# LASER-ASSISTED MICROMACHINING OF HYDROGEL FILMS FOR BIOMEDICAL APPLICATIONS

by

**Hongjie Jiang**

**A Dissertation**

*Submitted to the Faculty of Purdue University*

*In Partial Fulfillment of the Requirements for the degree of*

**Doctor of Philosophy**


School of Electrical & Computer Engineering

West Lafayette, Indiana

December 2018

# THE PURDUE UNIVERSITY GRADUATE SCHOOL
# STATEMENT OF COMMITTEE APPROVAL

Dr. Babak Ziaie
Department of Electrical & Computer Engineering
Dr. Zhihong Chen
Department of Electrical & Computer Engineering
Dr. Saeed Mohammadi
Department of Electrical & Computer Engineering
Dr. Çağri Savran
Department of Mechanical Engineering

**Approved by:**

Pedro Irazoqui
Head of the Graduate Program

*This dissertation is dedicated to my parents, Xibo Jiang and Jianping Huang, and to my wife, Jia Liu, with my endless gratitude for their unwavering support, love, and encouragement.*

# ACKNOWLEDGMENTS

The route to pursue a Ph.D is never straightforward; the work in this dissertation could not have been completed without the help from many people along the way. My endless gratitude first goes to my parents, Mr. Xibo Jiang and Mrs. Jianping Huang, and my wife, Ms. Jia Liu. Their patience, encouragement, and support stay with me all the time when I pursued this academic endeavor; their love and care embrace me at every moment I feel frustrated. My priceless gratitude also goes for my twin sons; they were born at Oct.2017 and their arrival is more than the responsibility also to encourage me to create a better future for them. In addition, I would also like to thank my sister-in-law, Professor Yan Liu of Texas A&M University, who is always supportive to provide me the professional advice/analysis. It is only because of them (my entire family), I can achieve what I have accomplished so far.

I'd like to thank my academic advisor, Professor Babak Ziaie, for all of his valuable guidance, support, and advice throughout my Ph.D. study at Purdue. He always shows a strong scientific enthusiasm and passion for a variety of research interests, which encourages me to pursue the latest topics. I appreciate his research philosophy as the guide for my Ph.D research, his understanding when the students face a life problem outside of research, and his motivation through the team building, which together create an exceptional atmosphere for conducting the doctoral research.

I would also like to thank all the wonderful people I met during my time at Purdue who offered their support and suggestion to my research. Firstly, I thank all my committee members, Professor Zhihong Chen, Professor Saeed Mohammadi, and Professor Çagri Savran, for their precious instruction and feedback to improve my graduate studies. I am also especially grateful to Dr. Manuel Ochoa, Dr. Jun Hyeong Park, Mr. Wuyang Yu, as our direct cooperation created this work in this dissertation and it would not have been possible without them. A very dear thanks goes to all my friends that have helped to keep me motivated throughout this endeavor. These include the helpful staff at the Birck Nanotechnology Center and all my colleagues from the Ziaie Biomedical Microdevices Laboratory (ZBML). They are Dr. Rahim Rahimi, Mr. Vaibhav Jain, Mr. Mark Oscai, Mr. Tejasvi Parupudi, Mr. Jiawei Zhou, Mr. Tianshuo Zhang and all my other lab colleagues. We are not only coworkers but also friends who also share life experience and advice to each other. In this lab, they provided me with collaboration and contribution to the nature of my graduate studies. Furthermore, I am thankful to Mr. Neil Dilley in Birck Nanotechnology Center and

Professor Ronald A. Siegel of the University of Minnesota at Twin Cities for their help and guidance in the magnetic susceptibility experiment of the ferrogel.

Finally, I would like to take this opportunity to thank those who provided me with professional development and financial support. This thank goes to the Purdue ECE Department for the two semester teaching opportunities of ECE 255 class. This equipped me the experience of academic teaching and understanding the undergraduate students.

# TABLE OF CONTENTS

# LIST OF TABLES

# LIST OF FIGURES

# ABSTRACT

Author: Jiang, Hongjie. PhD
Institution: Purdue University
Degree Received: December 2018
Title: Laser-Assisted Micromachining of Hydrogel Films for Biomedical Applications
Major Professor: Babak Ziaie

Hydrogels are soft polymers comprising of a three-dimensional network capable of absorbing significant amount of water or other aqueous bio-fluids. A group of hydrogels, commonly referred to as “environmentally-sensitive hydrogels” are designed such that they can undergo reversible volume change in response to a variety of physical and chemical stimuli. Although mechanically soft, embedding organic and inorganic micro and nanoparticles into the hydrogel network increases their mechanical strength. Hydrogels have been extensively explored as scaffolding for tissue engineering or smart materials for biomedical transducers. Hydrogels in the mm-scale are typically associated with a slow response time. At micro-scale, however, they can be fast and useful as smart sensors and actuators. Several micromachining techniques have been employed to pattern thin films of hydrogel. Micro-patterning methods are based on traditional fabrication techniques such as lithography, etching, and micro-molding. These methods are time consuming, expensive, and do not scale well to large production. In addition, they have limitations as related to processing composite gels (e.g., UV light cannot penetrate through the gel and particles can mask dry etch). In this work, we outline a doctoral research aimed at alternative solution based on direct laser patterning, allowing low cost, fast, and scalable fabrication for mass production.

We characterized and analyzed a series of transient features of the laser-engineered patterns, including the ablated width, sidewall quality and resolution, as a function of laser beam parameters and hydrogel thermal & optical properties by laser-machining the hydrogels at different moisture level of hydrogels till fully dry at an interval of one hour. All the optimal patterns appear at 1-2 hours of drying (hydrogel losing 35%-65% weight), thus identifying an optimal window for a rapid end-to-end fabrication. Then, two types of composite gels were created and laser engineered, consisting of nano-iron particles embedded hydrogel (“ferrogel”) and micro-silica beads loaded hydrogel (“silicagel”); the results show comparable features similar to the bare hydrogel, confirming the processability of laser micro-machining on the composite gels. Next, we studied

the swelling kinetics of the laser-machined hydrogels and identified tradeoffs between swelling speed and mechanical force. At the final, we used the laser patterning method to design and fabricate two pH-regulated autonomous drug delivery devices, a 3D printed smart capsule for targeted drug delivery in small intestine and a flexible patch for delivering antibiotics to infected chronic wounds. In both cases, their delivery capabilities can be tuned by either controlling the spatial resolution of the hydrogel actuator (the former) or using an n × n array (the latter).

# 1. INTRODUCTION

## 1.1 Motivation

Hydrogels are three-dimensionally crosslinked polymeric network which can absorb a large amount of water due to the hydrophilic side groups integrated in their backbone chains [1] and hence exhibit a swelling capacity (volumetric expansion) of several times of their initial weight (dimension). Not only imbibing the water from the surrounding medium into its network, the hydrogel also can expel the water into the external environment; therefore, this reversible shape/structure changing due to water uptake/expulsed into/out of the network is usually utilized to analyze and investigate the swelling kinetics of the hydrogel. Hydrogels can be physically or chemically crosslinked that the former is by ionic, hydrogen or Van der Waals bonds and the latter is through covalent bond; and both the crosslinking manners in gel network are capable of providing hydrogels with structural and physical integrity, thus rendering them the insoluble in the aqueous medium [2], [3].

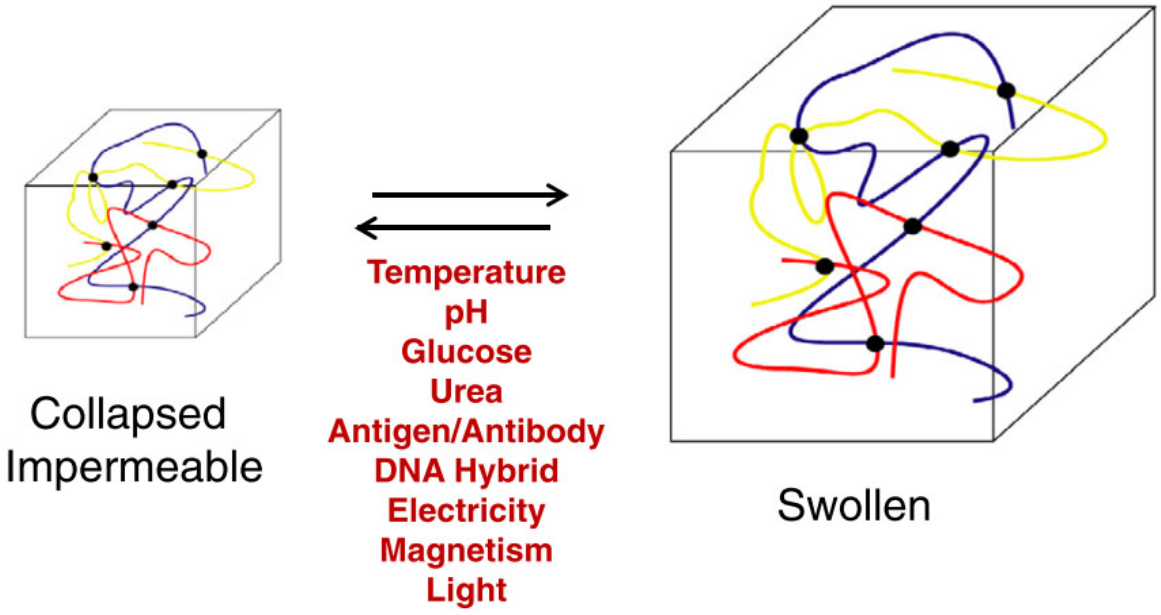


Figure 1.1 Environmental sensitive hydrogels swell and collapse when exposed to external stimuli Reproduced from Ref. [4] with permission from Elsevier.

As a type of ‘smart’ or ‘intelligent’ material, environmentally sensitive hydrogels can respond their volume and shape transition to the change of enclosing medium. Depending on the functional groups along their backbone chains, hydrogels can be sensitive/responsive to a variety of environmental stimuli, such as temperature, light, pH, glucose, magnetic/electrical signal and so on [4]–[6]; as a result, the hydrogel will exhibit not only changes in their dimensions/structures but also variations in their mechanical strength and permeability, whose degree depends on the encountered external surrounding stimuli, Figure 1.1. Environmental sensitive hydrogels usually respond to single stimulus, while they can be modified/tuned to response multiple stimuli through crosslinking different type of responsive monomers. Furthermore, the multiple environmental stimuli sensing capability can be easily achieved by incorporating functional organic or inorganic agent/particle into the gel network; this manner is also capable of physically customizing the hydrogel from being responsive one type stimulus to other stimuli. Due to all the aforementioned fascinating properties, environmental sensitive hydrogels can be applied as a promising option featuring various biomedical and pharmaceutical applications, such as biosensors, diagnostic imaging, drug delivery, etc., thus attracting the scientific interest for several decades [7]–[13], Figure 1.2.

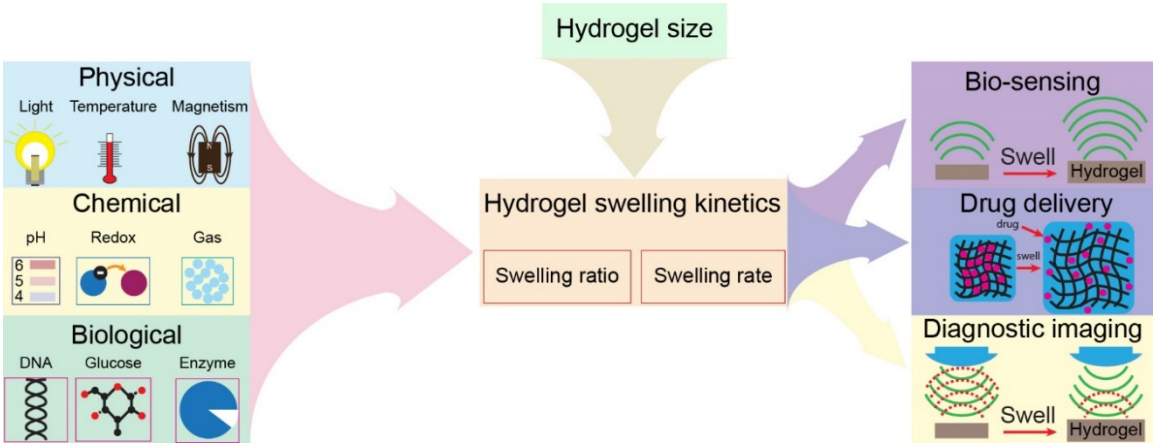


Figure 1.2 Typical bio-applications of envrionmental sensitive hydrogel regulated by external stimuli or different size.

Within most of the applications, hydrogels are required to fit into a cooperation with external mechanical or electrical system, which requires an in-situ polymerization of hydrogel instead of a time-consuming or destructive curing and transferring manner. Especially for sensing or actuation

purpose, which is dominated by the swelling kinetics of the hydrogel, like swelling ratio and swelling rate, the hydrogel thus requires a micro-patterning process, either within or after the polymerization. Besides, sometimes the hydrogel is required to be bonded to an adhesion promoting film to finish the sensing or actuation function, while this kind of bonding could give rise to the delayed stress relaxation and undesired hydrogel buckling during the hydrogel deformation period [14]–[16]. Therefore, the micro-machining process on the hydrogel is essential to achieve a repeatable and stable hydrogel-deformation induced micro biomedical systems.

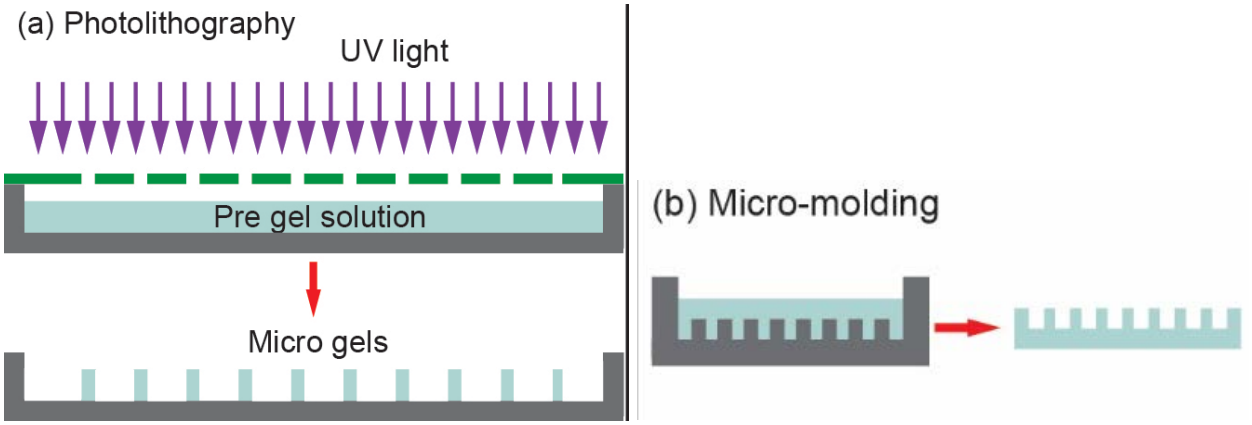


Figure 1.3 Tryditional micro-michaning techniques (a) UV-photolithography; (b) Micro-molding.

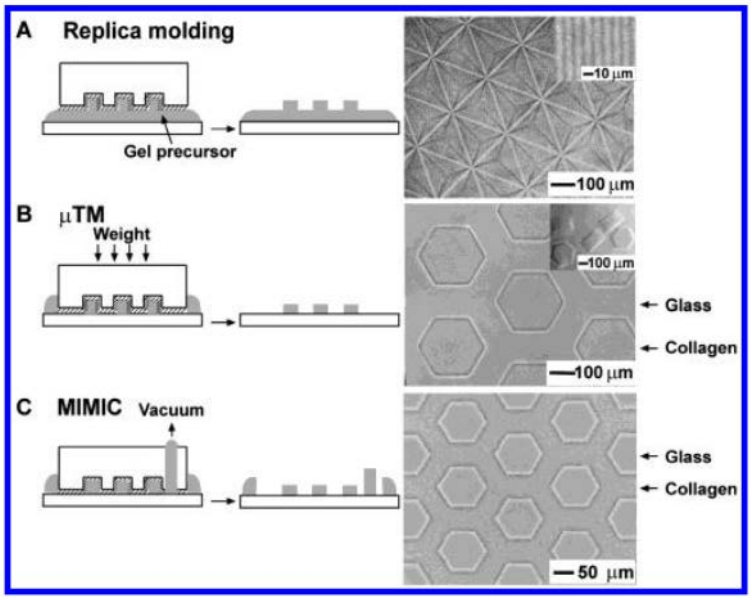


Figure 1.4 Micro-molding (soft lithography) applied for micro-machining of collagen. Reproduced from Ref. [17] with permission from ACS.

Current MEMS techniques for generating micro- and nano-patterns on polymeric materials include soft lithography and photolithography [18], Figure 1.3. Soft lithography is a rapid and low cost manufacturing technique without altering the integrity of polymers, whose procedure consists of fabricating and utilizing a micro-patterned elastomer (usually PDMS) to stamp, transfer, or mold micro-structures of hydrogels in series, Figure 1.4, [17]; although cost-effective and repeatable, its scalability and massive-fabrication capability are restricted by the development of appropriate masters. Photolithography is a powerful tool for high resolution patterning. One such example was well demonstrated in the published articles [19] that the UV-lithography was applied for direct photo-patterning a UV-curable pH-sensitive hydrogel in a microfluidic platform, serving as the pH-regulated valve to manipulate the flowrate, Figure 1.5. Another example involved a combination of photography and dry-etch of dehydrated hydrogels, a wide variety of hydrogel (three types of environmental sensitive hydrogels) and high resolution (2.5 μm) achieved and illustrated, [20], Figure 1.6. However, Photolithography usually suffers a low throughput limited by the complicated fabrication procedure and variable photomasks requirements; and the requirement of cleaning room techniques also puts the Photolithography at a disadvantage of being costly [21]. Besides, Photolithography does not fit the fabrication of composite hydrogels as UV will either compromise the properties of embedded particles or be blocked/scattered by those particles thus impacting the polymerization of hydrogels, Figure 1.7. Therefore, laser engraving system is chose in this work to micro pattern hydrogels without damaging the integrity and properties of hydrogels after processing. Moreover, compared to those abovementioned micro-machining techniques, the laser micro-machining is more advanced at the cost-effectiveness and throughput, thus more preferred for the scalable massive manufactory of micro-patterned hydrogels and concomitant the affordable development of complex biomedical micro-systems.

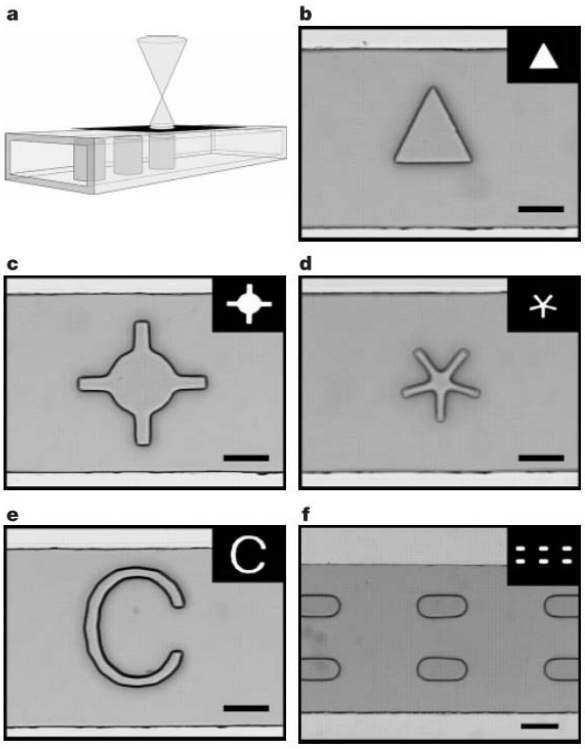


Figure 1.5 UV-photolithography applied for in-situ micro-machining of photocurable hydrogel for microfluidics. Reproduced from Ref. [19] with permission from Nature.

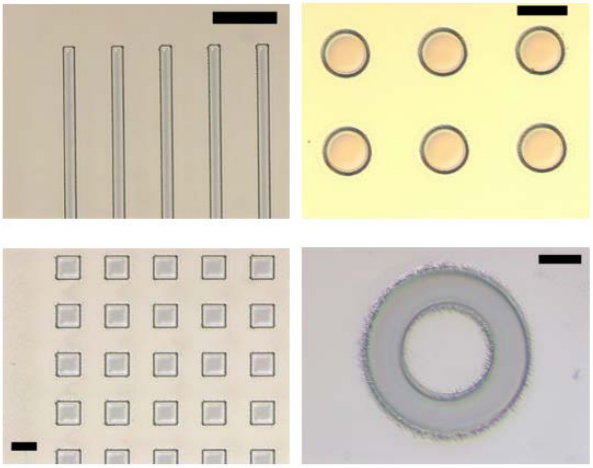

Figure 1.6 Photolithography and dry-etch applied for micro-machining of mAA-co-AAm hydrogel for biomedical applications. Reproduced from Ref. [20] with permission from IEEE®2005.

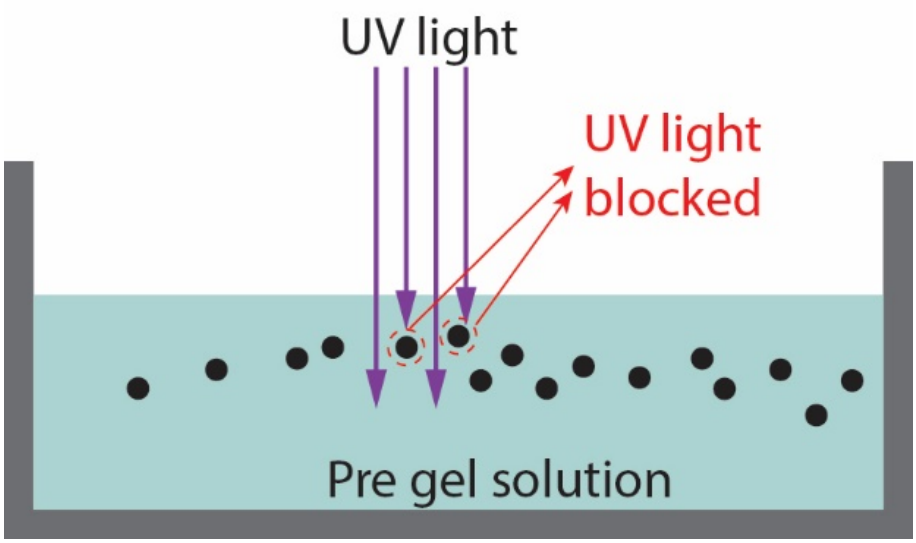


Figure 1.7 Limitation of photolithograph for composite hydrogels.

## 1.2 Organization of this document

This document is organized into eight chapters. The first chapter gives the motivation and significance for the proposed research. Chapter 2 provides background information regarding the pH-sensitive hydrogel-based applications for bio-medical micro-systems and a brief introduction of laser system. Chapter 3 presents the principle of the laser-micromachining technique and the experimental data of its application on hydrogel. Chapter 4 is the pH-sensitive hydrogel swelling kinetics analysis and characterization regulated by the laser micro-machined gel pattern and several typical physical/chemical stimuli, which are encountered in ordinary bio-applications. Chapter 3 and 4 are the theoretical and experimental basis for comprehending the operation principle of the first sensing system, which consist of the major parts of this thesis.

In the following chapters, two laser-engineered hydrogel-based bio-applications will be presented. Chapter 5 presents a smart capsule that can release its payload after a predetermined/adjustable delay subsequent to passing from stomach into the small intestine. Through the swelling of the pH-sensitive hydrogel, the accuracy and the resolution of the delay-time are autonomously controlled that the former is within ±5 min after one hour the small intestine increasing to ±40 min after 4 hours; the latter is one hour per 0.2mm gap.

Chapter 6 presents an inexpensive and closed-loop polymeric pump for topical/transdermal drug delivery which uses wound pH as a trigger for localized drug release. The device provides a slow drug release (< 0.1 μL/min) for up to 3 hours and can be tuned to $n^2$ times bigger through a

layer-by-layer fabrication to create an n×n drug delivery array (2×2 in this work). In addition, a simplified version using cationic pH-sensitive hydrogel (a reverse swelling kinetics of anionic one) could be achieved.

Finally, chapter 7 and 8 summarize the conclusion of this dissertation and discussions on prospective research for the improvement of the laser-micromachining technique applied on the pH-sensitive hydrogel and the extension of the hydrogel-based bio-applications presented here.

# 2. BACKGROUND: PH-SENSITIVE HYDROGEL AND LASER MICRO-MACHINING TECHNIQUE

## 2.1 pH Sensitive Hydrogels

As one type of environmental sensitive hydrogel, pH sensitive hydrogels can experience abrupt or gradual volume variations in response to the changes of pH levels of the surrounding environment due to their ionic moieties. pH sensitive hydrogels are composed of polymeric backbones with either anionic (e.g. carboxyl acid, sulfonic acid) or cationic pendant groups (e.g. amines); they contain a wide range of variable entities, including poly (acrylic acid) (PAA), poly (methacrylic acid) (PMAA), poly (ethylacrylic acid) (PEAA), poly (propylacrylic acid) (PPAA) copolymers of PAA and PMAA with PEG, PNIPAAm, poly (vinyl alcohol) (PVA), poly (hydroxyethyl methacrylate) (PHEMA), etc. Therefore, these side groups in the hydrogel networks offer the hydrogels different deformation (swelling/shrinking) kinetics [22].

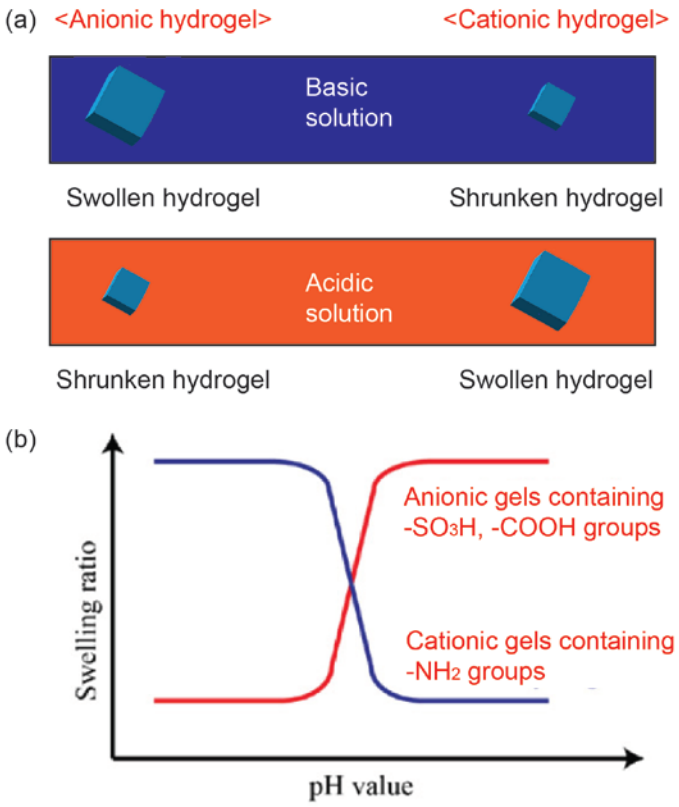


Figure 2.1 Illustration of (a) volume change and (b) swelling ratio curves of anionic and cationic hydrogels in response to different pH value.

Anionic hydrogels swell due to the increasing density of likewise charged groups within the network accompanied by an adequate generation of mobile counterions inside the gel when the pH value of a media is higher than pKa of the groups, like $–SO_3H$, -COOH, Figure 2.1. Therefore, the high degree of ionized pendant groups causes an enhanced electrostatic repulsion force among the groups, inducing an increase of hydrophilicity of the polymer thus leading to greater swelling response. In contrast, cationic hydrogels swell and shrink in an opposite behavior of anionic hydrogels as their ionization (protonation) begin at the pH level lower than pKa of the groups and deprotonation start at the pH level higher than pKa of the groups. Figure 2.1 describes and summarizes the general volume responses curves (swelling ratio versus pH value) of anionic and cationic hydrogels in acidic and basic solutions that the anionic hydrogels swell as pH increases and shrink as pH decreases and while the cationic hydrogels have a reverse deformation kinetics.

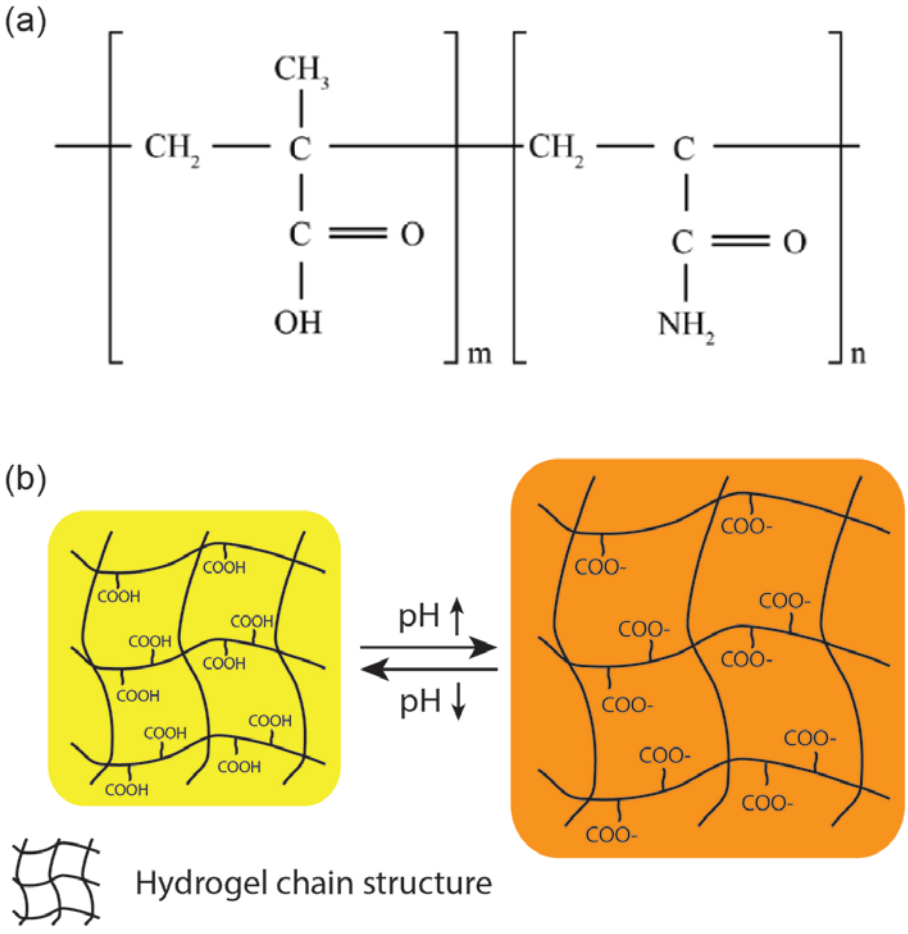


Figure 2.2 Chemical structure and (b) volume transition mechanism of poly (methacrylic acid-co-acrylamide) (mAA-co-AAm) hydrogel.

Poly (methacrylic acid) (mAA) is commonly copolymerized with poly (acrylamide) (AAm) to form a typical example of anionic pH sensitive hydrogels, poly (methacrylic acid-co-acrylamide) (mAA-co-AAm) hydrogel, whose chemical structure and volumetric deformation mechanism of are shown at Figure 2.2 (left: mAA, right: AAm). At high pH levels larger than its pKa, the carboxyl groups (-COOH) of mAA is deprotonated (thus ionized) to -$COO^-$, producing an internal electrostatic repulsion among the polymer chains as follows:

$$[RCOOH]_{gel} + [OH^-]_{aq} \rightarrow [RCOO^-]_{gel} + H_2O \quad (2.1)$$

Therefore, the degree of ionization density (thus ionic strength) within the hydrogel network strongly increases and concomitantly induces the phase transition due to the intensified electrostatic repulsion between the ionized groups ($-COO^-$). As a result, the increased hydrophilicity of the hydrogel leads to a greater swelling response. At low pH levels, the acidic gel is deionized/protonated as the -$COO^-$ is combined with $H^+$ ions back to the form of –COOH,

$$[RCOO^-]_{gel} + [H^+]_{aq} \rightarrow [RCOOH]_{gel} \quad (2.2)$$

thus reducing the electrostatic repulsion force and consequently causing hydrogels to turn into to a relatively shrunken status in contrast. Due to the dominant strong repulsion force of ionic hydrogels, ionic hydrogels exhibit a larger external stimuli regulated volumetric transition than neutral hydrogel, thus more applicable in pH-controlled drug delivery and sensors [23]. In this doctoral research, the poly (mAA-co- AAm) hydrogel is chose for demonstrating the laser micro-machining on hydrogels and proving the working principles of all its incorporated micro-systems for the health care applications.

### 2.1.1 pH-sensitive hydrogels for drug delivery

pH sensitive hydrogels are frequently utilized into implantable or digestible drug delivery applications since several human body sites, such as the gastrointestinal tract [24], [25], vagina [26] and blood vessels, have variable pH value in natural or locally changed by specific substrates, all thus providing a suitable base for pH-responsive drug release. The manner of pH-regulated drug delivery is to diffuse different sizes of drug molecular into (drug loading) and out of (drug release) hydrogels by controlling the hydrogels from shrinking to swelling or the reverse behavior, which result in the controlled release of entrapped drug and thus can cover a broad range of drug administrations, including oral, nasal, buccal, rectal, vaginal, ocular, parenteral routes, etc.. Moreover, plenty of variable drug/agent composition (protein, enzyme, cell, etc.) in different

formation (disc, membrane, micro/nano-capsule) can be delivered through this kind of pH-regulated drug delivery system, [27]–[32].

Apart from single-stimulus (pH in this context) responsive hydrogel, drug delivery also can be benefited from a multiple-stimuli-responsive hydrogel by incorporating other stimulus sensitive monomers in the network. For example, a typical pH and temperature sensitive copolymer, poly (N-isopropylacrylamide) / BMA (butyl methacrylate) / AA (acrylic acid) hydrogel, has monomer NIPAAm as thermal-sensitive and AA as pH-sensitive. This copolymer has its lower critical solution temperature (LCST) profile tailored as a function of pH and hence can achieve the desired aqueous loading and release profile [33]. Another example is pH-, thermo-, and glucose- triple-responsive (DMAEMA-co-AAPBA) hydrogels using bovine serum albumin to model protein release behavior from the hydrogel matrix as a function of pH, temperature and glucose concentration with maximum drug release rate at physiological pH [34].

pH sensitive hydrogel can also be converted to other stimuli-sensitive hydrogels by incorporating other environmental sensitive organic or inorganic agents/particles into gel network, thus capable of delivering drug autonomously controlled by the change of other stimuli concentrations. A typical such application is to immobilize the glucose oxidase (GOx) in pH-sensitive hydrogel network; once immersing in glucose solution, the gel can achieve a volume transition following the pH decrease induced by the increase of hydrogen ion from gluconic acid produced through glucose oxidation according to the below reaction [35] [36]:

$$glucose + O_2 + H_2O \xrightarrow{\text{GOx}} \text{gluconic acid} + H_2O_2 \tag{2.3}$$

Such aforementioned drug delivery systems, either using hydrogels as drug-entrapped carriers or as shell wall of microcapsules, generally require gel network to involve simultaneous absorption of water and desorption of drug via a swelling-controlled mechanism, thus the rate of release of drugs are affected by a multitude of parameters such as the polymer matrix, properties of the drug, or drug-matrix interaction, etc. Therefore, it suffers from various limitations such as high cost, difficulty with sterilization, and toxic reactions, Table 2.1.

Table 2.1 Advantages and limitations of pH sensitive hydrogels based drug delivery system.

| Advantages | Limitations |
|---|---|
| biocompatibility | High cost |
| Delivered by various routes | Low mechanical strength |
| Easy to process | Difficult to load |
| Easy to modify | Difficult to sterilize |
| Controlled release rate | Nonadherent |
| High loading efficiency | Cause local reactions |
| Minimal toxicity | Cause systemic reactions |

Instead of using hydrogels as carriers entrapping or encapsulating drug for a passive-diffusion based drug delivery, small scale system/devices cooperation with pH-sensitive hydrogel are also developed in macro or micro scales to achieve a more controllable and programmable drug delivery. This manner is able to utilize the strength of hydrogels like stimuli-sensitivity while can circumvent the weakness of hydrogels like fragile, limited to drug type/form, [1], [4], [37].

Several academic efforts are developed for the fabrication of such prototypes. A smart micro-valve is created by sandwiching a phenylboronic-acid-based hydrogel between a rigid porous membrane and a deflectable diaphragm; when exposed to external pH, the gel deformation opens and shuts a flow channel for the on-off flow control of insulin delivery, Figure 2.3(a) [9]. A polymeric drug delivery system is developed by using poly HEMA and poly (methyacrylic acid-co-ethylene glycol) (MAA-co-EG) gels as a gate to regulate the self-folding induced drug release; while it suffers several limitations as the low drug-loading efficiency and the surfactant coating for targeted drug release, Figure 2.3(b) [38]. A soft micro-robot is created by encapsulating the drug into eight radial arms made of poly HEMA and PEGDA with Fe3O4 nanoparticles; when manipulated by an electromagnetic actuation (EMA) system to a low pH medium, it will unfold its shape and release the drug. Its semi-sealed drug reservoir could expose the drug to the ambient environment, which thus limits the delivered drug type, Figure 2.3(c) [39]. A closed-loop insulin delivery device is made of medical grade silicone tubing with one end sealed by glucose responsive

hydrogel, whose swelling and shrinking modulate the insulin release as a function of blood glucose concentration, while lacking the capability of targeting, Figure 2.3(d) [40].

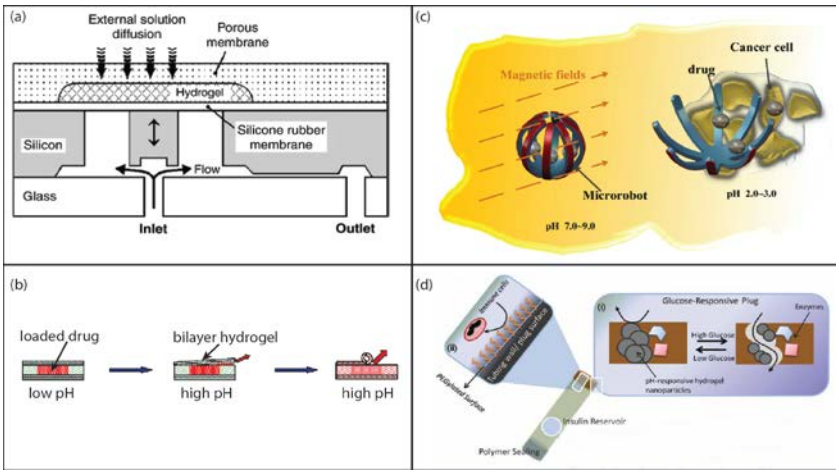


Figure 2.3 (a) illustration of smart micro-valve; (b) polymeric drug delivery system using bilayer of pH-sensitive hydrogels, Reproduced from Ref. [38] with permission from Elsevier; (c) magnetic actuated soft micro-robot, Reproduced from Ref. [39] with permission from IOP Publishing; (d) glucose-sensitive tube for insulin delivery, Reproduced from Ref. [40] with permission from John Wiley and Sons.

### 2.1.2 pH-sensitive hydrogels for wireless electrochemical sensing

Not only does the pH sensitive hydrogel can be utilized into the pH-controlled drug delivery with cooperation of a chemo-mechanical system working as a chemical engine to initiate the drug release, but also it can be applied into a chemo-electrical system, thus serving as the role for electrochemical sensing. As the ingestible “radio pill” is first demonstrated in 1957 [41], the wireless electrochemical sensing techniques for in-vivo physiological signal detection get rapid and extensively investigation. In order to overcome the need of on-board power source, a common drawback of most implantable chemical wireless micro-devices, the environmental sensitive hydrogels, which deform response to the surrounding external stimuli, have been employed to fabricate passive wireless chemical sensors [8], [11], [12], [42]–[48]. Our group first developed a MEMS-based passive LC transponder, whose capacitive-dependent resonance frequency is dependent on osmotic swelling and shrinking of a pH/glucose responsive hydrogel, thus achieving the interrogation between the LC resonator and the external pH/glucose level [49]. However, due to the requirement of cleanroom processing and the complicated fabrication of a hermetically

sealed MEMS capacitor, this MEMS-based LC resonator has a limited practical application by the low throughput and high manufacturing costs. Portions of the text in this section are taken from publications by the author [13].

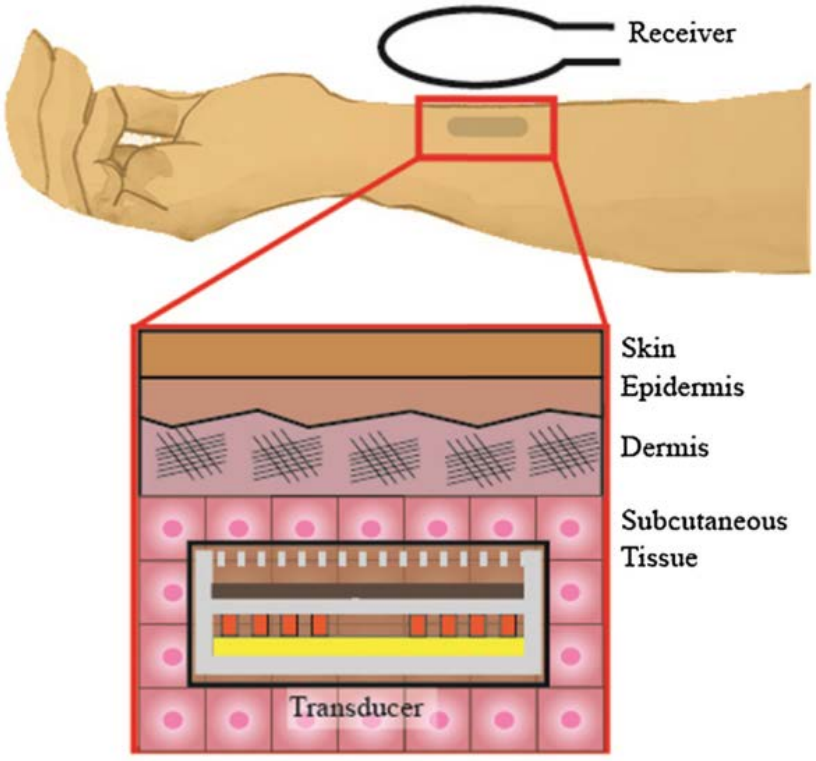


Figure 2.4 Sensing mechanisms of the ferrogel sensor using inductive-dependent resonance frequency modulation to measure the external enviromental stimuli concentration. Reproduced from Ref. [50] with permission from Elsevier.

An alternative pH-sensitive hydrogel-based wireless sensing mechanisms is to incorporate the micro/nano functional particles into the polymeric network of the hydrogels [51]–[53]. One such entity developed by our group using the composite gel for wireless sensing is to integrate magnetic nanoparticles into the pH-sensitive hydrogel in order to achieve a low-cost and easy-to-fabricate passive LC resonator, which can be applied into subcutaneous physiological pH detection, Figure 2.4 [53]. A magnetically functionalized hydrogel, “ferrogel”, is created in this manner and thus possesses volume-controlled magnetic permeability (i.e., lower permeability in the shrunken state and higher permeability at the swollen state), which can be used in conjunction with a planar coil to form a passive LC transponder whose inductance is modulated with pH variations.

While the fabricated ferrogel sensor has a significantly simpler fabrication process and lower cost than the MEMS-based one, the short interrogation range (~1 cm) and the requirement for a complicated readout circuitry limit its practical applications to scenarios in which the sensor is implanted subcutaneously. In order to remove/circumvent one of the major bottlenecks of passive sensing as to achieve a deep tissue penetration (>10 cm), our group later developed a different chemical sensing method, which features a silica-bead-embedded hydrogel (silicagel) whose volumetric response to the chemical stimuli can be remotely interrogated by ultrasonic imaging through evaluating the back-scattered wave intensity. The application was to insert the fabricated silicagel in either the subcutaneous space or deep tissue within the body and monitor the volume transition using ultrasonic waves at clinical imaging frequencies (2–20 MHz); as its volume transition would modulate the embedded silica bead density (a higher density at in the shrunken state and a lower density at in the swollen state), the change in intensity of back-scattered ultrasonic wave can be transformed into an ultrasonic image as a function of volume change and thus external stimuli variation. This biochemical monitoring scheme only requires a minimally invasive surgical procedure for implantation of the silicagel, thus featuring more clinically relevant since ultrasonic imaging equipment is commonly available in most clinics, Figure 2.5 [13].

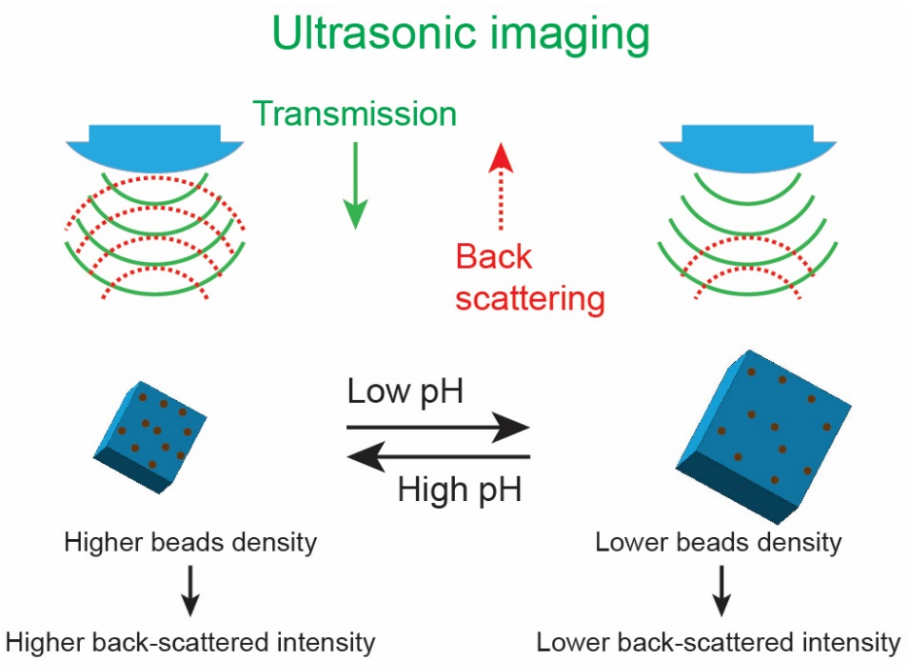


Figure 2.5 Sensing mechanisms of the silicagel sensor using ultrasonic back-scattered intensity measurement. Reproduced from publications [13] by the author.

## 2.2 Laser introduction

A laser system usually consists of three major parts, energy pumping source, lasing medium (source of emitted photons), and optical set up (direction, focusing and amplification). The initiation of laser generation starts to pump some types of energies, in electrical, light or other forms, on the lasing medium (in the form of gas or solid), which can excite the atoms of the lasing medium and concomitantly induce the transition of those atoms from their ground state to excited state; as these atoms return to their natural state, each one emits a photon. Then, the generated photon is allowed to travel randomly throughout the laser cavity until encountering another excited atom, which then cause another photon to be released with exact same properties and direction. This process is called 'stimulated emission'. Therefore, such multiple interactions between the produced photon and higher energy atoms emit more and more photons in the laser cavity, which results in high energy beam of light with coherent photons or laser. Eventually, the composed laser beam is guided and amplified to a desired direction through optical set up [54].

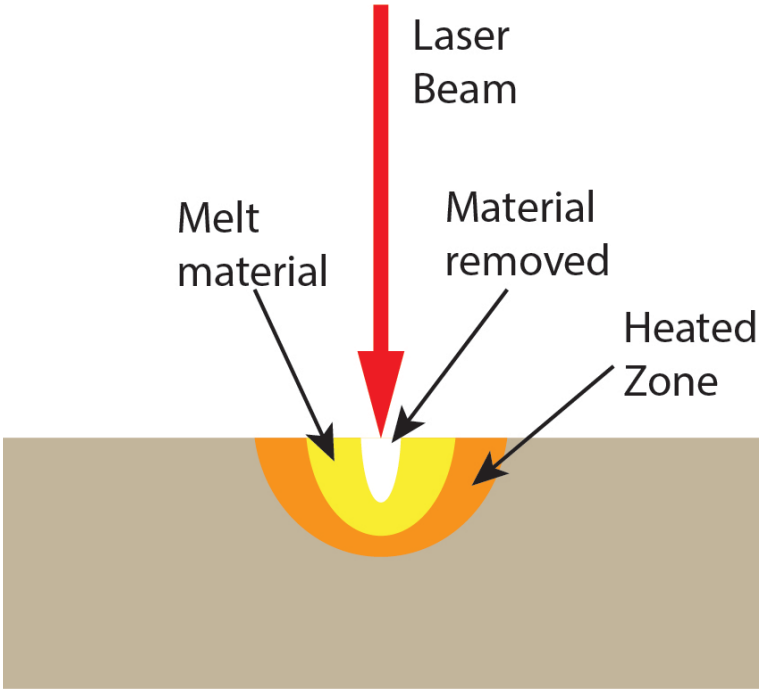


Figure 2.6 Laser interactions with material.

Figure 2.6 shows the laser-machining phenomenon and mechanism that when the laser imparts thermal energy on the surface of a substrate, the heat is created and deposited to the point of impact

and then propagate to the surrounding, the distance/damage dependent on the laser beam configuration and the thermal properties of the materials. At the center of the induced thermal energy, the temperature is maximum and evaporation takes place, resulting in removal of material; while at the surrounding of the focus, the temperature is lower than melting point, only causing the melting/softening of the materials (no decomposition occurs).

Due to its high lateral resolution, low heat input, and high flexibility, Laser beam is considered as a very useful in the micro-processes like cutting, welding, machining and other application where localized heating can be used. Moreover, as heat diffusion time is in the order of nanosecond to microsecond time scale, which is much longer than the electron–phonon coupling time of most materials (in the range of picosecond to nanosecond), laser energy can be deposited at a time scale much shorter than both the heat transport and the electron–phonon coupling to avoid collateral damage [55]. Thus, Laser beam is capable to be applied for micro-machining a wide range of variable materials, including metals, semiconductors, ceramics, polymers, etc. [55].

Laser-based micro-machining in polymers can be categorized into laser ablation, laser-assisted etching, laser-assisted deposition, stereolithography, and surface modification processes [56]. Laser ablation is used to break the chemical bonding of polymers in order to remove the directly interacted materials, including several mechanisms like photochemical (by directly breaking the chemical bonds of the substance during the process of photon absorption), photothermal (by releasing the heat of the excited molecules), or a combination of both [55], [56]. Based on that, laser ablation could be utilized to directly fabricate/write micro features on polymers, or create variable micro-machined polymeric masters for replication. Laser-assisted chemical etching (LCE or LACE) uses laser energy to create the local enhancement of a chemical etching reaction, which is thermally enhanced by substrate heating and/or generation of active species in the etchant by photo- or pyrolytic dissociation to produce deep structures in silicon [56]. Laser-assisted deposition processes can create material deposition through ablating the material from solid to gas phase in partial vacuum, which is capable of depositing high melting point and multi-element materials [56]. Stereolithography can selectively solidify the liquid photopolymer through adjusting the focus of UV beam, thus suitable to build complex 3D structures on layer-by-layer fabrication process [56].

According to the two main laser ablation mechanism (photochemical or photothermal), the laser system can be roughly divided into two categories, UV (the laser beam wavelength ≤ UV)

laser or IR (up to mid-infrared) laser [55], [57]–[60]. The former ablates the affected material through both mechanism; the latter removes the influenced material only by photo-thermally induced vaporization (due to a lower photonic energy); and the detailed comparison is in Table 2.2. As one type of the IR laser, $CO_2$ laser use $CO_2$ as the lasing medium to emitting light at a wavelength of 10.6 μm in the mid-infrared region. Although the $CO_2$ laser has a compromised range of the processable material when compared to the UV laser, it has proven to be well suited for micro-processing of ceramics/polymers as most of polymers have a good absorption coefficient at mid-infrared region and represented the best choice of the inexpensive commercial equipment for practical industrial applications [55], [61]–[63]. As a matter of fact, a $CO_2$ laser platform from Universal laser system is selected to micro-machine hydrogels include (poly (mAA-co- AAm) hydrogel and two derivative composite gels) through direct laser ablation in this research.

Table 2.2. Comparison of CO2 to other laser system.

| | **$CO_2$ laser** | **UV laser** |
|---|---|---|
| Wavelength(nm) | 10600 | 180-400 |
| Ablation mechanism | photothermal | Photochemical/photothermal |
| Pulse length | CW or us | ns |
| Cost | Low | High |
| Feature size | large | small |

# 3. CHARACTERIZATION OF LASER MICRO-MACHINING TECHNIQUE APPLIED ON THE HYDROGELS

## 3.1 Principle and theory

When the laser irradiates the surface of the hydrogel, the deposited thermal energy heats the hydrogel following the Gaussian distribution [55], [63]–[65] of the laser beam intensity; therefore, the micro-patterns/micro-channels created by the laser on the material usually has a U shape at a cross section view, where the removed width decreases from the surface to the bottom of the materials. For the practical application of micro-machined hydrogel, the laser-ablated width on the hydrogel should be defined to the smallest removed width at which this part of the hydrogel is completed ablated; in other words, the ablated depth equals to the gel thickness before laser process and the ablated width equals to that of the ablated bottom layer of U channel. The definition of ablated width aims at guaranteeing the enough space created for the micro-gels array to swell and thus eliminating the possible hydrogel buckling caused by the collision of swollen hydrogels.

From this point of view, the laser-machined hydrogel usually has the ablated width smaller or bigger than the laser beam diameter, which can be manipulated by decreasing/increasing either the laser beam intensity or beam radius. When laser ablating hydrogels, two regions on hydrogels are created that one is the laser direct-affected region due to the high temperature raised directly from the irradiation of the laser beam; and the other is the laser indirect-affected region, resulting from the heat lateral convection (vertical to the direction of laser scan) thus heating up to the evaporating point of the hydrogel away from the focus of laser beam. The regulation of the laser ablated width can be manipulated by controlling either the laser beam intensity or radius. As previously described, the laser beam usually follows the Gaussian distribution as follows [64]:

$$I(x,y,z) = \frac{P_i}{\pi d^2(z)} e^{-[(x^2+y^2)/d^2(z)]} \qquad (3.1)$$

, where I is the laser beam intensity, $P_i$ is the laser power and $d$(z) is the laser beam radius at distance z from the focal waist. This equation shows a linear relationship between the laser beam intensity and the laser power; therefore, by increasing the laser power, the beam irradiation imparted on the hydrogel surface will be intensified propotionally. The laser beam intensity also can be interpreted to the linear heat source (W s $m^{-1}$), the product of laser power and the reciprocal of scanning rate, $P_l = P_i/\upsilon$ ($\upsilon$ is the laser scanning rate), which can be enhanced either by

increasing the laser power or decreasing the scanning rate (more heat accumulation).

As discussed previously, the laser beam radius is one of the key parameters to manipulate the ablated width and the operation can be easily accomplished by altering the focal length of the laser beam. According to the definition of the laser beam radius[55]:

$$2d = 4\lambda f M^2/\pi D \qquad (3.2)$$

, where λ is the wavelength of laser radiation, f is the focal length of the lens, M is the beam quality and D is the spot size on the focusing lens, it is evident that the laser beam radius is an one-to-one function of the focal length assuming other parameter being constant and the fixed linear heat source. Therefore, by controlling the laser beam profile (linear heat source or beam radius), it is able to control the thermal ablation to the targeted dimensions and concomitant laser-engineer hydrogels to different desired patterns for fulfilling different requirements, Figure 3.1 (a).

At the other hand when at a fixed laser beam profile, the laser ablation also responds to the change of the hydration state of the hydrogel that when the heat diffusivity of the hydrogel increases or decreases, the ablated dimension (both width and depth) will also be expanded or compressed, Figure 3.1 (b). The mechanism between the hydrogel thermal properties and laser micro-machining can be further understood by the one dimensional thermal model of the heat conduction equation [66], [67]:

$$\mathrm{T} = T_0 + const\ t^{-1/2} e^{-(x_p^2/4\alpha t)} \qquad (3.3)$$

, where $T_0$ is the ambient temperature, t is the time and α is the heat diffusivity of the hydrogel. From this equation, it is evident that as the heat diffusivity increases, the temperature caused by the heat conduction from a fixed heat source will increase at the same position; in other words, the heat can propagate to a larger distance, thus extending the thermal ablation. The converse is also true; that is, when the heat diffusivity decreases, the laser ablated width will decrease. Note that this mechanism dominates in the laser indirect-affected region. Moreover, according to the definition of the heat diffusivity [67] as follows:

$$\alpha = \mathrm{k}/\rho C_p \qquad (3.4)$$

, where k is the heat conductivity, $\rho$ is the density and $C_p$ is the heat capacity of the material, the heat diffusivity can be raised by either increasing the heat conductivity or decreasing the heat capacity of the material, which, however, is not achievable for the hydrogel during a drying status. As the hydrogel contains a big amount of water, its thermal properties is dominated by the amount of the possessed water; when hydrogel is drying (losing water by water evaporation), both its heat

conductivity and capacity will decrease [68]; therefore, there would exist an optimal timing during the gel drying, at which the heat diffusivity reaches a maximum, and so is the ablated width.

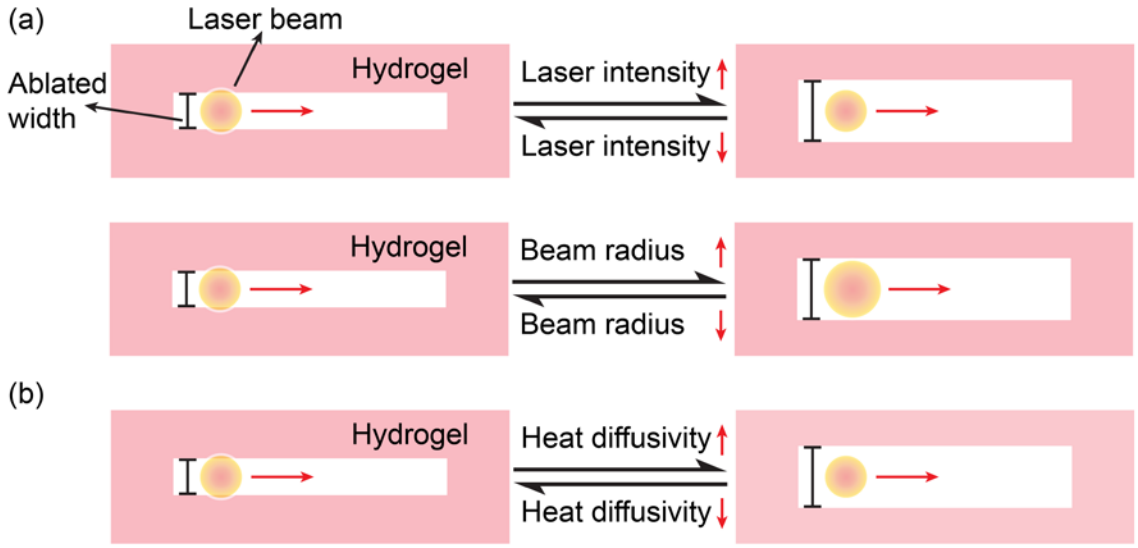


Figure 3.1 Conceptual illustration of laser-micromachining on hydrogel (a) The laser-ablated width regulated by laser beam profile (beam intensity and radius); (b) The laser-ablated width regulated by thermal properties of the hydrogel.

In addition, the thermal ablation on material removal approximately also follows Beer-Lambert's law, $I(z) = I_o e^{-\alpha z}$ where $I_o$ is initial intensity, α is absorption coefficient of the materials ($cm^{-1}$), and z is the depth laser intensity drops. The relationship between the etching depths per pulse and the laser fluence is given by $L_f = \left(\frac{1}{\alpha}\right) \ln(F/F_{th})$, where $L_f$ is etch depth per pulse (μm), F is laser fluence $\left(\frac{J}{cm^2}\right)$, and $F_{th}$ is threshold fluence $\left(\frac{J}{cm^2}\right)$ [55], [60]. When the hydrogel is drying, not only is the thermal properties of the hydrogel changed, but also both the mid-infrared absorption coefficient and the thickness of the hydrogel decrease [69]; therefore, the heat attenuation/propagation on the radial distance from the laser beam center is reduced/enhanced, which consequently increase the ablated width.

In summary, when fixing the optical parameters of the laser system, the quality of the laser micro-machining is a complicated balance among the thermal parameters, the absorption coefficient, and the physical dimension of the hydrogel, where only the thermal conductivity is proportional to the ablated width as its decrease would reduce the heat radial propagation and thus

the ablated width; while all other parameters, including the thermal capacity, the thickness and the absorption coefficient, are inversely proportional to the ablated width as their decrease can either expedite the material removal (water evaporation by reduced thermal capacity) or enhance the heat propagation (less heat attenuation by other two), thus increasing the ablated width.

Finally, the ultimate target of the laser micro-machining on the hydrogel can be summarized that the optical setting of the laser should be applied for finish the designed micro-patterning within one single laser scanning instead of a time-consuming laser cycling, which otherwise would damage the surrounding area or the substrate; and the laser-engineering window should be set as close as possible to the timing of the hydrogel gelation in order to shorten the entire fabrication period and consequently the cost. Therefore, the establishment of a dynamic profile (by hours) of the laser micro-machining on the hydrogel is essential not only to control the size of various patterns and but also to fulfill the requirement of a scalable, rapid and cost-effective massive manufactory, Table 3.1.

Table 3.1. Laser configuration and material properties for ablated depth and width.

| | | Ablated depth | Ablated width |
|---|---|---|---|
| Optical parameters of the laser | Laser power | **Large** | **Large** |
| | Beam radius (spot size) | **Small** | **Large** |
| | Ablation rate | **Slow** | **Slow** |
| | Focal length | **On Focus** | **Off Focus** |
| Thermal and optical properties of the hydrogel | Heat diffusivity | **Low** | **High** |
| | Absorption coefficient | **Low** | **Low** |

## 3.2 Experiment and general discussion

In current work, an adhesion promoting substrate (GelBond® PAG Film, Lonza) is utilized to provide chemical bonding for hydrogel to be held on place, eliminating the detachment of gels by probable vibration and rotation of capsule inside small intestine or bending of drug delivery patch upon chronic wound. First, this substrate is laser machined to create micro pores (~72 μm diameter) for allowing continuous ion exchange between gels and ambient aqueous environment since gels is confined in a cavity with one end sealed by an elastic membrane, making these micro

pores as the only channels for gels communicating with enclosing medium. Next, poly (mAA-co-AAm) hydrogels are casted and cured on the substrate. In order to control the thickness of gels on porous substrates, the pre-gel solution should not be casted directly on the porous substrate, since the porosity of the substrate allows some of the pre-gel solution to leak out at the edges of the substrate randomly, resulting in non-uniform gelation on and within the substrate. Instead, the pre-gel can be first casted onto a hydrophobic substrate (e.g., PDMS) and then sandwiched by placing the porous substrate on top of the pre-gel solution. Due to surface tension, the pre-gel will not spread on the PDMS solution until the porous substrate is placed on top of it, and then, it will only spread within the bounds of the substrate. Thus, with this sandwich method, it is possible to create uniform thin films of gel on a porous hydrophilic substrate, Figure 3.2. Finally, the hydrogel is allowed for one hour curing and then to be dried at room temperature; at an interval of one hour up to four hours by drying the hydrogel at room temperature, the $CO_2$ laser micro-machining on the hydrogel is applied and the weight of the hydrogel at each interval is also monitored. Moreover, both the laser work and the weighing of the complete dried hydrogel after 24 hours are also conducted as an extreme case of the change of both the thermal and optical properties of the hydrogel. In order to consider the hydrogel dimension effects on the laser machining, four types of hydrogels are fabricated to 0.5, 1, 1.5 and 2 mm thickness and laser micro-machined within one single laser beam scan with variable laser beam configuration and different moisture level, Figure 3.1.

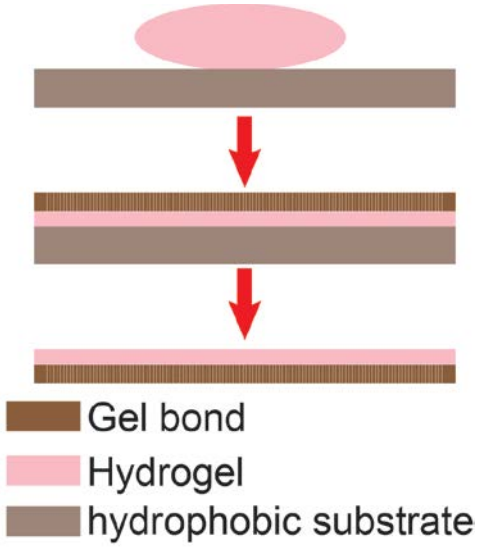


Figure 3.2 Fabrication of laser micro-machined hydrogels on adhesion promoting film.

As mentioned previously, when a laser beam imparts the thermal energy on the surface of the hydrogel, the Gaussian distribution of the laser beam intensity would form a U channel in the hydrogels, creating an inverse “Gaussian” pattern at the cross section view, Figure 3.3. Therefore, the laser micro-machining on hydrogels is expected to create a gradient decrease of the removed width, finally producing a truncated non-thermally ablated micro gels, Figure 3.3. Figure 3.4 (a) and (b) demonstrates the conceptual illustration and the photograph of the top view of the micro-machined hydrogel under a single scan of laser beam for a 5 mm length ablation. At the center of the laser beam, the hydrogel is completely removed/decomposed with the ablated depth equal to the gel thickness and the ablated width either larger or smaller than the laser beam radius, which depends on the laser beam profile and hydrogel thermal & optical properties. Meanwhile, at the position a little further away from the focus of the laser beam, the temperature raised by the heat radial propagation in the laser indirect-affected regions is unable to fully etch the gels; therefore, the hydrogels are partially removed as the ablated depth is smaller than the gel thickness, the debris shown as the dark part in the Figure 3.4 (b).

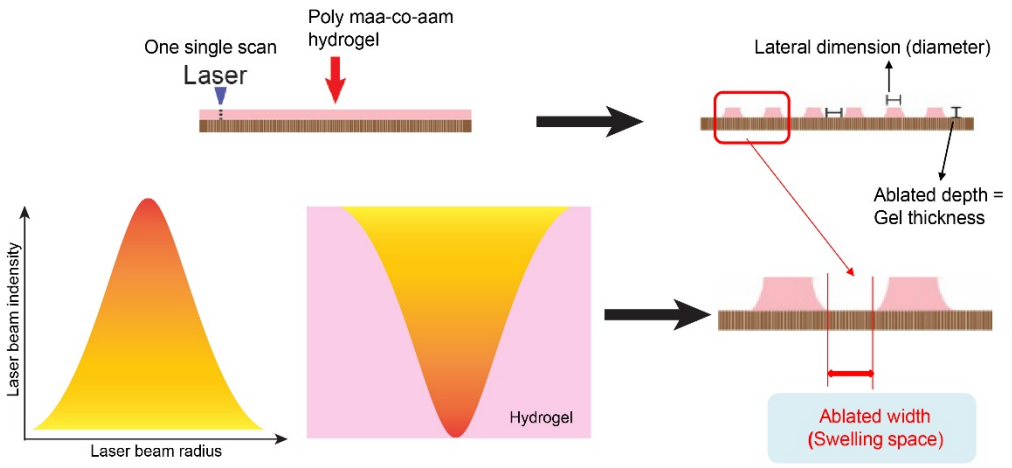


Figure 3.3 (up) Demostration of the fabrication and laser micro-machining of the hydrogel on an adhesion promoting substrate; (down) Ilustration of the Guassian patterned themally-etched hydrogels due to the Guassian laser beam profile.

So far, we are able to define several significant features which are chose to demonstrate the laser micro-machining quality in this research, including ablated width, sidewall quality (S.Q) and resolution. The ablated width is defined as the bottom layer width of the laser micro-machined U channel and serves the role of guaranteeing the swelling space of the fabricated micro gels, Figure

3.3. The sidewall quality (S.Q) is defined as the ratio of ablated width to laser affected width (the sum of completely and partially removed hydrogel), Figure 3.4 (c). From the definition of the S.Q, it is apparent that the degree of S.Q close to 1 is the key factor to identify the quality of the laser micro-machining on hydrogels in order to achieve a sharp/vertical laser-etched hydrogel edge. The third and the last important feature that should be used to investigate the laser micro-machining quality on the hydrogel is the resolution, which is defined as the ablated width versus the linear heat source.

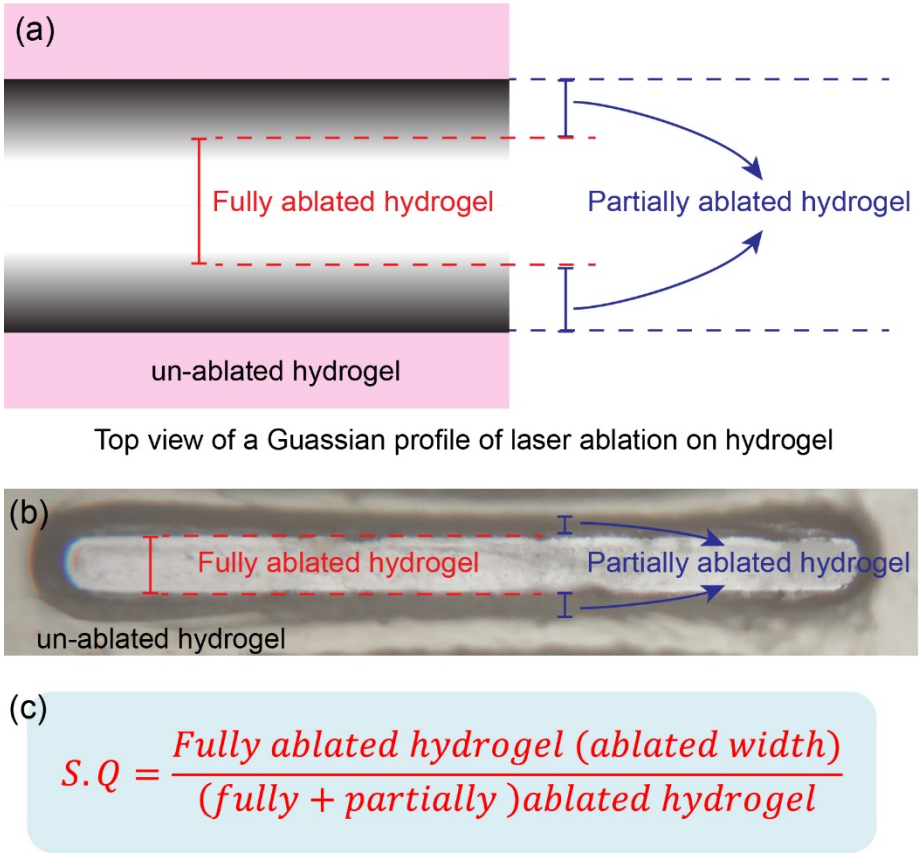


Figure 3.4 (a)-(b) Demostration and photograpgh of the topview of a 5 mm laser single ablation focused on the hydrogel surface, where two regions are created as the fully ablated hydrogel at the center of the laser beam and the partially ablated hydrogel due to the heat conduction parallel to the fully ablated area; (c) Definition of the sidewall quality.

In summary, the experiment procedure is designed to conduct a thorough and comprehensive characterization of the kinetic laser micro-machining of hydrogels that the ablated width should be precisely controllable to achieve different desired dimension so as to fulfill different sensing

(smaller ablated width, smaller lateral dimension, thus faster response time) or actuating (larger ablated width, larger lateral dimension, thus bigger mechanical force) or a balance of them; the optimal S.Q should approach as high as possible to 1 in order to induce less lateral damage to the micro-machined patterns, thus achieving the high-definition straight edges; and the resolution should be controlled within a high linearity to provide the tunable manufacturing scalability. Finally, the fully characterization of the laser-machining on the hydrogels at different drying state should help us to understand the time-dependent laser-machining kinetics on hydrogels and thus allocate a tunable and controllable processing window to achieve the desired pattern with the maximum S.Q and resolution under a rapid and scalable end-to-end fabrication. Note that as the hydrogels are covalent bonded to the substrate, the hydrogel swelling is not isotropical, which means that the swelling ratio at the top layer of hydrogels would be larger than that at the bottom layer as the top layer gels are free of any constraint; and this anisotropic swelling behavior is expected to balance the uneven laser ablation (Gaussian thermal removal of the targeted hydrogels), thus compensating the over-etched top layer of hydrogels and possibly reaching an equal equilibrium swollen width at both layers.

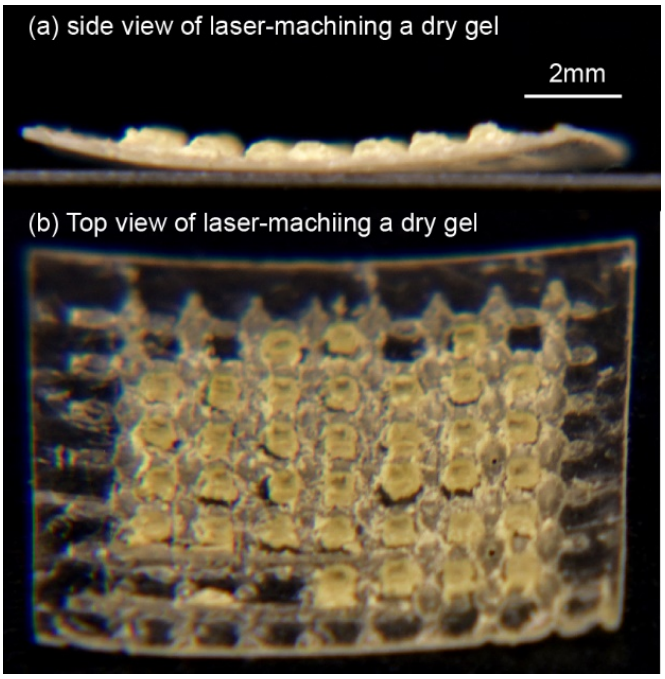


Figure 3.5 (a) Photograph of cross view of a bended adhension promoting substrate by non-uniform drying of the bonded hydrogels; (b) Photograph of top view of a non-uniform laser-machined microgel patterns on the curved substrate.

As described above, one main reason of managing the laser-machining process at different hydrogel moisture level is to find out the optimal window for achieving the time-saving and high quality fabrication. Besides, there exists a second reason, which was demonstrated in Figure 3.5. This demonstration involves an experiment conducted by drying the hydrogel on top of a 12 mm wide gel bond at room temperature for 24 hours until reaching a fully dried gel and laser micro-machining the gel afterwards. Since the hydrogel is bonded to the substrate, the anisotropic drying due to the water evaporation from the gel network will generate a non-uniform deformation (shrinking) between the bottom (large shrinking resistance by the gel bond) and up layer (free of shrinking resistance) of the hydrogel, thus bending the substrate, Figure 3.5 (a). Then, this curved substrate will cause a difficulty for allocating the focus of laser beam accurately and in turn creating a non-uniform fabricated micro gels, Figure 3.5 (b). Therefore, applying the laser micro-machining on the hydrogel after few hours of polymerization (thus no any deformation of substrate) is the guarantee to achieve a uniform micro-patterned hydrogel array.

Finally, a series of laser-machined hydrogel micro channels under different drying hours and laser beam profile were created and photographed for the analysis and measurement of the abovementioned features, including the ablated width, S.Q and resolution, so as to determine the optimal fabrication windows and conditions. Figure 3.6 presented the results of laser-machined hydrogels at 1 or 2 drying hours, where the optimal combination of laser machining qualities are capable to be accomplished, details explained in the next sections.

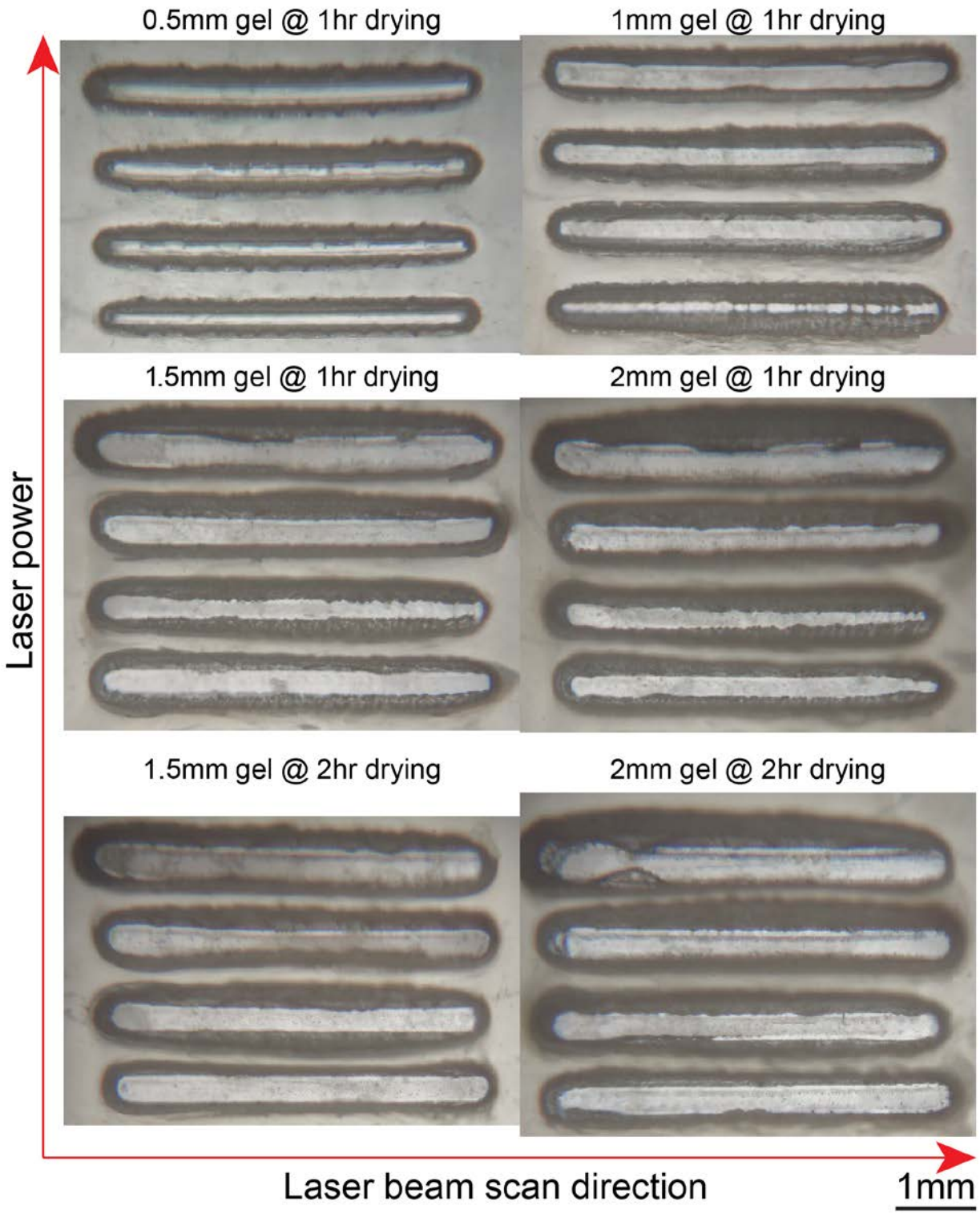


Figure 3.6 A set of selected photographs of the 5 mm laser single ablation on the four different thick hydrogels where the chosen hydrogel drying hours (1 or 2) for conducting the laser-machining are the optimal fabrication windows to achieve the best quality of a combination of laser ablated width, S.Q and resolution.

## 3.3 Ablated width analysis

Figure 3.7 shows the experiment results that for 0.5 mm thick hydrogel, the maximum ablated width processed under the linear heat source from 14 to 30 W s $m^{-1}$ occurred at the 1 hour drying except for that at 10 W s $m^{-1}$ (2 hour drying); and for the rest three thickness (1, 1.5, 2 mm), the maximum ablated width happened at 2 hour drying (only two exceptions including the 4 hour drying at 75 W s $m^{-1}$ and the 3 hour drying at 113 W s $m^{-1}$ for 1.5 and 2 mm thick hydrogel respectively). The maximum ablated widths that the four different thickness hydrogel can reach at the current optical setting of the laser beam are 0.27, 0.42, 0.43 and 0.43 mm respectively. The drying hour at which each type of hydrogel can achieve the maximum ablated width should be the timing that the largest heat diffusivity they can obtain, which are 1 hour for 0.5 mm thick hydrogel and 2 hour for the rest three thick hydrogels respectively. This difference can be understood that for a large aspect ratio of hydrogel (lateral dimension >> thickness) used in this work, its drying is mainly dominated by the evaporation of water through the upper surface; therefore, as the hydrogel becomes thinner, the distance for the water diffusing from the lower layer to the upper surface is decreased, thus increasing the evaporation rate and consequently accelerating the hydrogel drying. Finally, 0.5 mm thick hydrogel will lose almost the same amount of water as other three type of hydrogels and the detailed analysis of hydrogel drying kinetics is performed and explained later in the same section.

The relationship between the heat diffusivity and the ablated width is quantitatively demonstrated, and the effect of the laser optical configurations on the ablated width also can be gained by analyzing the experimental data, Figure 3.7. For example, for each type of hydrogel, in order to attain the maximum ablated width, more linear heat source is required. This observation is already discussed in the section 3.1 and confirmed by this experiment as the larger laser energy, the longer heat propagation. On the other hand, when the hydrogel thickness increased from 0.5 to 2 mm, the linear heat source required for achieving the maximum also increase (30 W s $m^{-1}$ for 0.5 mm, 75 W s $m^{-1}$ for 1 mm, 150 W s $m^{-1}$ for 1.5 mm and 300 W s $m^{-1}$ for 2 mm), which presented the proof of concept that the thicker hydrogel requires larger laser energy to conduct the heat to surrounding area for the complete thermal removal of hydrogels.

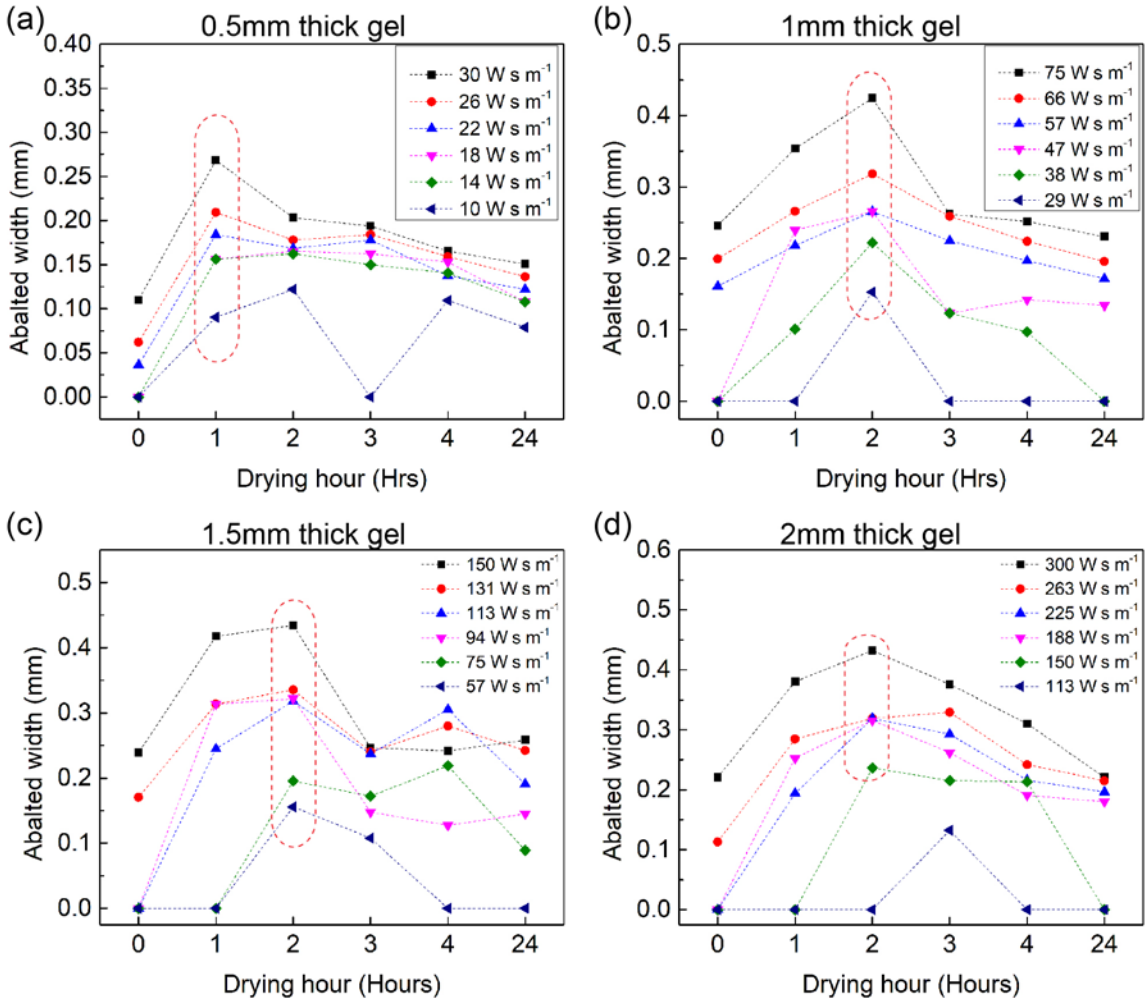


Figure 3.7 Experiment results of laser micro-machined hydrogels within one single laser beam scan for different thcikness of hydrogel (a) 0.5 mm thick hydrogel has the maximum ablated width of 0.27 mm after 1 hour drying at the linear heat source of 30 W s $m^{-1}$; (b) 1 mm thick hydrogel has the maximum ablated width of 0.42 mm after 2 hour drying at the linear heat source of 75 W s $m^{-1}$; (c) 1.5 mm thick hydrogel has the maximum ablated width of 0.43 mm after 2 hour drying at the linear heat source of 150 W s $m^{-1}$; (d) 2 mm thick hydrogel has the maximum ablated width of 0.43 mm after 2 hour drying at the linear heat source of 300 W s $m^{-1}$.

The above experiment presents the characterization of laser-micromachining under different hydrogel drying state and linear heat source, while one parameter that is missed over there and also is capable of tuning the ablated width is the laser beam radius. Therefore, this experiment is conducted by comparing the ablated width using two different laser beam diameter (0.13 vs 0.3 mm) immediately after the hydrogel curing (0 hour drying). Figure 3.8 shows the comparison that by increasing the laser beam diameter from 0.13 to 0.3 mm (2.3 times larger), the ablated width

has a maximum expansion of 1.75 times on 1.5 mm thick hydrogel (0.42 versus 0.24 mm) and a minimum one of 1.14 times on 2 mm thick hydrogel (0.25 versus 0.22 mm); the other two thick hydrogels (0.5 and 1 mm) has the ablated widths of 0.18 and 0.3 mm increased from 0.1 and 0.25 mm respectively. It should be noticed that compared to the 2.3 times increase of the laser radius, the increase of the ablated width can only reach 1.75 times, which is due to the decreased laser irradiation intensity by the increased beam radius demonstrated in the equation 3.1.

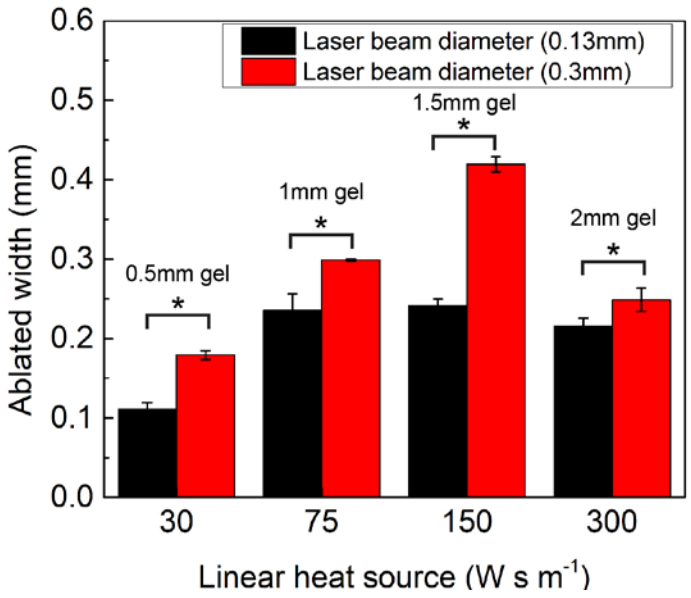


Figure 3.8 Experiment result of the ablated width by laser micro-machining with different laser beam radius that by using the 0.3 mm diameter laser beam, the ablated width has the ablated width of 0.18, 0.3, 0.42 and 0.25 mm increased from 0.1, 0.25, 0.24 and 0.22 mm on the hydrogel thickness of 0.5-2 mm respectively. One asterisk (*) indicates p value smaller than 0.05.

A simplified summary of Figure 3.7 is replotted in Figure 3.9 (a) showing the maximum ablated widths can be accomplished by different thick hydrogel under different linear heat sources and drying hours. Moreover, the experiment for the hydrogel drying kinetics is also conducted, whose result is shown in Figure 3.9 (b) that the decreased weight of hydrogels is an exponential function of the reciprocal of the time; and as the hydrogel gets thinner, the weight loss rate (by water evaporation) during the hydrogel drying increases, whose mechanism is already discussed and demonstrated in the section 3.1 as the water diffusion distance inside the hydrogel will be reduced following the shrunken thickness. Therefore, by coupling the drying kinetics to the laser ablation characterization, it is found that the optimal timing for laser-engineering the hydrogel is

at 1~2 hours drying where the hydrogel loses 35%~65% of water dependent on the initial thickness of the hydrogel.

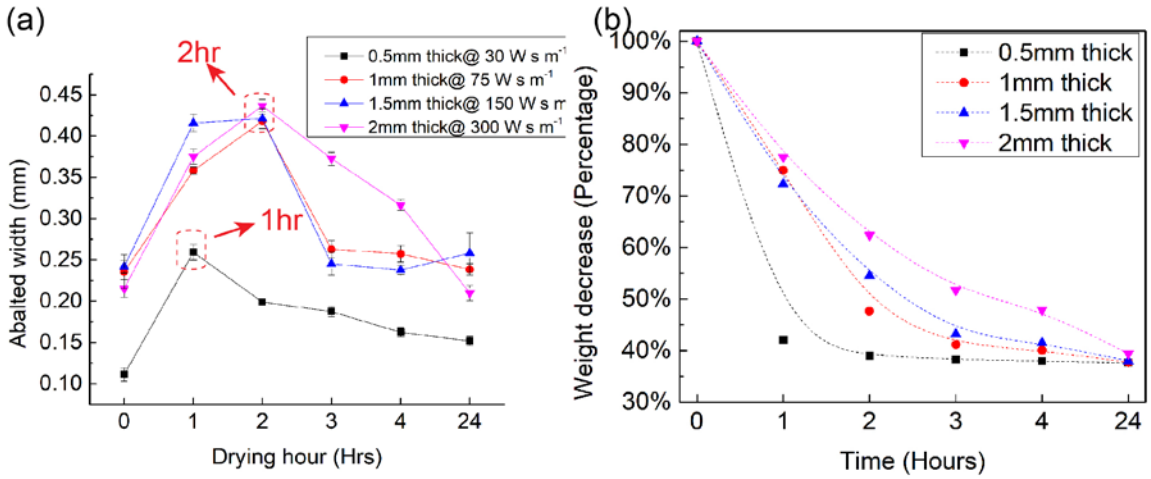


Figure 3.9 (a) The summary of the maximum ablated widths which can be achieved by different thick hydrogel under different linear heat sources and drying hours; (b) The drying kinetics of hydrogel at room temperature shows that the decreased weight is an exponential function of the reciprocal of the time, a complementary experiment for the laser-micromaching.

## 3.4 Sidewall quality analysis

Figure 3.10 shows the measured results of the sidewall quality (S.Q) that for 0.5 mm thick hydrogel, the maximum S.Q at the linear heat source from 14 to 26 W s $m^{-1}$ can reach ~0.45 mm/mm at 1~3 hours room temperature drying, which is around 1.5 times bigger than that of ~0.3 mm/mm at 24 hours drying (fully dried hydrogel); for other three thick hydrogels (1, 1.5 and 2 mm), the largest S.Q follow the same tend as that of 0.5 mm thick hydrogel, where the 1~3 hours drying are the best processing timing to achieve the largest laser-machined S.Q, which are between 0.45 to 0.5 mm/mm and hence 1.5~1.67 times bigger than that of ~0.3 mm/mm at 24 hours drying. Note that at several specific combination of linear heat source and the processing timing, a ~0.65 mm/mm high S.Q can be reached at both 1.5 and 2 mm thick hydrogels; otherwise, the general S.Q for all the other scenarios at 1~3 hours are mostly around 0.45 mm/mm no matter the thickness of the hydrogel and laser beam profile. This situation can be understood from the comparison of the $CO_2$ laser lens size to the hydrogel thickness that the $CO_2$ laser lens used in this work has the

spot size of 10.6 μm, much smaller than the thickness of 0.5 mm hydrogel, so by reducing the hydrogel thickness to a comparable value compared to 10.6 μm, a sharp edge (S.Q close to 1) is expected to be achieved.

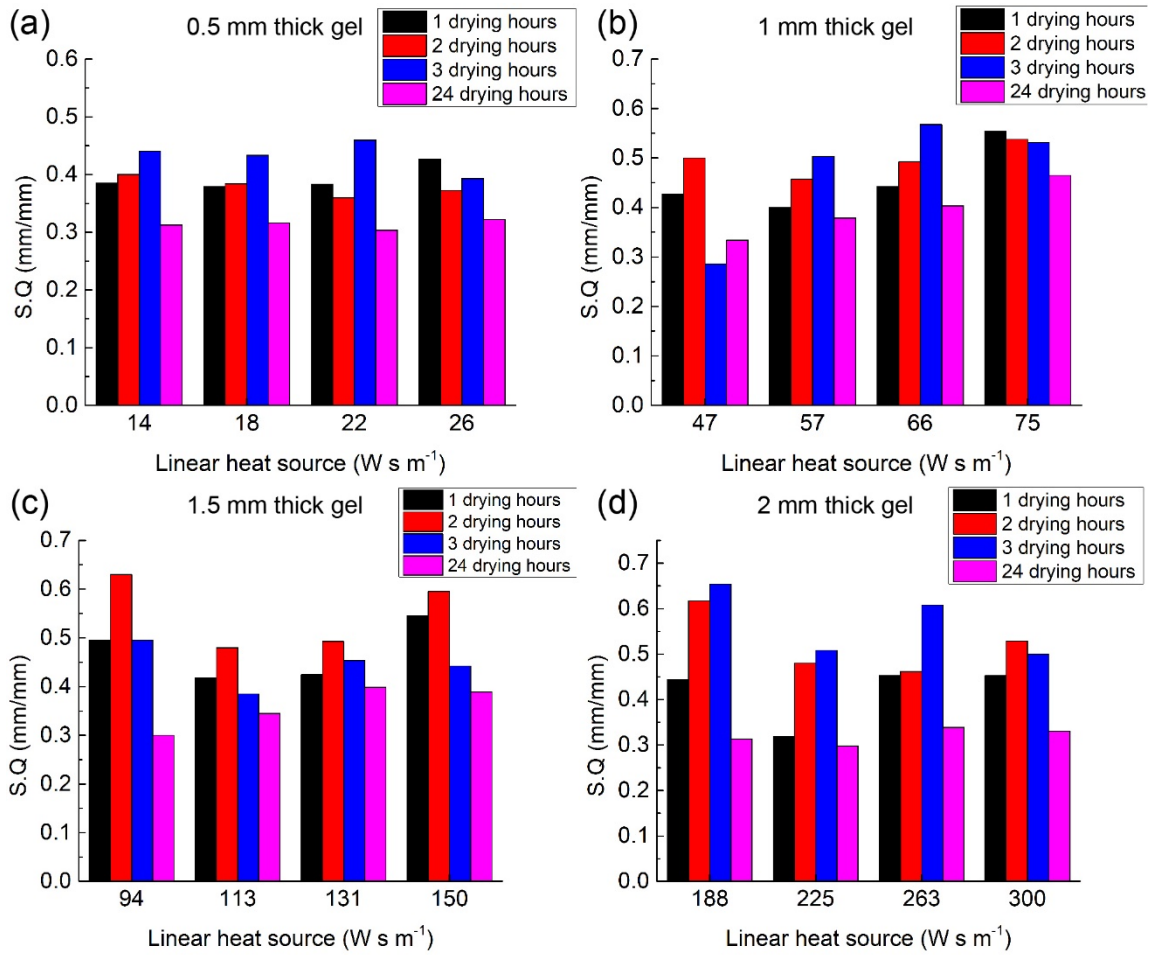


Figure 3.10 Analysis of the S.Q of laser micro-machined hydrogels for different thcikness of hydrogels that all the hydrogels have the largest S.Q occurring at 1~3 hours drying as 0.5~0.6 mm/mm, no statistics significant different among them and all bigger than that at 24 hours drying.

This S.Q identified an implied relationship between the ablated width and the fabricated pattern diameter. In this research, the maximum pH the two drug delivery devices deal with is around neutral value (pH 7) since that pH range is both the identification of the infected region on the chronic wound bed and the triggering signal of drug release from the smart capsule in the small intestine (especially in the jejunum); therefore, the swelling ratio of the hydrogel that actually matters is the one at pH 7, which is typically around 2 mm/mm (from to the swelling

characterization at Chapter 4). Moreover, for creating the enough internal space for the micro-fabricated gels to swell without collision, the ablated width should equal to the desired micro-machined pattern width assuming a straight edge (S.Q = 1). However, since the actual S.Q is less than 1, the top layer has a larger ablated width than that of the bottom layer, thus creating more swelling space on the top layer than the bottom layer of hydrogels, so the actual ablated width is allowed to be smaller than the micro-fabricated pattern width.

### 3.5 Resolution analysis

The resolution characterization is concentrated on the analysis of relationship between the ablated width and the linear heat source and the detection of the laser-processing timing to reach the maximum value (also involving its comparison to that at 24 hours), thus serving as the investigation and confirmation of why applying the laser-machining on the moisturized hydrogel instead of fully dried one. In this regard, two resolution curvatures are selected and compared in each thick hydrogel that one has the largest resolution and the other has that at 24 hours drying, which is expected to have the smallest resolution. Figure 3.11 presents the experiment results that for the 0.5, 1 and 2 mm thick hydrogels, all of their maximum resolutions appear at 1 hour drying, which are 0.0074, 0.0058 and 0.0012 mm/(W s m-1) and are 2.22, 1.59 and 4 times of 0.0033, 0.0036 and 0.0003 mm/(W s m-1) at 24 hours drying respectively; while for 1.5 mm thick hydrogel, the maximum resolutions are 0.0027 mm/(W s m-1) at 2 hours drying, which are 1.2 times of 0.0023 mm/(W s m-1) at 24 hours drying.

As known from the characterization of the ablated width, the evaporated water volume from hydrogel network during the hydrogel drying will first increase and then decrease the heat diffusivity of the hydrogel. It would reach the maximum after 1~2 hours drying dependent on the thickness of the hydrogel due to different drying kinetics, where the maximum ablated widths are reached. The same principle/mechanism also can be applied to explain the maximum resolution also occurring at 1~2 hours drying and the compromised one at 24 hours drying.

Compared to other three types of hydrogels (1, 1.5 and 2 mm thick), the 0.5 mm hydrogel has the largest resolution of 0.0074 mm/(W s $m^{-1}$), which is contributed to the absolute water amount (thus the thickness as they all share the same surface area) that as the hydrogel becomes thinner (less water contained), the same thermal energy induced by the laser should propagate farther distance radially, thus forming larger width or wider Gaussian distribution. Therefore, thinner

hydrogel requires less laser power to produce the same ablated pattern and the concomitant bigger resolution. Note that the same explanation can also go for interpreting the comparison of sidewall quality among the four types of hydrogels, where the S.Q of 0.5 mm hydrogel is slightly smaller than those of other hydrogels, which is because of the thinner hydrogel, the larger propagation of laser induced heat.

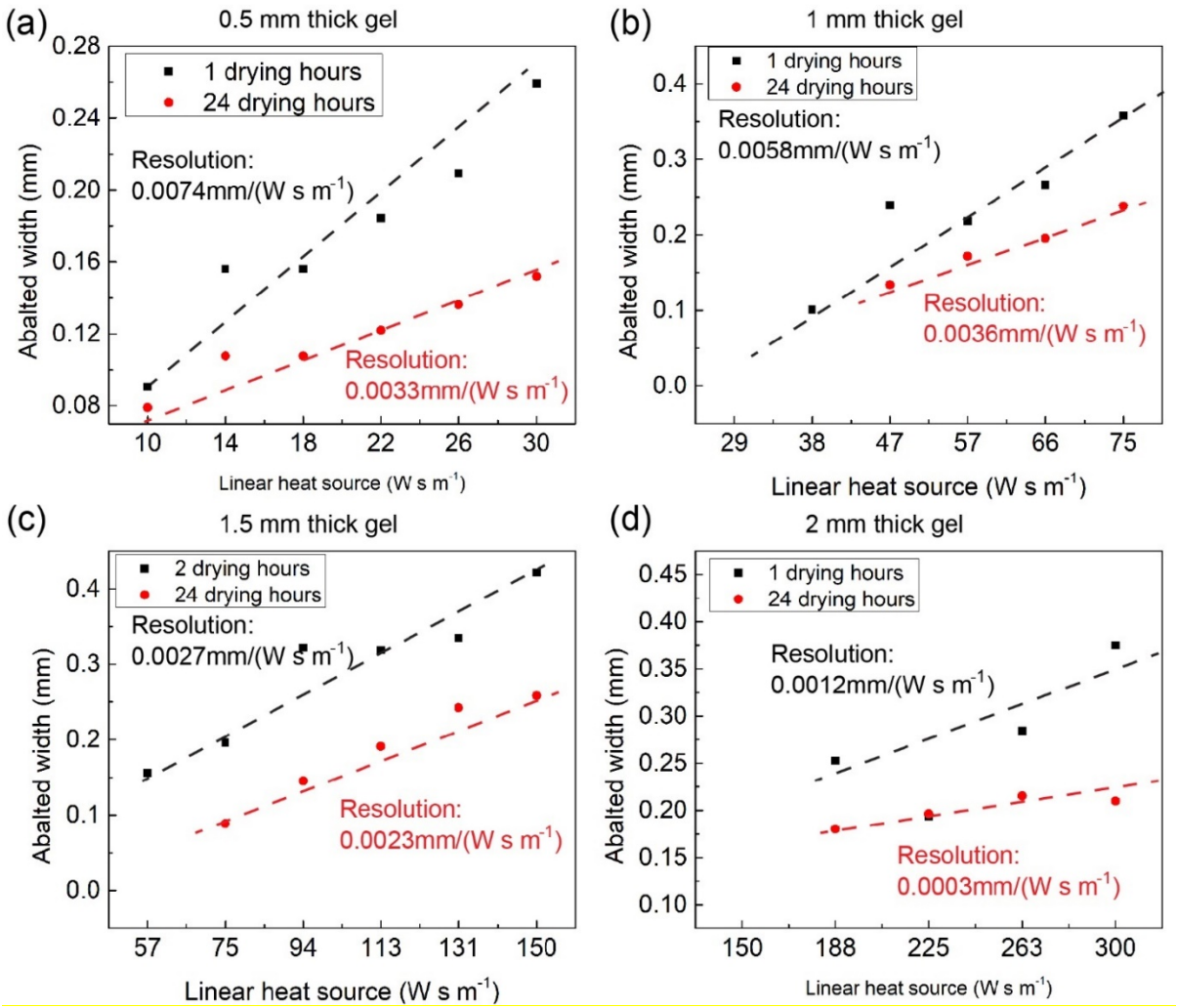


Figure 3.12 Resolution analysis of laser micro-machined hydrogels within one single laser beam scan (a) 0.5 mm thick hydrogel has the maximum resolution of 0.0074 mm/(W s $m^{-1}$) at 1 hour drying, 2.24 times of 0.0033 mm/(W s $m^{-1}$) at 24 hours drying; (b) 1 mm thick hydrogel has the maximum resolution of 0.0058 mm/(W s $m^{-1}$) at 1 hour drying, 1.6 times of 0.0036 mm/(W s $m^{-1}$) at 24 hours drying; (c) 1.5 mm thick hydrogel has the maximum resolution of 0.0027 mm/(W s $m^{-1}$) at 2 hour drying, 1.2 times of 0.0023 mm/(W s $m^{-1}$) at 24 hours drying; (d) 2 mm thick hydrogel has the maximum resolution of 0.0012 mm at 1 hour drying, 4 times of 0.0003 mm/(W s $m^{-1}$) at 24 hours drying.

### 3.6 Laser-machining of composite gels

As mentioned at the beginning of this research, one of the key advantages and also one of the motivations of the laser-machining on hydrogels are the processability to etch and pattern the composite gel by using the same fabrication procedure applied on the bare hydrogel (0% embedded micro or nano particles), since the composite gels play a significant role of equipping the bare hydrogel with additional or enhanced functionalities by incorporating various micro/nano functional particles into the polymer network. Aiming at demonstrating this capability, two types of 1 mm thick composite gels are fabricated that one is the 2 w/v% ~0.3 mm diameter MNP-PS (magnetic nano particle polystyrene sphere) mixed hydrogel ("ferrogel") and the other is the 0.1 w/v% 9~13 μm diameter silica beads loaded hydrogel ("silicagel"). The same laser-machining protocol is applied to the laser-machining of the two composite gels and all the features including ablated width, S.Q and resolution are analyzed.

The experiment results of the ferrogel were shown in Figure 3.12 that the ferrogel had the optimal combination of all the investigated features occurring at 2 hours drying, where both the maximum ablated width and S.Q reached 0.42 mm and 0.51 mm/mm at the linear heat source of 75 W s $m^{-1}$ respectively with the linear resolution of 0.006 mm/(W s $m^{-1}$).

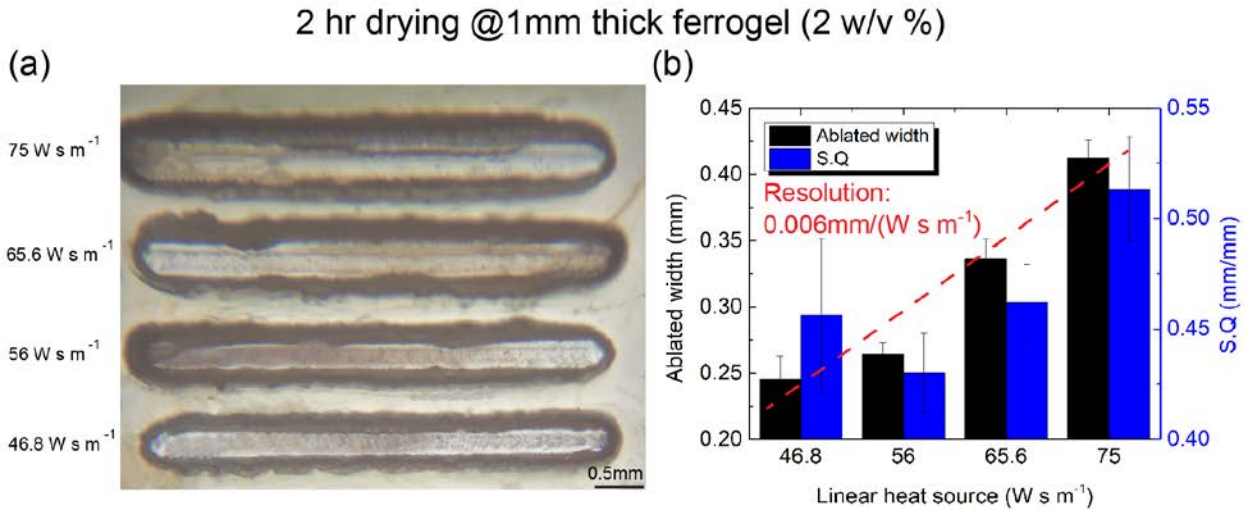


Figure 3.13 (a) Photograph of laser micro-machined 1 mm thick ferrogel after 2 hours drying at a range of linear heat source from 46.8 to 75 W s $m^{-1}$; (b) The experiment results showed a resolution of 0.006 mm/(W s $m^{-1}$) and both the maximum of ablated width of 0.42 mm and S.Q of 0.51 mm/mm.

The experiment results of the silicagel were shown in Figure 3.13 that the silicagel had the optimal combination of all the investigated features occurring at 1 hours drying, where both the maximum ablated width and S.Q reached 0.285 mm and 0.495 mm/mm at the linear heat source of 150 W s $m^{-1}$ respectively with the linear resolution of 0.002 mm/(W s $m^{-1}$).

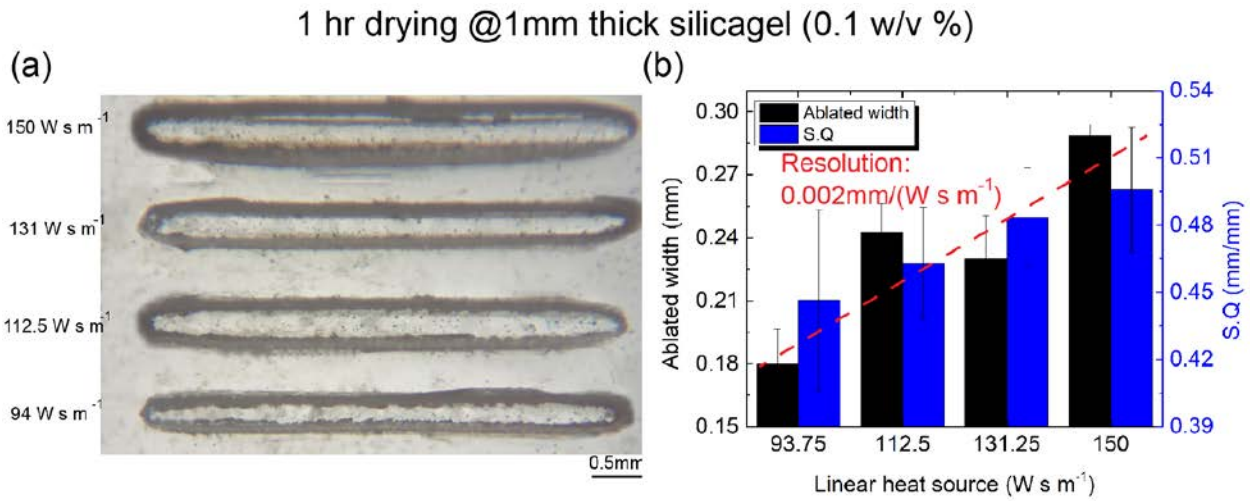


Figure 3.14 (a) Photograph of laser micro-machined 1 mm thick silicagel after 1 hours drying at a range of linear heat source from 94 to 150 W s $m^{-1}$; (b) The experiment results showed a resolution of 0.002 mm/(W s $m^{-1}$) and both the maximum of ablated width of 0.285 mm and S.Q of 0.495 mm/mm.

Compared to the ferrogel, the silicagel has its maximum laser-machining features smaller than those of ferrogel, which also appear at different processing timing and require more laser power. One of the reasons would be the different size of embedded particles (~9 µm silica beads and 0.3 µm MNP-PS) in the two hydrogels that although the silicagel has a smaller volume fraction (0.1 w/v% silica beads) of embedded particles compared to the ferrogel (2 w/v% MNP-PS), the total space the silica beads occupied is larger than that of the MNP-PS with the detailed calculation as follows:

- The volume ratio of silica beads to MNP-PS is about $(9/0.3)^3 = 27000$;
- The volume fraction ratio of silica beads to the MNP-PS is 0.1/2 = 0.05;
- So, the total occupied space ratio of silica beads to the MNP-PS is 27000 * 0.05 =1350 assuming the silicagel and ferrogel share the same dimension.

Therefore, as the silicagels contain less water than the ferrogels, the processing timing to achieve

the optimal feature on the silicagels is thus 1 hours ahead of that of the ferrogels (2 hours drying), where both gels have the similar water volume fraction and thus approximate thermal & optical properties, which then require a longer time for ferrogels to lose more contained water. Besides, since the silicagels incorporate more particles in their network, more thermal energy could be reflected or scattered by the embedded silica beads, which then compromise the heat propagation, thus reducing both the ablated width (32% smaller than that of ferrogel) and resolution (67% smaller than that of ferrogel) while requiring more laser power (100% additional power required to achieve the 67% ablated width of the ferrogel) at the same time. Notice that both the laser micro-machined features of the two gels are comparable or close to that of the bare hydrogel (0 w/v% silica beads or MNP-PS), which verified and confirmed one of the claims in this research that the laser micro-machining methodology can be transferred to the composite gels smoothly, thus capable of integrating a wide range hydrogels into variant environmental responsive systems.

## 3.7 Conclusion

At this chapter, the principle and mechanism of the laser-machining on hydrogels are first presented. It points out that two set of parameters regulate the quality of laser micro-machining on hydrogels. One is the laser beam profile, including the laser beam radius and the linear heat source defined as the product of laser power and the reciprocal of the laser beam scan rate; and either the increase of laser beam radius or the increase of linear heat source can expand the thermal ablation. The other are the dynamic thermal and optical properties of the hydrogel when drying the hydrogel at room temperature till a fully dried state. Therefore, by tuning the laser beam configuration and selecting an appropriate processing window, it is able to fabricate the hydrogel to the desired micro-patterns and concomitant satisfy the sensing or actuating requirements of the incorporated system for variable biomedical applications. Next, the experiment protocol is introduced that four different thick hydrogels (0.5, 1, 1.5 and 2 mm) are laser-machined at different drying state (0-24 hours drying at room temperature) under a wide range of linear heat source (10-300 W s $m^{-1}$) and within a single laser beam scan (5 mm ablation length); and the detailed characterizations include the comprehensive analysis of ablated width, sidewall quality and resolution, Figure 3.14.

Later, the ablated width, sidewall quality and resolution of laser-machining on the hydrogel are measured and analyzed in series that the optimal processing timing to get the best qualities (referring to the maximum features) of laser-machining on the hydrogels is detected to be mainly

focused on 1~2 hours drying (the hydrogel loses 35%~65% weight), Table 3.2. The overall maximum values of the characterized features include 0.43 mm ablated width on 2 mm hydrogel at 2 hours drying, 0.65 mm/mm sidewall quality on 1.5 mm hydrogel at 1 hour drying, and 0.0074 mm/(W s $m^{-1}$) resolution on 0.5 mm hydrogel at 1 hour drying. Besides, two composite gels, ferrogel and silicagel, are also fabricated and laser-machined under the same procedures and conditions that the results show the similar qualities as those of the bare hydrogels, thus verifying the capability of laser micro-machining on the micro/nano particles embedded hydrogels.

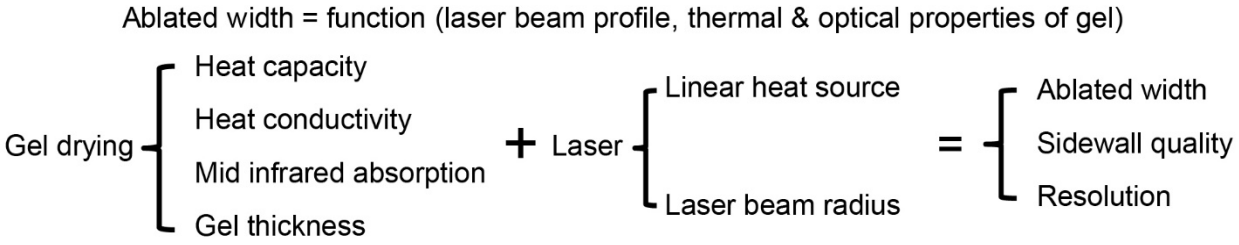


Figure 3.15 The summary of the quality of laser-machining of the hydrogel as the function of laser beam profile and the thermal & optical properties of hydrogel.

Table 3.2. The summary of the processing windows of all the optimal features (ablated width, S.Q and resolution) for the four different thick hydrogels.

| **Drying hours versus laser-machining features** | | | | |
|---|---|---|---|---|
| Optimal features | 0.5mm hydrogel | 1mm hydrogel | 1.5mm hydrogel | 2mm hydrogel |
| Ablated width | 1 hour | 2 hours | 2 hours | 2 hours |
| Sidewall quality | 1~3 hour | 1~3 hour | 2 hours | 2~3 hours |
| Resolution | 1 hour | 1 hour | 2 hours | 1 hour |

Finally, the proof of the concept is demonstrated that the laser micro-machining technique can be applied to the hydrogel to create a scalable pattern under a rapid and cost-effective fabrication manner. The photographs of a set of laser micro-machined hydrogels with a variety of patterns are illustrated in Figure 3.15.

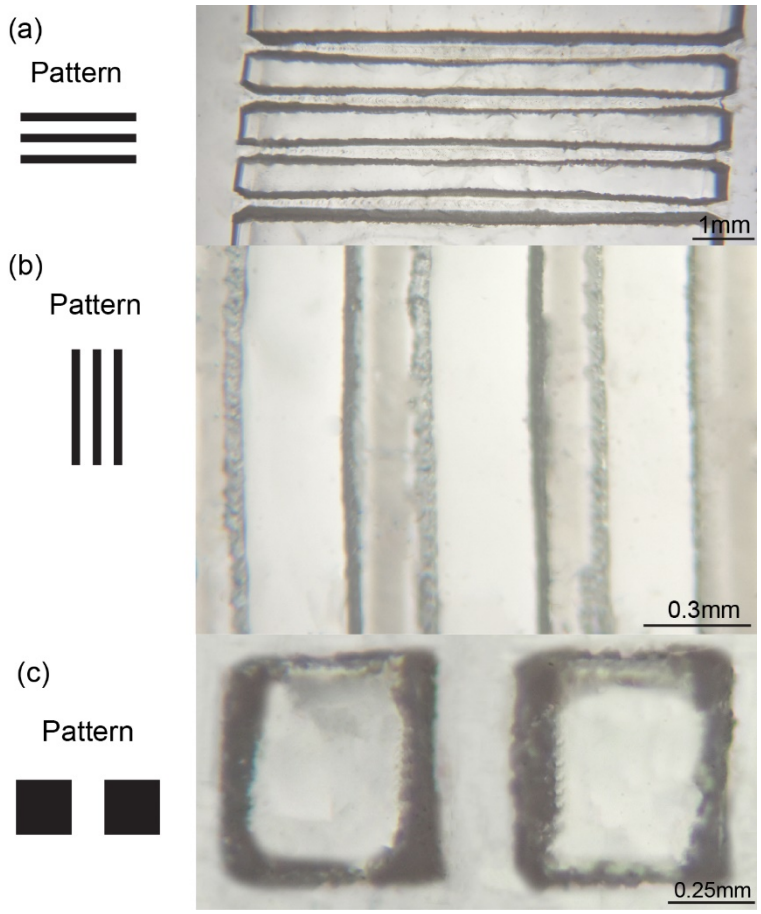


Figure 3.16 The photographs of micro-patterned hydrogels.

# 4. SWELLING KINETICS OF LASER-MACHINED HYDROGELS

## 4.1 Principle and mechanism of pH-sensitive hydrogel swelling

The swelling principle of the pH-sensitive hydrogel is simply described in chapter 2 that as a type of anionic hydrogels, poly (mAA-co-AAm) hydrogel swells due to the enhanced electrostatic repulsion force within the gel network induced by the increasing density of ionized carboxyl groups (-COOH to -$COO^-$) when the pH value of the medium increases over the pKa of –COOH. A more comprehensive discussion of the swelling kinetic model and the correlated experimental demonstration of the pH-sensitive hydrogels are presented in the chapter.

pH sensitive hydrogel is a type of ionic gel or polyelectrolyte gel as its pedant group in the polymer chains can be protonated or deprotonated when the surround pH lower or higher than its pKa, which then creates an increased/decreased ion concentration in the network. The ionization inside gel then gives rise to an osmotic pressure resulting from the Donnan equilibrium inside and outside the gel, which can be described in terms of the ion osmotic swelling pressure $\pi_{ion}$ and finally causes the gel to swell [70]. Besides, the pH-sensitive hydrogel swelling/shrinking in a solution is also regulated by two other contributions, $\pi_{mix}$ and $\pi_{el}$ . The former is the mixing swelling pressure attributed to the thermodynamic force when mixing the gel with the solution, favoring swelling of hydrogel by promoting the movement of the hydrophilic polymer chains; the latter is the elastic pressure induced by the crosslinked hydrogel network which provides a retractive/repulsive force which inhibits the deformation of polymer chains from their most probable configuration. Therefore, the osmatic swelling pressure $\pi_{swelling}$ can be wrote as the sum of the three independent contributions as follows [22], [23], [71]–[75]:

$$\pi_{swelling} = \pi_{ion} + \pi_{mix} + \pi_{el} \qquad (4.1)$$

At the other hand, for ionic hydrogel or polyelectrolyte gel, the mixing swelling contribution, described on the Flory-Huggins model [76], is usually much smaller than the ionic swelling pressure and thus is negligible in the swelling kinetics of the pH-sensitive hydrogel. Therefore, the kinetic swelling behavior of the pH-sensitive hydrogel is a dynamic counteraction between the ion swelling pressure and the elastic pressure as when the hydrogel is swelling, the ion osmotic pressure acts as an expansion force while the elastic term works as the opposite force; and finally the swelling equilibrium of the hydrogel occurs when the inward elastic restoring force of the gel

network balances the outward ionic osmotic force (thus the total osmotic swelling pressure equals to zero) as follows:

$$\pi_{swelling} = \pi_{ion} + \pi_{el} = 0 \qquad (4.2)$$

The ionic osmotic pressure $\pi_{ion}$, attributed to the difference of the mobile ion between the gel network and the external solution can be calculated based on the following equation [77]:

$$\pi_{ion} = RT[\Phi \sum_i \overline{C_i} - \varphi \sum_i C_i] \qquad (4.3)$$

where $\overline{C_i}$ and $C_i$ are the concentrations of mobile ions in the gel and in the external solution, $\Phi$ and $\varphi$ are the corresponding osmotic coefficients respectively, R is the gas constant and T is the absolute temperature. This equation shows that the ionic contribution to the osmotic swelling pressure of the ionic hydrogel is linearly proportional to the total concentration of the charged groups attached to the gel network, which is then independent to the crosslink degree of the gel. Note that the temperature also plays an essential role in swelling phenomena of the ionic hydrogel as its increase/decrease would add a positive/negative effect on the osmotic pressure. In most case, the ion concentration in the gel is much larger than that in the external solution, thus the equation 4.2 can be rewritten to as follows [71], [75], [77]:

$$\pi_{ion} = RT[\Phi \sum_i I\overline{C_i}] \qquad (4.4)$$

$$I = \frac{k_a}{10^{-pH} + k_a} \qquad (4.5)$$

where I is the ionization and $k_a$ is the acid dissociation constant. From the above equations, it is evidence that as the pH value of the external solution increases, the ionization in the gel will increase, concomitantly increasing the ionic swelling pressure.

The elastic contribution to the osmotic swelling pressure $\pi_{el}$, resulting from the configurational entropy changing of polymer chains caused by the gel deformation, can be expressed [71], [75], [76]:

$$\pi_{el} = nRT[\left(\frac{1}{w}\right)^{\frac{1}{3}} - \frac{1}{2w}] \qquad (4.6)$$

where n is the crosslink density of the gel network and w is the swelling ratio. This equation proposes that the elastic restoring force is linearly proportional to the crosslink density of the network and inversely proportional to the swelling ratio; therefore, assuming the ionic swelling pressure does not change, when the crosslink density of the gel increases, the swelling ratio would be decreased to maintain the $\pi_{el}$ unchanged; and so is the converse (the decrease of crosslink density of the gel would increase the swelling ratio).

Actually, based on the above mentioned equations, especially from the equation 4.4 and 4.6, we are able to know that the swelling ratio is a counterbalance between the crosslink density and the mobile ion concentration; therefore there would be a threshold upon/below which either the crosslink density or the mobile ion concentration in the gel network will dominate the swelling of the hydrogel. This deduction is very important to understand the swelling kinetics of the hydrogel (especially the composite gel) in a complicated situation where several chemical or physical parameters co-exist, and this multiple parameter co-regulated swelling kinetics of the pH-sensitive hydrogel will be demonstrated in the next section.

## 4.2 Characterization of the hydrogel swelling kinetics

When a hydrogel is brought into contact with solution, the solvent (mainly water in this context) move into the gel network based on the increased osmotic swelling pressure inside the gel as explained in the section 4.1. Meanwhile, the water uptake during hydrogel swelling is also a diffusion-limited process regulated by the diffusion equation [78]. The diffusion regulated swelling process can be understood from the mechanism of the semipermeable membrane that the hydrogel network serves as the semipermeable membrane to immobilize the ionized carboxylic group inside the network, and then the solvent (water) becomes to the solute that diffuse into or out from the gel network due to the unbalanced osmotic pressure. The one-dimensional solution of the diffusion equation proposes that the characteristic time $\tau$ of the swelling transition is directly proportional to the square of the linear size $t$ of the gel and inversely proportional to the diffusion coefficient of the network (D) as follows:

$$\tau = t^2/D \qquad (4.7)$$

From this equation, it is evidence that as the gel size increases, the time required for the gel reaching an equilibrium swelling will be doubled; therefore, in order to achieve a fast environmental responsive sensing, hydrogels need to be micro-machined to a designed small size. This size-dependent swelling behavior of the hydrogel is especially important to the two applications in this research (the smart capsule and the chronic wound dressing, both pH-regulated), where the swelling of the micro-machined hydrogel is accomplished by imbibing the water only through a porous gel promoting adhesion substrate and the one dimensional size t of the gel is interpreted to the gel thickness in the three dimensional scenario.

The pH-responsive poly (mAA-co-AAm) hydrogel is prepared by mixing two pregel solutions [21]. Solution A is made by mixing 100 µL of methacrylic acid (mAA), 335 mg of acrylamide (AAm), 100 µL of tetra-methyl-ethylene-diamine (TEMED), and 3.27 mg of methylene-bis-acrylamide in 1.2 ml of DI water. Solution B is prepared by dissolving ammonium persulfate (APS) in DI water (80 mg/ml) added to the sonicated solution A in a volume ratio of 5.9:1 to form the hydrogel [79], [80]. Two type of composite gels are also fabricated and characterized in this work to demonstrate the processability of the laser-machining on hydrogels. One is the so called "ferrogel", which is made by mixing 10% and 2% w/v MNP–PS (magnetic nanoparticles in polystyrene beads, ~0.3 mm diameter) into the pregel solution A; the other is named as "silicagel", which is created by mixing 0.5% and 0.1% w/v silica micro-beads (9-13 µm diameter) into the pregel solution A. Before blending with the solution B for the polymerization, the mixtures (the pregel solution A and the magnetic or silica beads) were sonicated and vortex-mixed around one hour to reach a uniform dispersion. Finally, the mixed solution A and B are allowed for the complete polymerization around one hour.

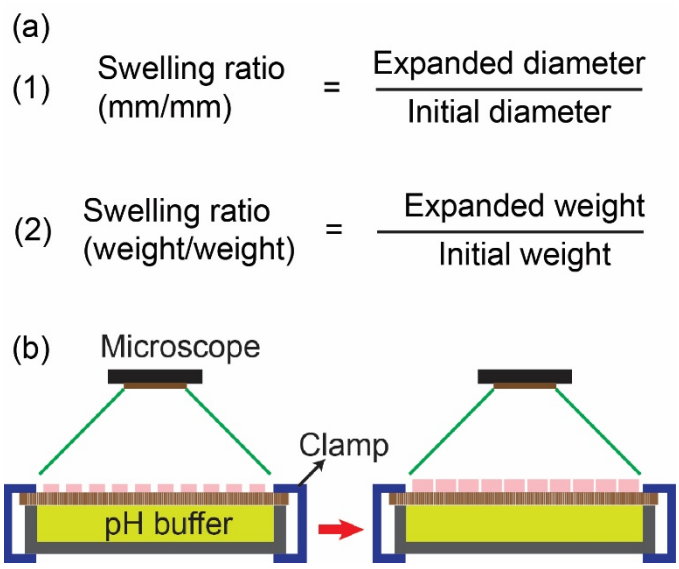


Figure 4.1 (a) Definition of the swelling ratio of the laser micro-machined hydrogels in a pH buffer; (b) The visual measurement for the hydrogel swelling ratio (mm/mm).

After the fabrication, the hydrogel is laser micro-machined to the designed patterns for later swelling or actuation characterization. According to different application scenarios, the swelling ratio is defined and measured by two methods that one is the value of the expanded diameter of

the gel at certain time during swelling over the initial diameter upon one hour curing (synthesis) through the microscopic images of the top view of the micro-gels, which is mainly used in the characterization involving both the swelling rate and swelling ratio; the other is the ratio between the weight of the gel at swelling and the initial weight, which is only utilized in the applications where the swelling ratio at equilibrium is the solo focus, Figure 4.1. All the experiment are conducted in triplicates and in room temperature (21$^{o}$C) except for the characterization of the temperature-regulated hydrogel swelling, which is exerted in three different temperatures.

### 4.2.1 Size dependent swelling behavior of hydrogel

As discussed previously, the swelling kinetics of hydrogels, thus their integrated environmental responsive sensors, are strongly dominated by the dimension, so the micro-machining is applied on hydrogels to reach a fast response time. On the other hand, within the two drug delivery applications of this research, the hydrogel is first bonded to a porous substrate and then utilized to provide the mechanical force/actuation so as to accomplish the drug release process. Therefore, the hydrogel is only exposed to the surround medium through the attached micro-pores, at which its thickness dominates the swelling kinetic behavior. To test this hypothesis, two different thick hydrogel films are cured to 0.4 and 2 mm and laser-ablated to different diameters, 0.36, 0.5 and 4 mm. Then the fabricated micro-gels are allowed to swell through the porous substrate on top of a constant pH solution, Figure 4.1 (b).

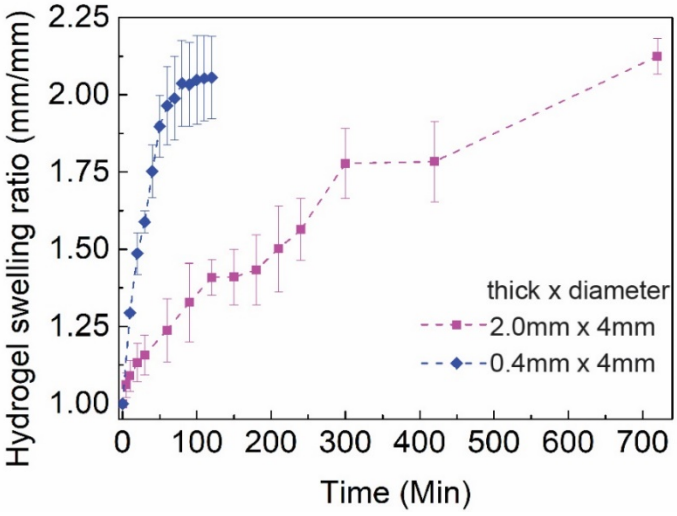


Figure 4.2 Comparison of swelling behavior between 2 mm thick and 400 um thick hydrogels in pH 7 buffer. n =3.

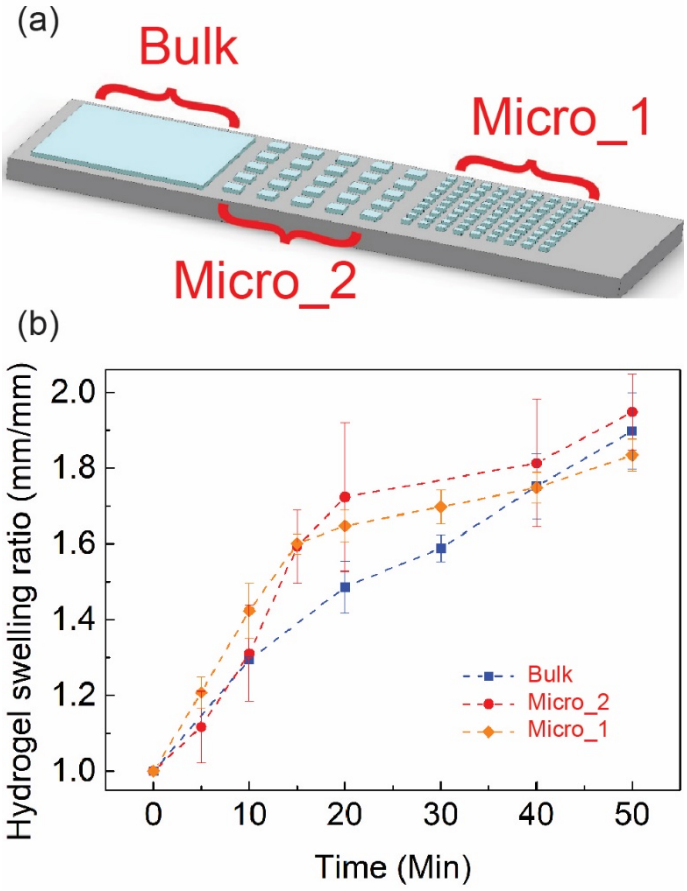


Figure 4.3 Comparison of hydrogels swelling on porous membrane for three different diameters, 4mm, 0.5mm and 0.36 mm; all have the same thickness of 0.4 mm. n = 3.

Figure 4.2 shows a comparison of swelling behavior between 2 mm thick and 0.4 mm thick hydrogels (both 4 mm diameters) in pH 7 buffer, where 0.4 mm thick hydrogels show a faster swelling rate. The 2 mm thick hydrogels need 700 minutes to reach almost the same swollen ratio (x2.1) instead of 120 minutes by the 0.4 mm thick hydrogels. Since the two types of hydrogels share the same diameter but different thickness, the different swelling kinetics (especially the swelling rate) can be attributed to the different thickness. Figure 4.3 illustrates the comparison of hydrogel swelling with different diameters (4mm, 0.5mm and 0.36mm) but same thicknesses (0.4 mm thick) that both 0.5 mm and 0.36 mm diameter hydrogels have a similar swelling ratio as x0.85/min in first 20 minutes faster than 4 mm diameter hydrogels (x0.74/min). While the final swollen ratios for three patterns are close and all arrive at their maximum within one hour, it then confirms the assumption that when hydrogels are confined in a chamber and allowed to contact the ambient environment only through a porous substrate, the thickness of the hydrogel dominates

the swelling behavior of hydrogels with high aspect ratio (thickness/lateral dimension >> 1), as both the ion exchange and water diffusion channels between hydrogels and surrounding are confined in the vertical direction instead of the lateral directions. These data provide the experimental profile of the transient performance of different micro-patterned hydrogel, whose swelling rate can be tuned by the laser micro-machining and thus can be applied to the time-sensitive bio-applications.

### 4.2.2 Other physical/chemical parameter regulated Swelling behavior of hydrogel

In this research, the pH-sensitive hydrogel is chose to be the poly (mAA-co-AAm) hydrogel, which swell/deswells as the pH value increase/decreases; the mechanism is already well explained in section 4.1 that the increased pH value of the solution will promote the ionization of the carboxylic group in the gel network and consequently raise the ionic swelling pressure, thus causing the hydrogel swell, equation 4.5. The demonstration of the pH-regulated swelling behavior is performed by using a similar setup as the size-dependent swelling kinetic characterization and the only difference is that the pH dependent swelling experiment would monitor the hydrogel swelling in three different pH buffer (2.2, 4 and 7) instead a single one for 120 minutes. The experimental results are presented in the Figure 4.4. In pH 4 buffer, the hydrogel had a faster swelling rate as x0.048/min during the first 30 minutes than in the remaining 90 minutes, reaching a maximum of x1.56 after 30 min. In pH 7 buffer (small intestine), the hydrogel had a slightly larger initial swelling rate of x0.053/min reaching a maximal swelling ratio of x2.0 after 90 min. In the highly acidic (stomach) solution (pH of 2.2), as expected, both the initial swelling rate and final swelling ratio were smaller (x0.043/min and x1.33, respectively). Into the two drug delivery applications, the significant swelling capabilities of pH-sensitive hydrogel in the neutral/alkaline environment is thus able to deflect the elastomeric PDMS membrane and initiate the triggering of drug release based on the actuation of the flexible membrane. Portions of this text are taken from publications by the author [80].

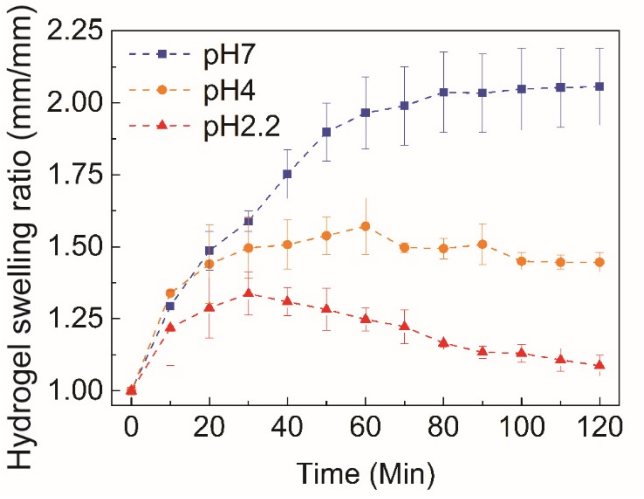


Figure 4.4 Comparison of hydrogels swelling through porous membrane in three different pH buffer, 2.2, 4 and 7.

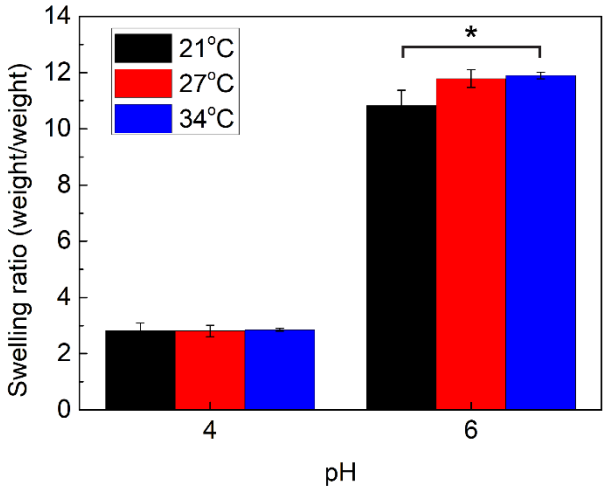


Figure 4.5 The temperature characterization on the hydrogel swelling in pH 4 and 6 shows that higher temperature is significantly pronounced at higher pH value. One asterisk represents $p < 0.05$.

Except the pH level, the temperature also affects the swelling behavior of the hydrogel in a positive way as the higher temperature will produce the larger ionic swelling pressure, equation 4.4; besides, the temperature is a common parameter the hydrogel would encounter in many bio-applications, whose influence should be carefully considered. Therefore, it is necessary to analyze the quantitative effect of the temperature to the hydrogel swelling at different pH level, thus revealing a co-regulation by both the pH and temperature. The experiment is conducted by

measuring the swelling ratio of the hydrogel (expanded weight by initial weight defined previously) in different pH solution (4 and 6) and at different temperatures (21$^{o}$C, 27$^{o}$C and 34$^{o}$C) respectively. Figure 4.5 shows the experiment results that at pH 4, the pH-sensitive hydrogel has a similar swelling ratio of x2.8 at all the three temperatures; while at pH 6, the swelling ratio at 34$^{o}$C is x11.9, 1.1 times larger than x10.8 at 21$^{o}$C ($p < 0.05$). This comparison exhibits that the temperature response is significantly pronounced on the hydrogel swelling at higher pH 6; in other words, at a lower pH level, the temperature effects on the hydrogel swelling is counteracted by the decreased ionization level in the gel (the protonation of ionized carboxylic group as $–COO^{-} + H^{+}$ = -COOH). This feature is essentially important to the chronic wound dressing as it can be used to autonomously tune the drug delivery rate based on a combination of wound pH and temperature, especially at high pH level when the wound is not in a healing status.

As described previously, composite gels have been the research focus for several decades and their fabrications are developed by incorporating various micro/nano scale materials into the polymer network, which offer the hydrogel with extra or enhanced functionalities. There are two types of composite gels involving this work to demonstrate the processability of laser micro-machining on hydrogels. One is the ferrogel which is produced by mixing the ~0.3 mm diameter MNP-PS into the gel network and can be utilized to couple its volumetric deformation into any magnetic change induced wireless sensing system [53]. The other is the silicagel, which is fabricated by mixing the 9~13 μm diameter silica beads into the gel network and can be applied to respond its swelling/shrinking to the scattered ultrasonic wave intensity thus for achieving a longer distance wireless sensing, compared to the magnetic wireless sensor system, [13]. The experiments are set to compare the equilibrium swelling ratio of the hydrogel (0 w/v% of magnetic beads or silica beads) to that of the ferrogel (10 w/v% and 2 w/v%) or the silicagel (0.5 w/v% and 0.1 w/v%) in different pH (4, 5, and 6) respectively.

The results show an inverse relationship between the swelling ratio of the ferrogel and the concentration of the embedded magnetic particles at all selected pH level that as the concentration of magnetic particles is reduced from 10 w/v% to 0 w/v%, the swelling ratio increases from 2.5 to 3.6 at pH 4, from 7.9 to 8.6 at pH 5, and from 10.5 to 13.1 at pH 6, Figure 4.6 (a). This diminished swelling ratio of the ferrogel can be explained by the enhanced crosslink density as the added magnetic beads bring extra crosslinking into the gel network through hydrogen bonding or physical absorption [81]. Although the compromised swelling capabilities, the ferrogel has its swelling

kinetics well maintained. Firstly, the response of the ferrogel to the pH variation is similar to that of a bare hydrogel; expanding at the elevated pH levels and shrinking at low pH levels. On the other hand, the sensitivities (the slope of the swelling ratio versus pH value) are approximately the same for the three types of ferrogels; x4/pH for 10 w/v%, x4.1/pH for 2 w/v%, and x4.7/pH for 0 w/v%, Figure 4.6 (b). Therefore, the ferrogel, whose swelling/shrinking is maintained, can work as a magnetic core to regulate the inductance and thus the resonance frequency of its incorporated wireless sensing system once in the chemical stimuli (pH in this context) present medium.

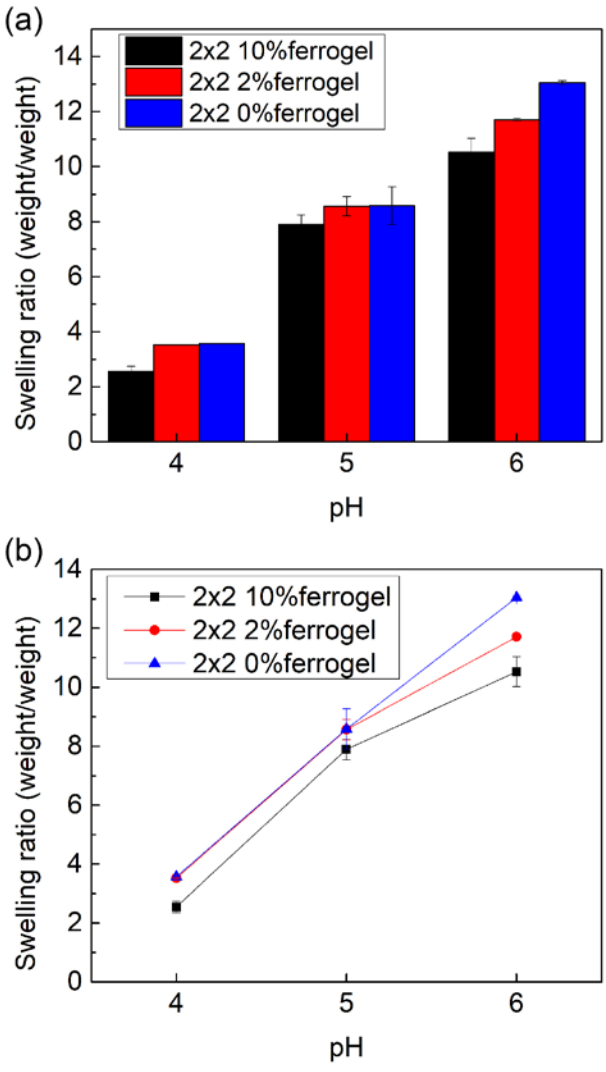


Figure 4.6 Swelling behavior of ferrogel in different pH buffer showing that the swelling behavior of the ferrogel is decreased by the increased crosslinking density.

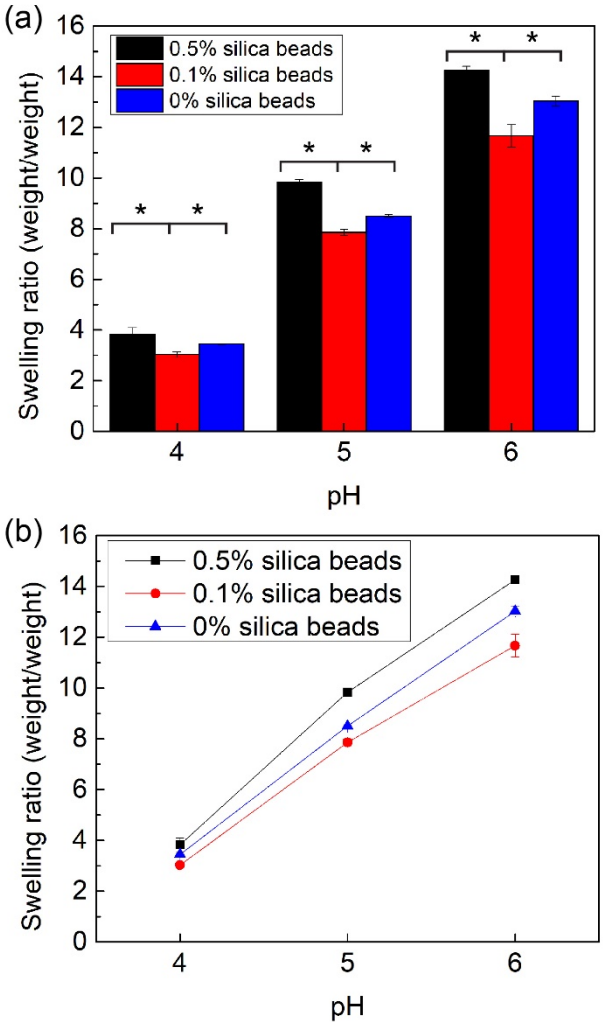


Figure 4.7 Swelling behavior of silicagel in different pH buffer shows that the swelling properties of the silicagel is the counteracted result between the crosslinking density and negative charges (from the beads); above a threshold of between 0.1% and 0.5% w/v mixed silica beads, the gel swelling become proportional to the beads concentration inside the gel. One asterisk represents $p < 0.05$.

The ferrogel shows a one-direction relationship between the particle concentration and the swelling ratio; the more embedded particles, the less swelling ratio, which however is not the case of the silicagel. Figure 4.7 shows the experimental result of the silicagels swelling in different pH solution that the silicagel first exhibits a compromised swelling ratio reduced from x3.4, x8.5 and x13 to x3, x7.9 and x11.7 at pH 4, 5 and 6 respectively when the concentration of the beads increases from 0 w/v% to 0.1 w/v%; and later the silicagel presents an enhanced swelling ratio of x3.8, x9.8 and x14.3 by increasing the concentration of the beads up to 0.5 w/v%, Figure 4.7 (a).

This bidirectional relationship between the concentration of the beads and the gel swelling can be well explained by the examining the relationship between crosslink density and the ionization of the gel that the swelling properties of the silicagel depends on a balance between crosslinking density and negative charges as the adding of the silica beads involve both mechanisms. The former is elevated by increased hydrogen bond, ionic bond, or physical absorption inside the gel network from the silica beads (same mechanism as the magnetic beads) [82], thus reducing the swelling ratio; the latter is raised by the increased negative charges on the surface of the beads (silica beads exhibit negative charges when in aqueous medium [83], [84]), thus increasing the swelling ratio. Finally, the experiment indicates that the positive effect of the silica beads dominates the gel swelling at higher concentration while the negative effect of the beads prevails at lower concentration as the monomers which can be crosslinked is limited but the increased ion concentration would be continuously increased by adding more and more silica beads.

Besides, like the ferrogel, the silicagel also has its swelling kinetics (the slope of the swelling ratio versus pH value) undisrupted by addition of the silica beads as x5.2/pH for 0.5 w/v%, x4.3/pH for 0.1 w/v%, and x4.8/pH for 0 w/v%. Therefore, the silicagel can be applied to tune the hydrogel deformation-based drug delivery performance and increase the hydrogel mechanical strength thus the device robustness at the same time. Note that the excellent swelling capabilities of the silicagel hence guarantee its functionality in an integrated wireless sensing system to interrogate the external chemical stimuli to the silicagel volumetric response through the ultrasonic imaging [13].

The hydrogel would only swell in the aqueous medium, once it leaves the solvent, it will go through a dehydration process till reaching a complete dry (losing all the contained water molecule). Then when the hydrogel is put back to the solvent, the swelling kinetics of the hydrogel is required to be preserved as a well-maintained hydrogel swelling performance is crucial for retaining the repeatability/reusability of its integrated system. For this reason, it is essential for conducting the characterization of the hydrogel swelling reversibility. The experiment is set to the following protocols. At first, the hydrogel (2 mm diameter and 2 mm thick cylinder) is immersed in different pH buffer (4, 5 and 6) for one day swelling to reach the equilibrium; then the hydrogel is allowed to dry completely at room temperature; finally, the dried hydrogel is re-immersed in the same pH buffer to achieve the equilibrium swelling again. At each equilibrium swollen state, the swelling ratio is measured and calculated by the swollen weight over the initial weight, Figure 4.8 (a)-(b). All the experiments are done in triplicates.

Figure 4.8 (c) shows the results that the hydrogel can reach the first maximum swelling of x2.5, x7.9 and x10.5 and the second one of x2.5, x7.6 and x10.2 in the pH 4, 5, and 6 respectively. No significant statistical difference is detected between the two swelling cases, which identifies the reversibility of the pH-sensitive hydrogel swelling, thus validating the reusability of the devices.

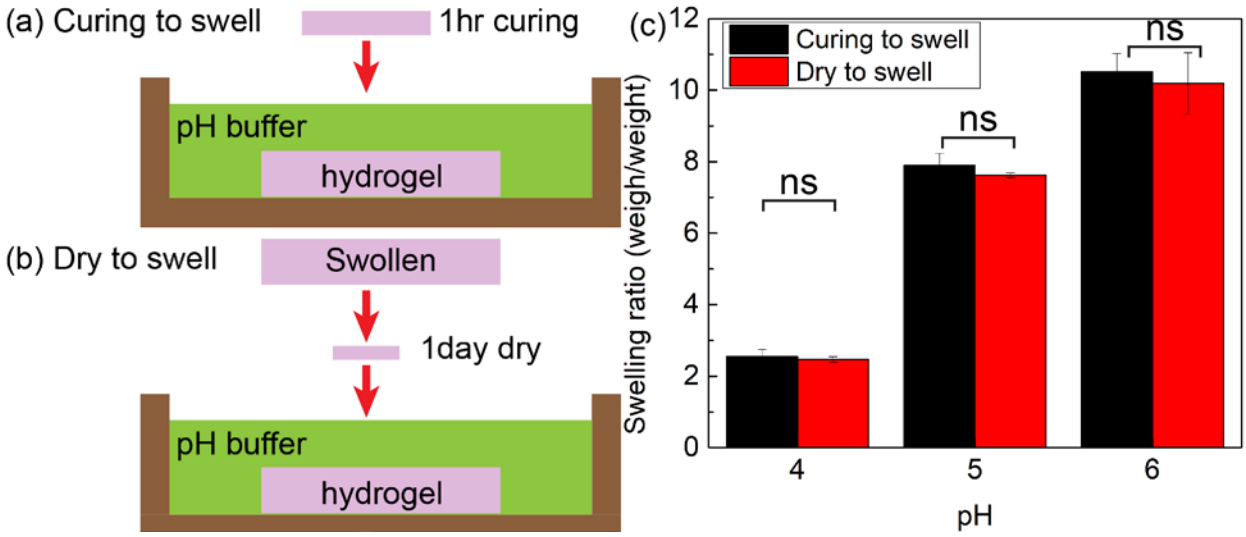


Figure 4.8 pH sensitive hydrogel reversibility in pH 4, 5 and 6 buffer. (a)-(b) Illustration of the experiment setup that hydrogel first swells in pH buffer for one day to reach the equilibrium swollen state, then is allowed to dry completely, and is finally re-immersed in the same pH buffer for swelling; (c) the results show that the swelling properties of the pH sensitive hydrogel are reversible, and thus the reusability of the device is validated. ns represents nonsignificant difference ($p > 0.05$).

## 4.3 Hydrogel swelling based actuation of a deflectable polymeric membrane

As discussed previously, one significant application of the pH-sensitive hydrogel is to work as a chemo-mechanical engine to lift a weight or deflect a flexible polymeric membrane, which then is utilized as the trigger to start a drug release process. To identify this mechanism, the hydrogel swelling kinetics is first testified in the section 4.2, and then its actuation capability will be evaluated in this section. Moreover, from the aforementioned mechanism of the hydrogel swelling, the outward force to cause the gel swelling is mainly from the increased osmotic pressure; when the hydrogel swelling is adopted for any mechanical job, the size of the hydrogel would matter the finally delivered force assuming the osmotic pressure is homogeneous (size-independent).

Therefore, it is essential to assess the size-dependent actuation capability of the hydrogel before the characterization of the corresponsive applications.

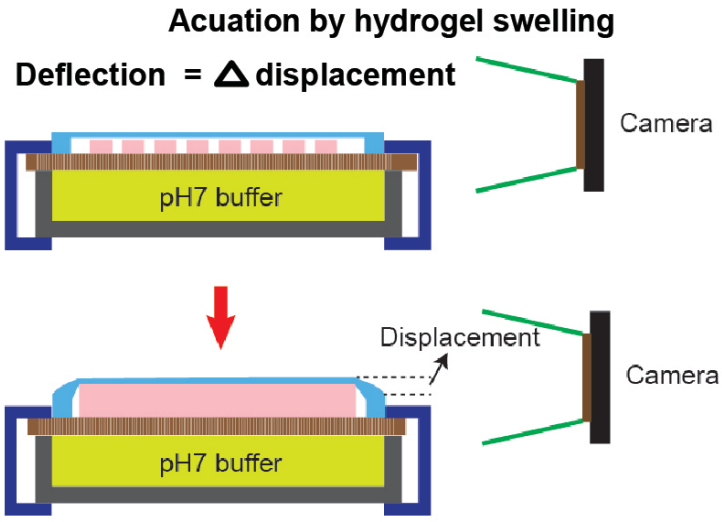


Figure 4.9 Illustration of the experiment setup for investigating the acutation capability of the micro-gel integrated actuator.

The experiment setup is to laser-machine two different thick (0.8 mm and 0.4 mm) of 5 × 5 $mm^2$ hydrogel films into two different micro-gel arrays on the porous substrate. The 0.8 mm thick hydrogel array has the micro-gel lateral dimension of 0.36 mm and the 0.4 mm thick one has the lateral dimension of 0.3 mm; both have the ablated space among the micro-gels created to be around 0.4 mm. Later, a PDMS gel chamber is glued to the porous membrane and then sealed by a PDMS thin membrane (0.12 mm), encapsulating the micro-hydrogels inside gel chamber and working as the chemo-mechanical actuator. Finally this actuator is put on pH 7 buffer to test its actuation ability. The quantitative analysis of the actuation ability is defined to be the vertical displacement of the PDMS membrane, measured by a digital camera at the side view, Figure 4.9. All the experiments are done by a set of three samples.

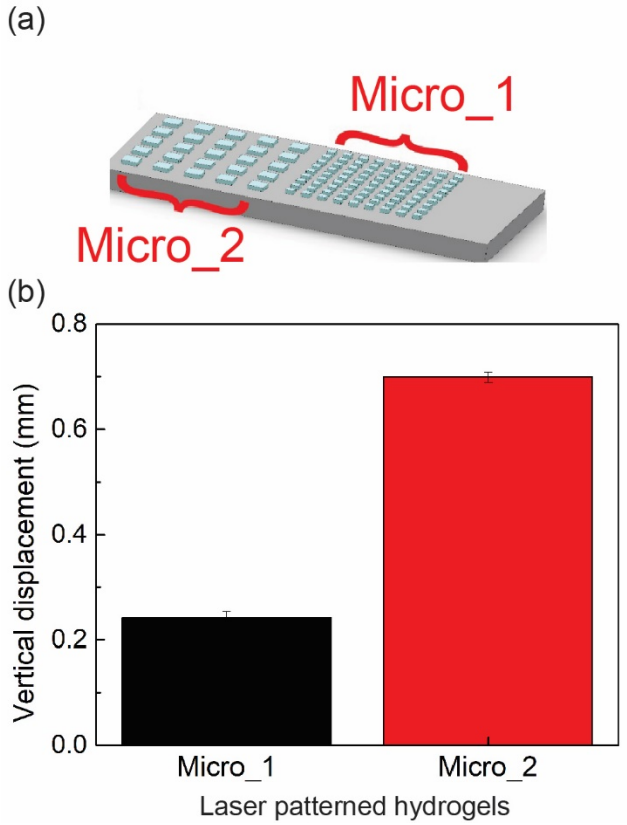


Figure 4.10 (a) Illustration of two different micro-gel matrix, 0.3mm diameter × 0.4mm thick (micro_1, black) versus 0.36mm diameter × 0.8mm thick (Micro_2, red); (b) The actuation results present the maximum PDMS membrane deflection due to swelling of pH-sensitive hydrogel at pH 7.

Figure 4.10 shows the comparison of the maximum vertical displacement of PDMS thin membrane actuated by hydrogels swelling with different laser-engineered micro-patterns. As shown, the PDMS membrane deflection can reach an averaged maximum of 0.7 mm by using 0.36 mm × 0.8 mm micro-gels (Micro_2), a value 2.9 times larger than that of 0.24 mm by using 0.3 mm × 0.4 mm micro-gels (Micro_1). These measurements provide experimental data for the design of the drug volume.

Not only the maximum deflection (thus the largest dispensed drug volume) but also the actuation performance under different pH level is one of the imperative features to autonomously initiate the pH-regulated drug release profiles; therefore the pH-regulated actuation behavior of the fabricated actuators is investigated by using 4 mm × 0.4 mm hydrogels in different pH buffers (7, 4 and 2.2) at an interval of 10 minutes in the first 60 minutes and an interval of 30 minutes in the rest 180 minutes, total 240 minutes. Figure 4.11 demonstrates the results that upon the

equilibrium swelling of the hydrogel, the deflection in pH 7 buffer reached an averaged maximum of 0.7 mm with the averaged deflection rate of 2.92 μm/min, whereas both the averaged maximum deflection in pH 4 and 2.2 were only 0.29 mm and 0.06 mm with the averaged deflection rate of 1.2 μm/min and 0.25 μm/min, respectively. Compared to the maximum deflection measurements in Figure 4.9, the pH-dependent transient performance are more essential for the design of the correlated bio-applications, where the transient since they provide more dynamic and steady-state information to design the correlated bio-applications. For example, they (the temporal performance of the fabricated hydrogel actuators) can be used to design the isolation gap of the smart capsule in order to achieve a controllable on-and-off transition in the GI tract; they also are able to control the drug delivery rate (faster or slower) for the pH-regulated drug delivery device upon the healing state of the chronic wound. Portions of this text are taken from publications by the author [80].

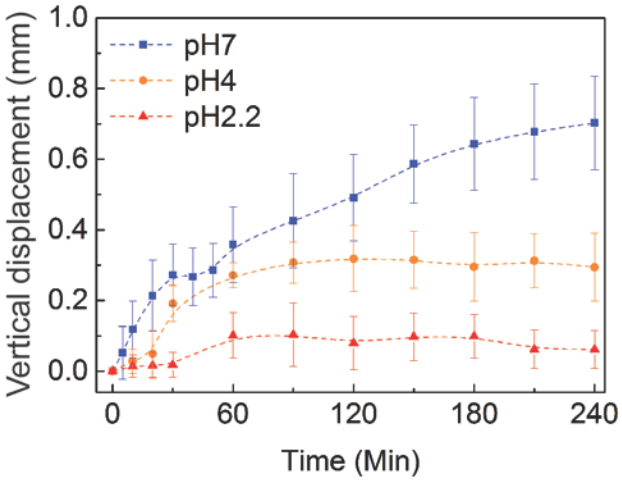


Figure 4.11 Comparison of PDMS membrane deflection due to swelling of pH-sensitive hydrogel in pH 7, 4 and 2.2 buffer solutions over 4 hours.

## 4.4 Conclusion

At this chapter, we first discussed the principle and mechanism of the hydrogel swelling, which is mainly dependent on the counterbalance between the elastic retractive force (inward) from the hydrogel network and the ionic osmotic pressure induced outward swelling force in the hydrogel. The former is strongly dominated by the crosslink density of the hydrogel; the latter is primarily regulated by the difference mobile ion concentration between the gel and the external solution.

The poly (mAA-co-AAm) gel used in this work is pH-sensitive as the increase pH will increase the ionization degree in the gel by converting more –COOH to $–COO^-$, thus finally enhancing the swelling ratio.

Then, we conducted and accomplished the characterization of the swelling kinetics of the laser micro-machined hydrogel. Two different micro-gel patterns are created on a porous substrate and tested at pH 7; the transient gel deformations are continuously monitored through the microscopic imaging. The experimental result shows that at the situation of gel only absorbing the water from the bottom, the swelling rate of the gel is dominated by its thickness instead of its lateral dimension. This phenomenon confirms the diffusion-limited hydrogel swelling process and is essential for the design of any hydrogel based response-time sensitive sensing system, whose large-scale manufactory can be achieved by the laser-machining.

Next, several other important parameters which also play an important role in the regulation of the hydrogel swelling are testified, including the temperature, the crosslink density, and the ionization. The result shows that the temperature and ionization have a positive effect on the hydrogel swelling while the crosslink density has a negative effect; these measurement confirm the theoretical description, which thus can be utilized to tune the performance of the incorporated actuation/sensing system. The composite gel, which is fabricated by mixing micro/nano particles into the gel network before gelation, is also investigated. Although its swelling ratio is changed, the swelling kinetics does not get severe compromised, thus the composite gel is proved to be capable of applying its volumetric response not only to detect the change of the external chemical stimuli but also to accomplish multiple jobs at one time, like more mechanical force (silicagel) or wireless inductive sensing (ferrogel). Moreover, the reversibility of the hydrogel, thus the repeatability of its integrated biomedical system, is identified.

Finally, as the two drug delivery devices (chronic wound dressing and smart capsule) have their drug release initiation strongly dependent on the deflection of the hydrogel actuator, the hydrogel swelling induced actuation capabilities are measured. The experiment result presents a size-dependent performance of the fabricated hydrogel actuator that the larger size (especially the thickness), the bigger deflection of the flexible PDMS membrane. The reason is not hard to understand that as the osmotic swelling pressure is size-independent, the lifting force become a one-by-one function of the gel size. Therefore, through the laser micro-machining process, different micro-gel patterns can be rapid fabricated to fulfill different mechanical works. The

actuation performance at different pH level also are measured, which certainly follow the pH-dependent hydrogel swelling kinetics as the higher pH value, the larger deflection of the PDMS thin membrane.

In summary, this chapter is the fundamental research and characterization of laser-machined hydrogel swelling/actuation behavior, which then would define the functionality and feasibility of the incorporated micro device/systems.

# 5. A SMART CAPSULE WITH A HYDROGEL-BASED PH-TRIGGERED RELEASE SWITCH FOR GI-TRACT SITE-SPECIFIC DRUG DELIVERY

## 5.1 Introduction

In this work, we present a smart capsule that can release its payload after a predetermined/adjustable delay subsequent to passing from stomach into the small intestine. The described capsule (9 mm × 22 mm) comprises of a pH-sensitive hydrogel-based switch, an electronic compartment containing a capacitor charged to 2.7 V, and a drug reservoir capped by a taut fusible thread intertwined with a nichrome wire. The nichrome wire, capacitor, and pH-responsive electrical switch are connected in series. The pH transition the capsule encounters when it enters small intestine, triggers controlled swelling of the pH-responsive hydrogel, which pushes a conductive elastic membrane to close an electrical switch. This initiates a sequence of events, i.e., the discharge of the capacitor, heating the nichrome wire, breakage of the fusible thread, and release of the payload stored in the capsule reservoir through the un-latched cap. The time lag between initiation of hydrogel swelling (by the near-neutral pH of the small intestine) and payload release is controlled by the deflection of the conductive elastic membrane and the gap separating the contacts. The release time can be set to within ±5 min after one hour in the small intestine (start of the swelling) increasing to ±40 min after 4 hours. Portions of this text are taken from publications by the author [80].

## 5.2 Motivation

Site-specific drug release within the GI tract, for increased therapeutic efficacy in preferential absorption positions or protection of the drug from detrimental chemical conditions (extreme pH values or enzymatic degradation) has been the focus of research in academia and industry for several decades [85]. Being a pharma-compatible method, polymer carriers that can dissolve in a predictable manner and deliver entrapped drugs have been the main target of such efforts [86]. For instance, enteric [87] or time-delayed coatings [88] which can shield the drug in the stomach and release it later in the small intestine have been in the market since the introduction of shellac in the 1930s. Stimuli-sensitive hydrogels are another class of polymeric delivery systems that can entrap

the drug and release it, upon swelling, at low or high pH levels [5]. Although convenient and low cost, polymer carriers suffer from various limitations such as low mechanical strength, poor absorption, difficulty with drug loading, and local toxic reactions. Moreover, their drug release profile depends on passive/diffusion mechanism, compromising their targeting capability.

Recent advances in miniaturization of sensors and actuators has allowed the development of multi-functional delivery systems that can protect the drug in hard-shell capsules and release the payload at certain locations. Most such systems have been used for drug abruption studies where the location of the capsule is tracked by various imaging techniques (e.g., fluoroscopy [89] or radioactive methods [90]). This limits the application of such systems to controlled clinical settings. Furthermore, the release mechanisms are typically complicated and require sophisticated assembly and integration, such as the use of an external oscillating magnetic field to induce an electric current in a receiving coil, heating and straightening a bent shape memory alloy wire to rotate and align holes in an outer sleeve and drug reservoir, releasing the drug through the holes (InteliSite®) [91]. Another similar approach uses a heat-actuated mechanism to release a compressed spring, pushing a piston and hence the drug formulation through a small vent (Enterion™) [89]. In order to simplify the targeting and release mechanism, our group recently demonstrated a smart capsule that is capable of releasing the payload in the GI tract at a specific location, pre-determined by a magnetic fiducial marker [92]. This, we believe is still not patient-friendly since it requires the implantation of a miniature magnet or an externally worn larger one.

A way to circumvent the tracking problem is to use anatomic-specific physio-chemical variations within the digestive system (e.g., pH variations, microbial presence, etc.) to actuate the release mechanism. For example, a recent work by van der Schaar et al., uses a pH sensor to locate the capsule in the gut and a stepper motor that is remotely actuated to expel the contents of the drug reservoir (InteliCap®) [93]. This capsule, which is marketed by Philips, is not autonomous and requires user intervention. In addition, it needs an on-board power supply, interface electronics, microcontroller, and RF transmitter.

In this work, we describe a simple alternative solution to the aforementioned shortcomings by using a pH-sensitive hydrogel to trigger the release mechanism by closing an electrical switch and discharging an on-board supercapacitor. Since the pH profile within the GI tract is variable and changes from highly acidic (1.0-2.5) in stomach to near neutral/alkaline (mean of 6.6) in the small

intestine [24], [25], the swelling of the hydrogel (anionic ones that swell at high pH values [22], [94]) in conjunction with the mechanical design of the switch can be used to set the release time once the capsule is within the small intestine. This described device is totally autonomous, converting the pH variations within the GI-tract into mechanical work to initiate the release process. Portions of the text in this section are taken from publications by the author [80].

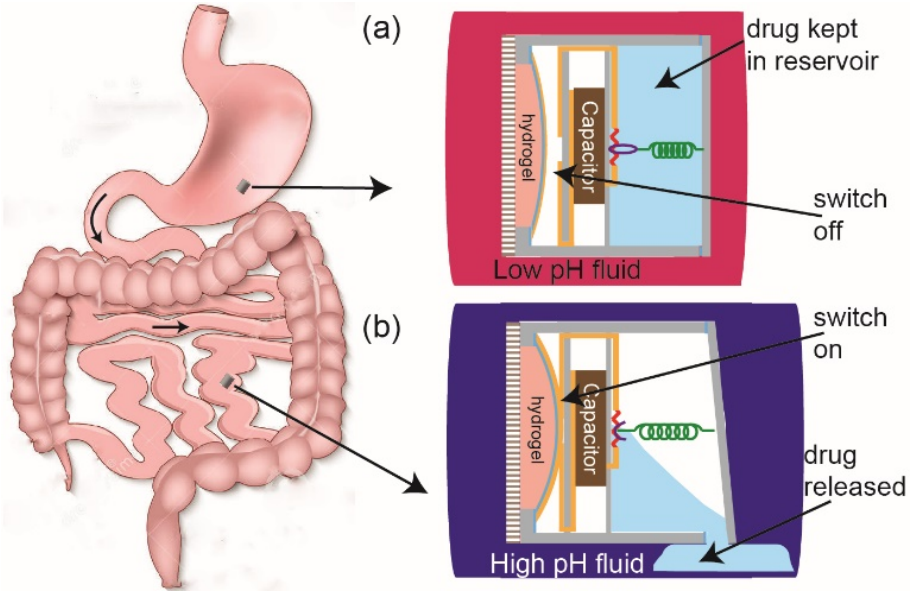


Figure 5.1 Conceptual illustration of the smart capsule: (a) in stomach with low pH, the deflection of the elastic conductive membrane is not sufficient to close the switch, (b) in small intestine, the higher pH values cause the gel to swell and deflect the membrane. After a certain time delay the switch is closed and drug release mechanism is activated.

## 5.3 Design and operation

Figure 5.1 shows a schematic illustration of the smart capsule at different locations within the GI tract. Once swallowed, the capsule passes through the stomach where the low pH values keep the hydrogel in a shrunken state, Figure 5.1 (a). Upon arrival in the small intestine, hydrogel starts swelling, deflecting the switch membrane. After a certain time delay, determined by the mechanical design of the switch (i.e., the membrane thickness and the gap) the switch is closed and drug release mechanism is activated, Figure 5.1 (b). A more detailed working principle of the capsule is shown in Figure 5.2. Initially, in the un-actuated state, the switch is open, the super capacitor is charged (this is done through an inductive link, see Section III.C), and the taut rubber

band holds the reservoir cap closed, preventing drug leakage while ensuring good contact between the fusible thread and the nichrome wire, Figure 5.2 (a). Once the capsule passes the stomach and enters the small intestine, the hydrogel encounters a sharp increase in pH and begins to swell over a certain period, pushing the deflectable conductive membrane against a fixed electrical terminal to close the switch, Figure 5.2 (b). As the switch is shorted, the capacitor discharges a current across the nichrome wire, heating it to a temperature higher than the melting point of nylon thread (60~85 ºC). Subsequently, the reservoir cap opens, releasing the drug, Figure 5.2 (c). An additional elastic (PDMS) rod, under compression in its initial state, is also used to ensure the opening of the cap after actuation (push-pull mechanism). Portions of the text in this section are taken from publications by the author [80].

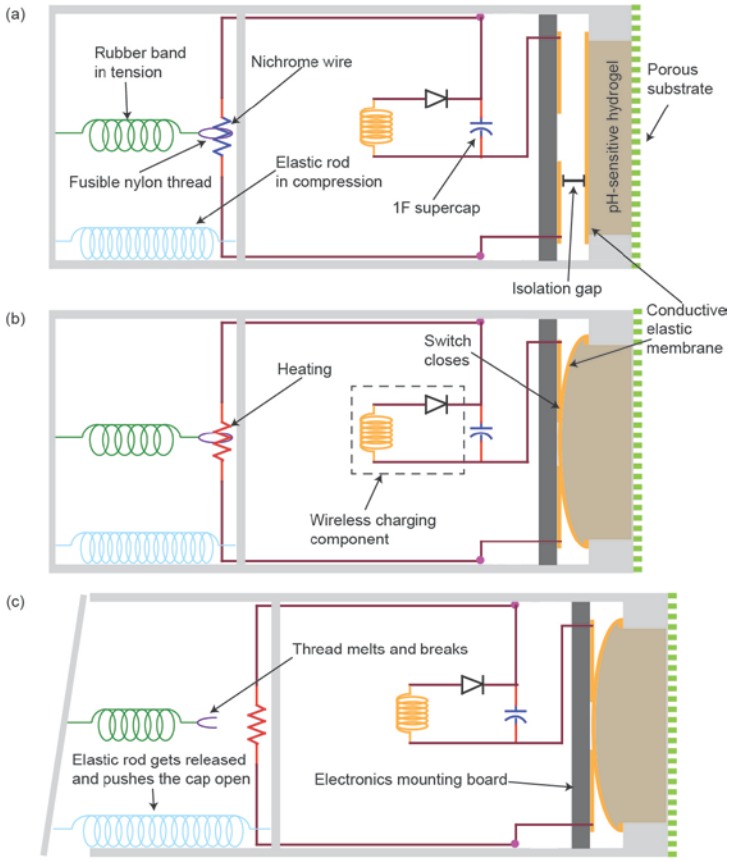


Figure 5.2 (a) Before actuation, the rubber band is in tension, the elastic rod is in compression, the electrical switch is open, and the nylon thread hooks up to the cold nichrome wire; (b) once in the small intestine, the gel swells and deflects the conductive membrane; as the switch closes after a certain time, the capacitor discharges, heating the nichrome wire; (c) after a short time, the nylon thread melts and both the rubber band and the elastic rod return to their original states, releasing the cap.

## 5.4 Fabrication and assembly

### 5.4.1 Capsule enclosure/casing

The detailed 3D structure of the capsule is shown in Figure 5.3 (a). The capsule consists of three main compartments/reservoirs, from bottom to top: 1) the pH-triggered switch compartment, 2) electrical compartment, and 3) drug reservoir. All the enclosures/casings are 3D printed from a photo-reactive resin (mixture of methacrylic acid esters and a photoinitiator) and stacked/bonded together during the assembly process. The switch compartment is 1.7 mm in height, while the electrical compartment and drug reservoir are taller, 12.2 mm and 7.2 mm in height, respectively. A porous plate with 60-70 µm holes laser-drilled onto a 9 mm diameter and 0.15 mm thick GelBond® film (Lonza Group AG, Switzerland) covers/protects the hydrogel while simultaneously allowing its exposure to the aqueous contents of the GI-tract. An electronics mounting board (9 mm outer diameter and 2.1 mm height) is also 3D printed with two 1.45 mm × 0.60 mm windows opened at the edge for extending electrical connection to the pH switch (this also works as a dividing wall between the pH switch and the electrical compartment). At the other end of the electrical compartment, another plate of similar size (1.45 mm × 0.60 mm) having two windows opened for exposing the nichrome wire separates the electrical compartment from the drug-reservoir. Figure 5.3 (b) shows the photograph of a completely assembled capsule having a diameter of 9 mm and length of 22 mm, smaller than a standard 000 size gelatin capsule (9.97 mm × 26.14 mm).

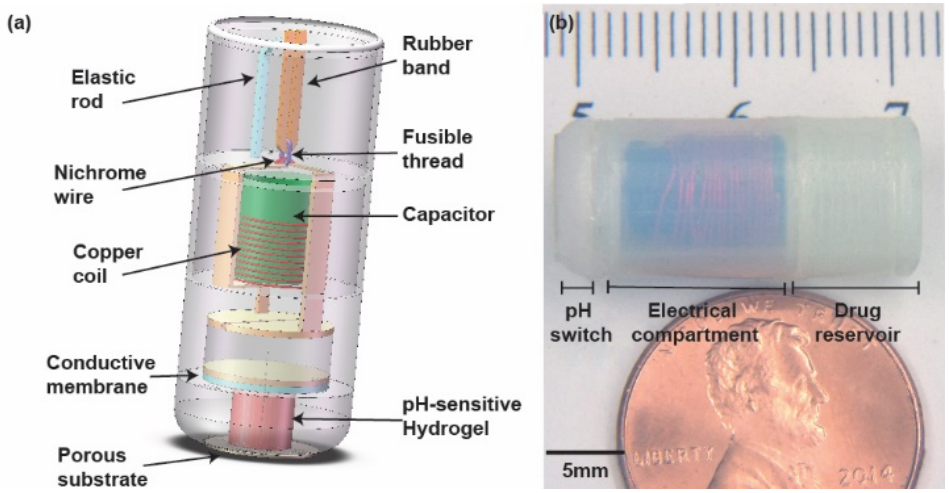


Figure 5.3 (a) Detailed 3D illustration of the smart capsule; (b) photograph of a 3D printed prototype.

### 5.4.2 pH-triggered switch

First, a 4 mm diameter and 0.5 mm height cylindrical hydrogel is cured on the porous plate and covered by the conductive elastic membrane. This is made of bonding a copper tape to a thin (0.12 mm thick) PDMS (polydimethylsiloxane) membrane and acts as the movable terminal of pH switch. Next, two copper pads are attached to one side of the electronics mounting board. This acts as the other (fixed) end of the pH switch. Finally, the two ends of pH switch are joined by a 3D-printed gasket serving as the isolation gap, which can be designed to different thicknesses for the timing control of drug release, Figure 5.2.

### 5.4.3 Electrical compartment

First, a supercapacitor (Electric double layer supercapacitor, 1 F, 2.7 V, 10.5 mm × 6.3 mm, Digi-Key Corp.) is connected to wireless charging components, including a copper coil (20 turns and 7 mm inner diameter) and a Schottky diode (SD0603S040S0R2, Mouser Electronics), all soldered on the electronics mounting board. Next, the two windows on electronics mounting board bring the electrical connections of the fixed end of pH switch into the electrical compartment. Finally, through the two windows on the other end of electrical compartment, electrical connections are extended to the nichrome wire in the drug reservoir, connecting supercapacitor, nichrome wire and the fixed end of pH switch in series. Figure 5.4 shows the wireless charging circuit schematic and a picture of the setup used to charge the capacitor to 2.7 V in 5~6 minutes.

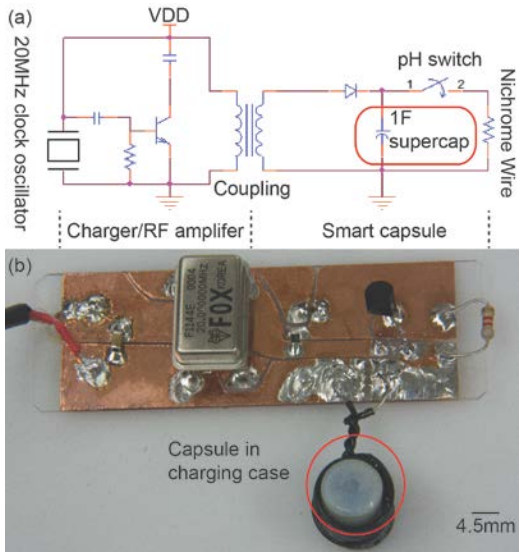


Figure 5.4 Wireless charging of the capacitor (a) schematic and (b) setup.

### 5.4.4 Drug reservoir and capsule assembly

The capsule assembly starts with first soldering a 2~3 mm segment of nichrome wire (Nichrome 60, 70.2 ohms/foot, Dia. 0.0031 inches, Jacobs Online LLC) to two copper wires that connect the supercapacitor and pH switch in series through the two windows of electrical compartment (sealed later to prevent any leakage form of the drug reservoir into the electrical compartment). Next, a length of fusible nylon thread (Grilon bonding yarn, EMS-GRIVORY, Switzerland) is passed through the loop shaped by the nichrome wire and its two ends are joined by heat melting to form a ring. Then, a strip of rubber band (1 mm × 1 mm cross section) is trimmed by a blade and intertwined through the thread ring. Before final closure, a flexible PDMS rod slightly longer than the height of drug reservoir, acting as a pre-loaded spring, is placed inside to ensure its opening following the switch-on.

Table 5.1. Specifications of the capsule

| Capsule enclosure | | | |
|---|---|---|---|
| Outer diameter Length | | 9 mm | |
| Length | | 26 mm | |
| Inner diameter | | 8.4 mm | |
| Separating wall and caps' thickness | | ~1 mm | |
| Drug reservoir volume | | 0.288 mL | |
| Capacitor | | | |
| Diameter | 6.3 mm | Capacitance | 1 F |
| Height | 10.5 mm | Rated voltage | 2.7 V |
| Nichrome wire | | | |
| Resistance/unit length | | 2.3 Ω/cm | |
| Length | | 2~3 mm | |
| Fusible nylon thread | | | |
| Melting point | | 60~85 ºC | |
| PDMS rod | | | |
| Height | | 6 mm | |
| Cross section | | 1.2 mm ×1.2 mm | |

The pH-triggered switch, electrical compartment and drug reservoir are stacked and glued together to form the smart capsule. Table 5.1 summarizes different components used in the construction of the capsule and their major specifications. Portions of the text in this section are taken from publications by the author [80].

## 5.5 Experimental Results and Discussion

### 5.5.1 Characterization of the pH-sensitive hydrogel based electrical switch

Both static and dynamic electrical performance of the pH-triggered switch are critical parameters in the design of the smart capsule. In the off-state, the switch should have high resistance to prevent drainage of the charged supercapacitor. It must also have a small series resistance in the on-state. On the other hand, the dynamic resistive change of the switch during the off-to-on transition should be sufficiently abrupt such that large parasitic contact resistances are not present for too long, posing potential problems such as dissipating power and leading to malfunctioning. Figure 5.5 (a) illustrates the experiment setup used for the electrical characterization of the switch. For static measurements, an isolation gap of 0.4 mm was used while the device was immersed in a pH 7 buffer. The conductance was continuously monitored over 2 hours. The tests revealed a transition conductance of 0.41 S (on resistance of 2.5 Ω) after 62 minutes of exposure to pH of 7 and a stable resistance of 2 Ω thereafter. Fig. 6 (b) shows the results of dynamic switching tests. Initially, the device was immersed in pH 2.2 followed and after a certain time period it was moved to pH of 7. Since the gastric emptying pattern is different in various individuals depending on the digested volume and type of the food [95], [96], two different time durations (70 and 180 minutes) were chosen for these tests. As shown in Figure 5.5 (b), the conductance stayed at 0 S in pH of 2.2 and increased to about 2 S (0.5 Ω) after being transferred and immersed in pH 7. This transition happened after around 70 minutes in both cases with switch showing a rise time of within one second.

For the purpose of controllable targeting at different locations inside the small intestine, the switch time-delay tunability was characterized by varying the height of the isolation gap. For a 0.4 mm isolation gap the mean delay time was 66 minutes (SD=5.3 min), increasing to 105 minutes (SD=8.3) and 230 minutes (SD=42.3) for 0.6 and 0.9 mm isolation gaps, Figure 5.6. The results show an approximate 1 hour/0.2 mm tunability for switching action, thus covering the small

intestine transit time of an average 3.5 hours. The switches with smaller gaps (0.4 and 0.6 mm) can be set to have a more accurate time delay (smaller SD) than on the ones with larger gap (0.9 mm). This is anticipated since as the hydrogel keeps swelling, its behavior becomes non-linear and the polymer network starts exhibiting creep behavior. This incidentally can be used to our advantage since most drug absorptions occur in the jejunum which the capsule covers within the first 1-2 hours.

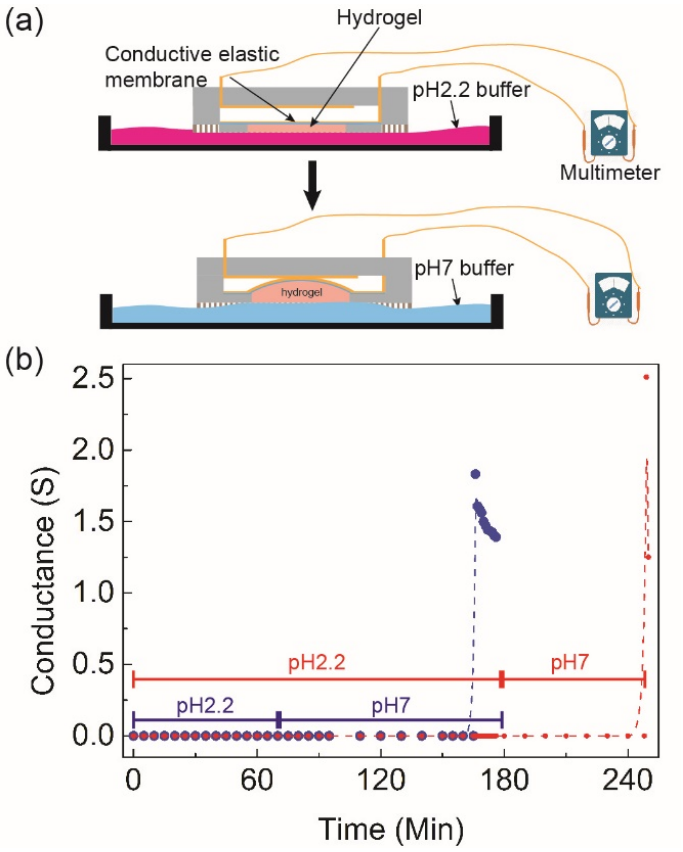


Figure 5.5 (a) Experiment setup for static an ddynamic electrical evaluation of the pH-triggered switch; (b) characterization of the conductance change, blue: first 70 minutes in pH 2.2 buffer and the rest 110 minutes in pH 7 buffer; red: first 180 minutes in pH 2.2 buffer and the rest 70 minutes in pH 7 buffer.

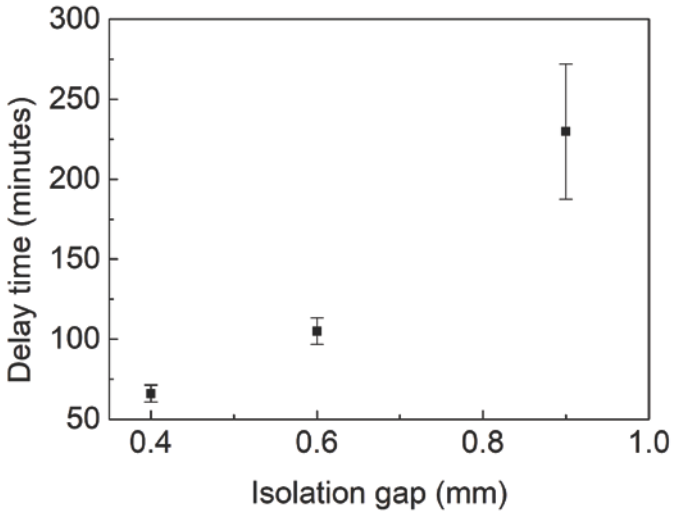


Figure 5.6 Actuation delay time for devices with three different isolation gaps (0.4, 0.6, 0.9 mm).

### 5.5.2 Reliability tests and evaluation

The successful drug release from the capsule requires the triggering action to be only dependent on the hydrogel swelling and the subsequent closure of the electrical switch. This implies that other external mechanical forces such as gastric contraction does not interfere with the device operation. In order to verify this, we first evaluated the reliability of pH-triggered electrical switch under axial stresses. This experiment was done by pushing a 4 mm diameter metal stick against the porous substrate of pH-triggered switch (controlled by a manipulator) and simultaneously monitoring the resistance of switch. A set of 3 samples were tested and the result showed that a minimum 10140 mmHg applied pressure was required to punctuate the porous substrate and close the switch. The experiment confirmed that the capsule can easily withstand the highest stomach contraction pressures of 80 mmHg [97], [98] without accidently being triggered. The radial (in-pane) force required to deform the gel chamber is expected to be larger than the axial one as the gel chamber wall (>1.2 mm) is much thicker than the porous substrate (0.15 mm).

Since the gel chamber is the weakest link, we do not anticipate other capsule components to be disturbed or compromised by any force during the gastric emptying or intestinal peristalsis. We have performed similar evaluations in our previous work and did not notice/record any leakage or disintegration [92].

### 5.5.3 In-vitro evaluation of the release mechanism

For in-vitro evaluation of the release mechanism, smart capsule was loaded with Evans blue powder (mimicking lyophilized drug and allowing easy visual recording). The capsule was then immersed in a pH 7 buffer, representing the alkaline environment of the small intestine. Figure 5.7 shows photographs of multiple stages of release. The capsule starts to open in frame “b” after immersing in buffer over 260 minutes. The powder was released continuously, diffusing from the drug reservoir into the buffer over a period of 15 minutes, frame “b-f”, Figure 5.7.

The above experiment demonstrated a successful drug release in pH buffer solution, a more sophisticated experiment was designed to evaluate the release capabilities of capsule quantitatively. As the mechanical processing of food in the small intestine is dependent on food formulation, four types of solutions were prepared to represent different digestion environments. These included DI water, 0.5% (w/v) guar gum, 1% (w/v) guar gum, and 0.5% (w/v) guar gum with 30% (w/v) added cooked rice. These concentrations (0, 0.5 and 1% w/v) were chosen to model the variations in the chyme viscosity, where 0% (water) corresponds to 1 cP, 0.5% to 300 cP, and 1% to 2500 cP at the shear rate 0.1/s [99]. The quantifications were gravimetric and done by retrieving the capsule and measuring its weight after 4 hours of dry-out at 70 oC. Considering a possible weight change from dehydration of the 3D-printed parts, control experiments were conducted with capsules having an empty load. The results revealed an average of 12.66 mg (SD = 3.72) weight loss through these spurious routes.

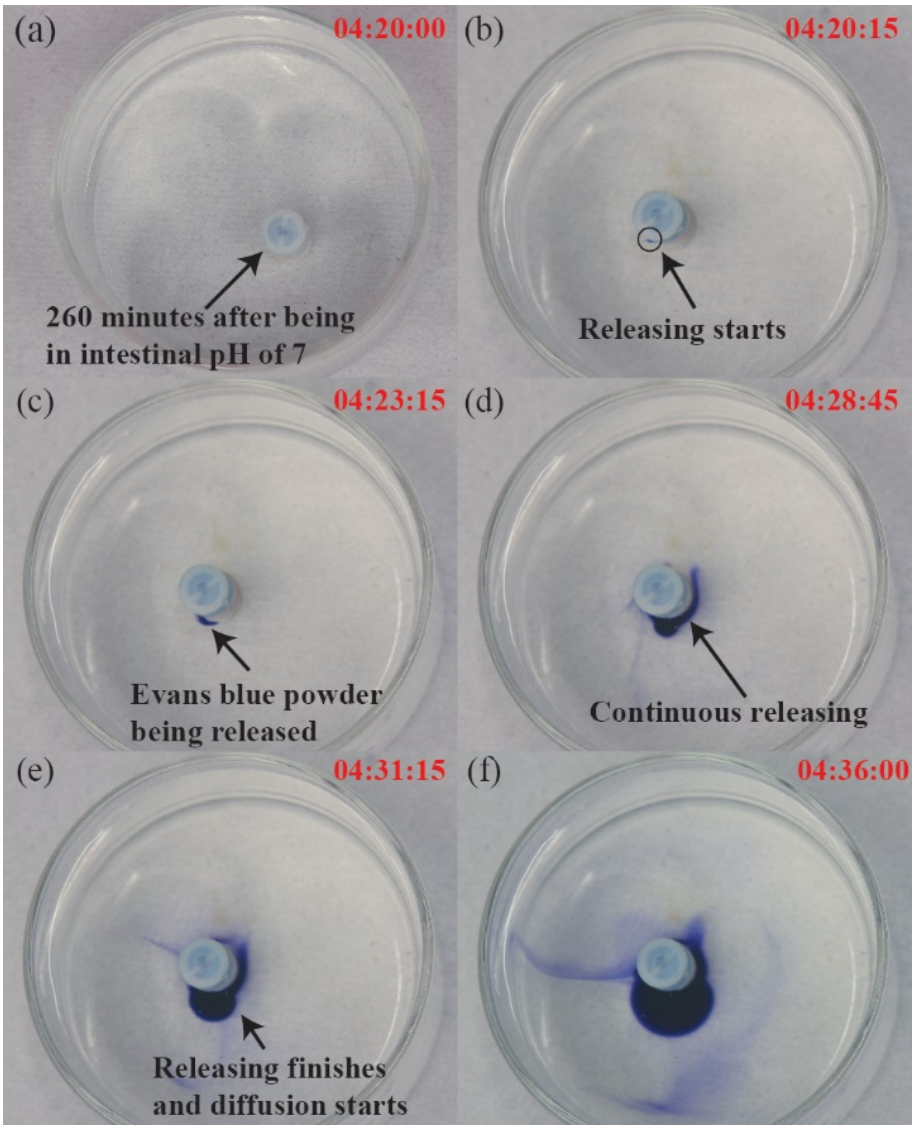


Figure 5.7 Snapshot photographs of the in-vitro experiment of the drug release from the capsule. Frames (a-b) show the cap starting to open after capsule stays in pH 7 buffer for 260 minutes. Frames (c-d) show the Evans blue powder being released from the drug reservoir into the buffer over 5 minutes. Frame (e) shows a complete discharge of the drug after 11 minutes. Frame (f) shows the released blue-dyed drug diffusing to the ambient buffer over a period of 5 minutes.

Figure 5.8 presents the characterization results of capsules releasing 100 mg of Vitamin C (Emergen-C® drink mix) in different environments, clearly indicating an increased payload release associated with a decrease of the surrounding environment viscosity. Note that the result for 0.5% guar + 30% rice was somewhere between 0.5% and 1% guar concentrations, with starchy food and undissolved pellets contributing to an increased viscosity. Portions of the text in this section are taken from publications by the author [80].

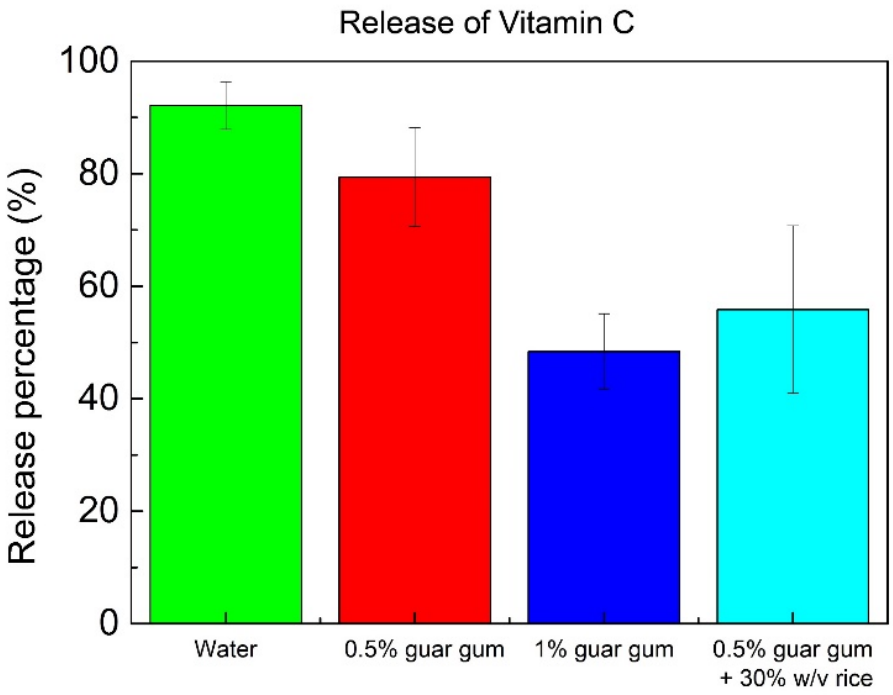


Figure 5.8 Payload release of smart capsule in different environments.

# 6. A PH-REGULATED DRUG DELIVERY DEVICE FOR TARGETING INFECTED REGIONS IN CHRONIC DERMAL WOUNDS

## 6.1 Introduction

This work presents a low-cost, passive, polymeric pump for topical/transdermal drug delivery which uses wound pH as a trigger for localized drug release. Its operation relies on a pH-responsive hydrogel actuator which swells when exposed to alkaline pH (an indicator of certain dermal infections) to displace a drug volume. The pump enables slow release (< 0.1 μL/min) of aqueous solutions for up to 3 hours and sustains against up to 8 kPa of backpressure, making it suitable for automated drug release in chronic wounds and for transdermal delivery applications. Moreover, this patch can be expanded to a 2 × 2 array or converged into one chamber. The former can release 4 times volume of a single cell; the latter is to use the poly (HEMA-co-DMAEMA) gel, which swells/shrinks as the pH decrease/increases, to control the drug release on-to-off from the shrinking-to-swelling of this type of hydrogel, instead of from the swelling-to-shrinking by using poly (mAA-co-AAm) gel.

## 6.2 Motivation

Unlike acute wounds, chronic wounds do not heal in an orderly or timely manner and usually remain for months or sometimes worsen rather than improving, resulting from complex biological factors behind wound healing, such as local tissue ischemia, presence of tissue necrosis, impaired cellular and systemic host response to stress, etc.; therefore, these combinations or overlaps of bio-factors in the wound contribute to a sustained pro-inflammatory state, which inhibits normal wound healing progression and tissue integrity [100]. The recent statistics reveals that the chronic wounds affect an estimated 6 million people in the US and cost the health care system $20 billion annually [101].

There are various types of wound dressing products available in current market, including standard gauze pads or hydrogel/hydrocolloid products, which is designed to fulfill one or multiple complicated requirements, like physically protection, exudates absorption, optimal moisture levels restoring/maintaining, Figure 6.1 [100], [102], [103]. The former is the most common base component in multi-layer dressings for a shallow wound; the latter is for increased exudate

absorbing. All these materials can promote the tissue regeneration within a balanced moisture environment, while a more efficient method is to target the chronic wounds based on different physicochemical and physiological parameters, acting as “biomarkers” of chronic wound, including temperature, moisture, nutrition factor, inflammatory mediator, uric acid, etc. [104].


Figure 6.1 Typical commercial wound dressing products.

Among those above mentioned biomarkers, the pH level in wound bed is a key indicative parameter for assessing the healing progress of chronic wounds as it can indirectly and directly influence all biochemical reactions taking place in this process of healing. Healthy skin or healing acute wounds have a slightly acidic pH in a small range (4–6), chronic wounds have pH distributed from 5.4 up to 9.0, which is attributed to the alkaline byproducts of proliferating bacterial colonies [104]. Therefore, current dermal drug delivery systems can include physical/chemical pH sensors or using pH sensitive polymeric materials to achieve a pH-regulated would dressing. pH sensitive monomers, like Poly(acrylic acid), can be copolymerized into semi-interpenetrating polymer network (IPN) films to diffuse therapeutic agents through a swollen polymer matrix to infected wound beds [105], [106]. Nanoparticles, like nanodiamond, use high surface area-to-volume ratio to bind protein-based therapeutics such as insulin to release increased amount of insulin in alkaline environment [107]. However, such aforementioned methods have a common shortcoming as

acting in open-loop manner, unable of receiving physical or chemical feedback from wound physio-chemical microenvironment to modify or adjust the treatment. Further, Chronic dermal wounds often exhibit a spatial irregularity of infection development due to their non-uniform healing rate, resulting in drastic pH variations throughout the affected area [108], thus further compromising their point of care drug delivery capabilities.

In this work, we describe a simple alternative solution to the shortcoming of the current treatment methods, which is the pH-sensitive hydrogel based flexible patch consisting of two polymeric chambers molded and bonded together. The top chamber serves as the drug reservoir and the bottom one works as the gel chamber, a little bit smaller than the drug reservoir; a thin flexible membrane is applied to separate the two chambers and force the drug out of the reservoir once deflected by the gel swelling; and the drug outlet is made by creating two micro vertical channels in the gel chamber wall to connect the drug reservoir to the outside. As the two micro-channels are made of hydrophobic polymer (PDMS), the drug wouldn't be released unless being actuated by the deflectable membrane. The working mechanism of this described device is straightforward that when the device is contacted to the inflamed regions of the wound bed (high pH), the hydrogel will start to swell and against the thin membrane, thus releasing the drug to the wound; then at the non-inflamed regions (low pH), the hydrogel will shrink (as transferred from high pH to low pH) or have a very limited swelling, thus stopping the drug releasing or releasing no drug. Hence, the entire wound could benefit from selective delivery of drugs targeted to only the infected regions using this closed loop drug delivery manner, Figure 6.2.

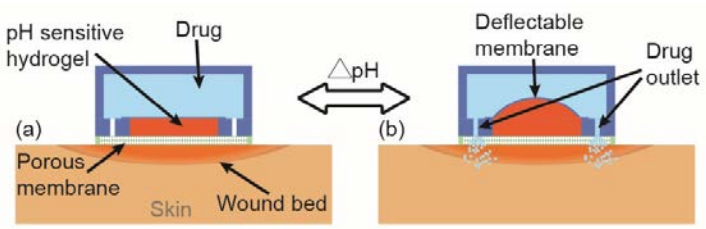


Figure 6.2 Conceptual illustration of pH-regulated drug delivery for the infected regions of chronic wounds, (a) no drug is released at non-infected region where pH is low. (b) pH-sensitive hydrogel swells against a deflectable membrane when pH is high, allowing drug to be pumped out from the drug chamber into the wound.

## 6.3 Fabrication and experiment

The fabrication process of the pump is shown in Figure 6.3 (a). First, laser-cut acrylic is used as a mold for PDMS to create the deflectable membrane (150 µm thick), the liquid drug reservoir ($11.5 \times 11.5 \times 1.8$ mm$^3$), the hydrogel chamber ($7 \times 7 \times 1.8$ mm$^3$), and drug outlets (0.6 mm diameter). The layers are all bonded together via plasma. The drug chamber is loaded with the drug solution (blue-dyed water for testing) using a syringe while the hydrogel chamber is filled with a yellow-dyed poly mAA-co-AAm gel pre-solution, Figure 6.3 (b); this gel swells as pH increases [21]. The final device is shown in Figure 6.3 (c). Moreover, a $2 \times 2$ array of such device is created through the same protocol as the single cell, which contains 4 pairs of drug reservoirs and gel chambers and is expected to deliver 4 times of volumes of a single cell, Figure 6.4 (a). The top and side view of the fabricated pH drug delivery array are shown in Figure 6.4 (b) and (c) respectively.

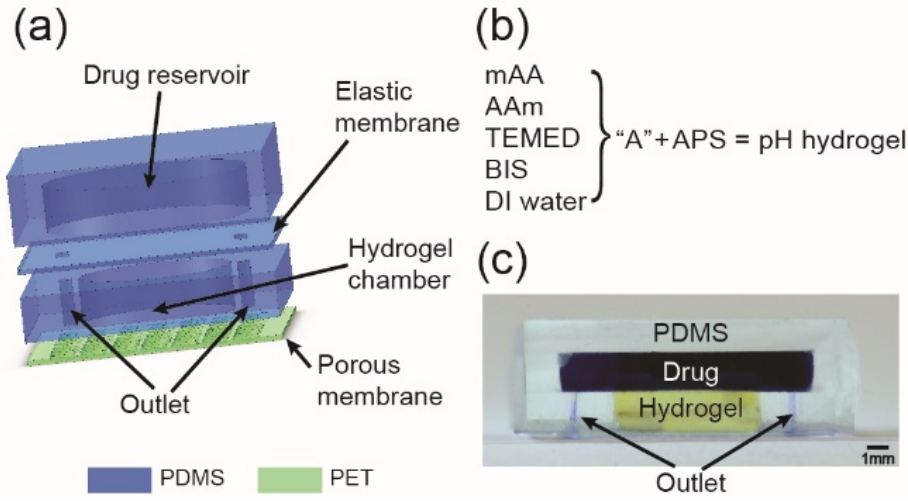


Figure 6.3 (a) 3D exploded view of the pump, from top to bottom: drug reservoir, deflectable elastic membrane, pH hydrogel chamber with micro via hole (for releasing drug), and laser-cut porous membrane. (b) Fabrication of pH sensitive hydrogel. (c) Photograph of the device.

For characterizing the in situ pumping performance of this fabricated device, we first created a wound tissue phantom using a 0.5 %w/v agarose gel substrate made with phosphate buffered saline (pH 7.4). Subsequently, two platinum wire electrodes were inserted into agarose gel (2 cm apart) to simulate bacterial infections and a voltage of 3 V across them was applied to continuously increase the pH near the cathode to mimic the alkaline pH at the infected regions of the wound,

thus resulting in a reusable test platform, Figure 6.6 (a). The fabricated device is then fixed near the cathode and all the correlated characterizations are conducted.

To measure the flow rate, the device was modified to seal the two hydrophobic PDMS micro channels and create an extra drug outlet at the top center of the device. Then, a graduated capillary tube (1.22 mm in diameter) was connected at the top drug outlet to allow for the measurement of flow rate, Figure 6.5 (a). The drug delivery capability of the 2 × 2 array was also investigated by using the same experiment protocol, which is designed to compare the maximum drug delivery capacity of the array to the single cell.

Another important factor to assess the transdermal drug delivery performance of the micro-devices is their pumping capability under certain high backpressure. The correlated experiment uses the same procedure as the flow rate measurement above that the device is put on top of the agarose gel near the inserted electrode at the cathode and connected to the graduated capillary tube and a pressure-regulated nitrogen source in series with the flow rate measured at different applied pressure, Figure 6.5 (b).

The reliability of this claimed wound dressing depends on the swelling kinetics of the hydrogel and the elasticity of the thin PDMS membrane. The former was investigated in Chapter 4.2 that the applied hydrogel is pH sensitive and its swelling is repeatable, thus guaranteeing the pH-regulated pumping requirement and the reusability of the integrated device. The latter relies on the mechanical properties of the flexible PDMS membrane. Therefore, the reliability examination of the fabricated device in this chapter is concentrated on the robustness of the PDMS thin membrane, as its deflection performance was also already characterized in Chapter 4.3. The experiment is conducted by using a solid rod to push against the PDMS thin membrane and monitoring the membrane deflection and applied load through the universal test machine (ADMET) at the same time, Figure 6.5 (c). The maximum pressure that the PDMS thin membrane can endure is defined as the recorded pressure immediate before the membrane is broken.

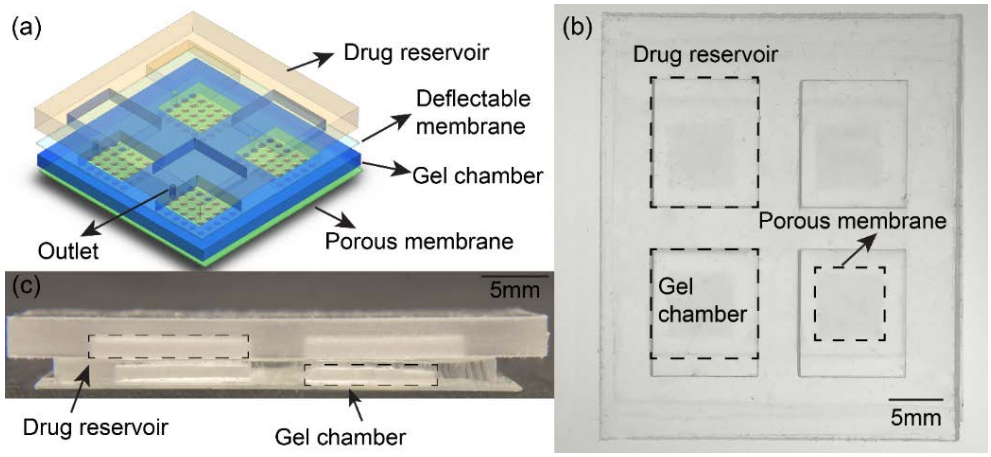


Figure 6.4 (a) The conceptual 3D illustration of the autonomous pH sensing and drug delivery dressings array, containing 4 pairs of drug reservoirs and gel chambers and able to deliver 4 times of volumes of a single cell; (b) Top view of the fabricated pH drug delivery array; (c) Cross view of the fabricated pH drug delivery array.

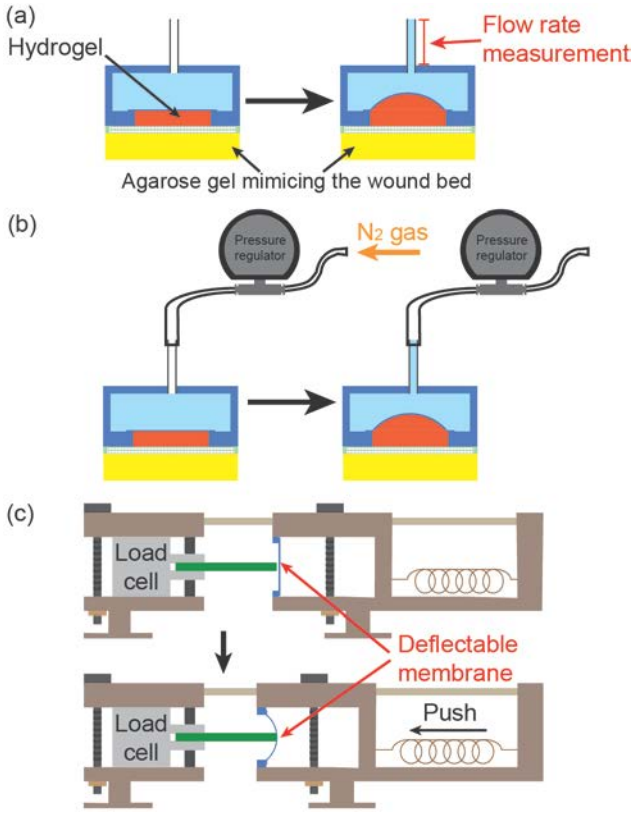


Figure 6.5 (a) The illustration of the flow rate measurement setup that the drug is released at the top outlet and continueously monitored; (b) The illustration of the flow rate versus backpressure; (c) The demonstration of the robustness characterization of the PDMS thin membrane using the universal test mechaine.

## 6.4 Results and discussion

The swelling kinetics of the poly (mAA-co-AAm) gel in this research has been already fully characterized in Chapter 4.2. Additionally, the swelling behavior of the pH-sensitive hydrogel placed adjacent to a negative electrode on top of an electrolyzed agarose gel (mimicking the wound bed) was also investigated. Figure 6.7 (a) shows the results that over 165 minutes, the pH within 0.5 mm of the cathode increases from 7.4 to 10.6 and a sample ($4 \times 4 \times 1$ $mm^3$) of the pH-sensitive hydrogel is capable to reach an equilibrium swelling of 2.6 times of its original diameter. Therefore, this created gel platform can create a gradient pH distribution and induce a dramatic deformation (swelling) of the pH-sensitive hydrogel, thus qualifying to be a simulation of chronic wound bed. Note that compared to the swelling kinetics characterized previously, the swelling ratio of the hydrogel near the negative electrode is slightly larger (2.5 vs 2.1), which can be attributed to the further escalated pH level (~10) over 7 (the pH value used to measure the hydrogel swelling in Chapter 4.2.

The flow rate experiment results are shown in Figure 6.7 (b) that the output volume from the pump reaches 11.31 µL at 180 min and provides up to 100 Pa of hydrostatic pressure; the flowrate is stable between 0.05 µL/min and 0.1 µL/min with maximum of 0.13 µL/min. Moreover, a set of photographs are also captured and presented to demonstrate the drug delivery of the fabricated device visually, showing the blue dye being delivered into the agarose gel over 210 min, Figure 6.6 (b). Note that the difference in expelled volume between outlet ports results from a non-uniform hydrogel swelling due to the created gradient pH distribution.

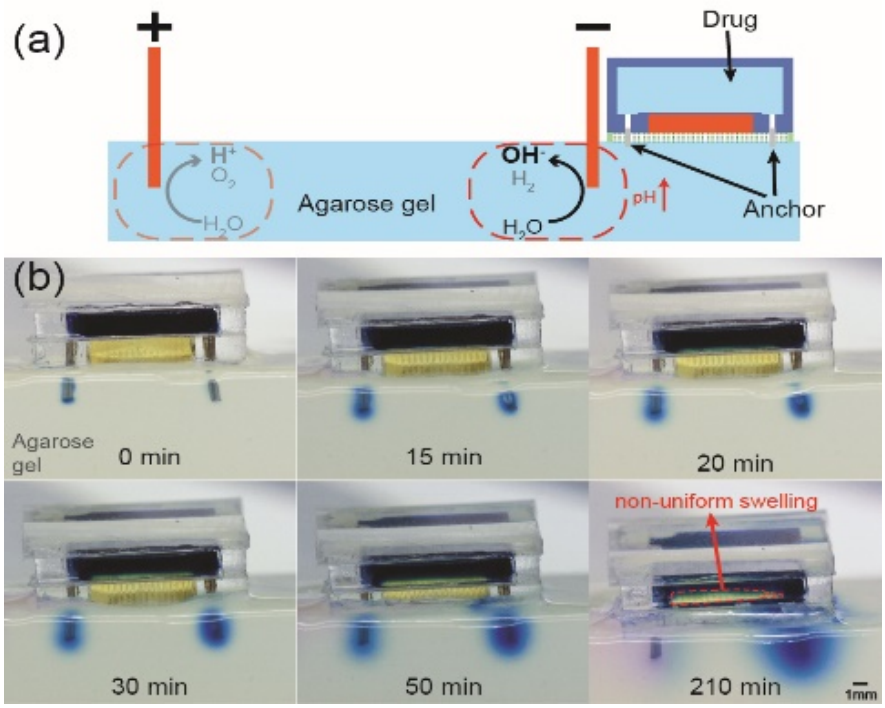


Figure 6.6 (a) 3D exploded view of the pump, from top to bottom: drug reservoir, deflectable elastic membrane, pH hydrogel chamber with micro via hole (for releasing drug), and laser-cut porous membrane. (b) Fabrication of pH sensitive hydrogel. (c) Photograph of the device.

Figure 6.7 (c) presents the characterization of the robustness of the PDMS thin membrane (thus the reliability of the device) that this PDMS membrane (150 μm thick) can take a maximum pressure of 206.8 kPa and a longest deflection (vertical displacement) of 1.8 mm. As the inner height of the drug reservoir is 1.8 mm, the measurement results actually render an implication that the drug release required actuation work would not damage the deflectable PDMS membrane even in case the hydrogel swelling produces a pressure equal or bigger than 200 kPa, thus securing the reliability of the entire device.

Figure 6.7 (d) shows the flow rate response with an applied backpressure provided from a gas source connecting to the outlet of the pump. The flowrate is inversely proportional to the backpressure, with the average flowrate decreasing from 0.082 μL/min to 0.022 μL/min as the backpressure increases from 0 kPa to 8kPa, thus able to fulfill the typical subcutaneous pressure requirement of 3kPa, [109], [110].

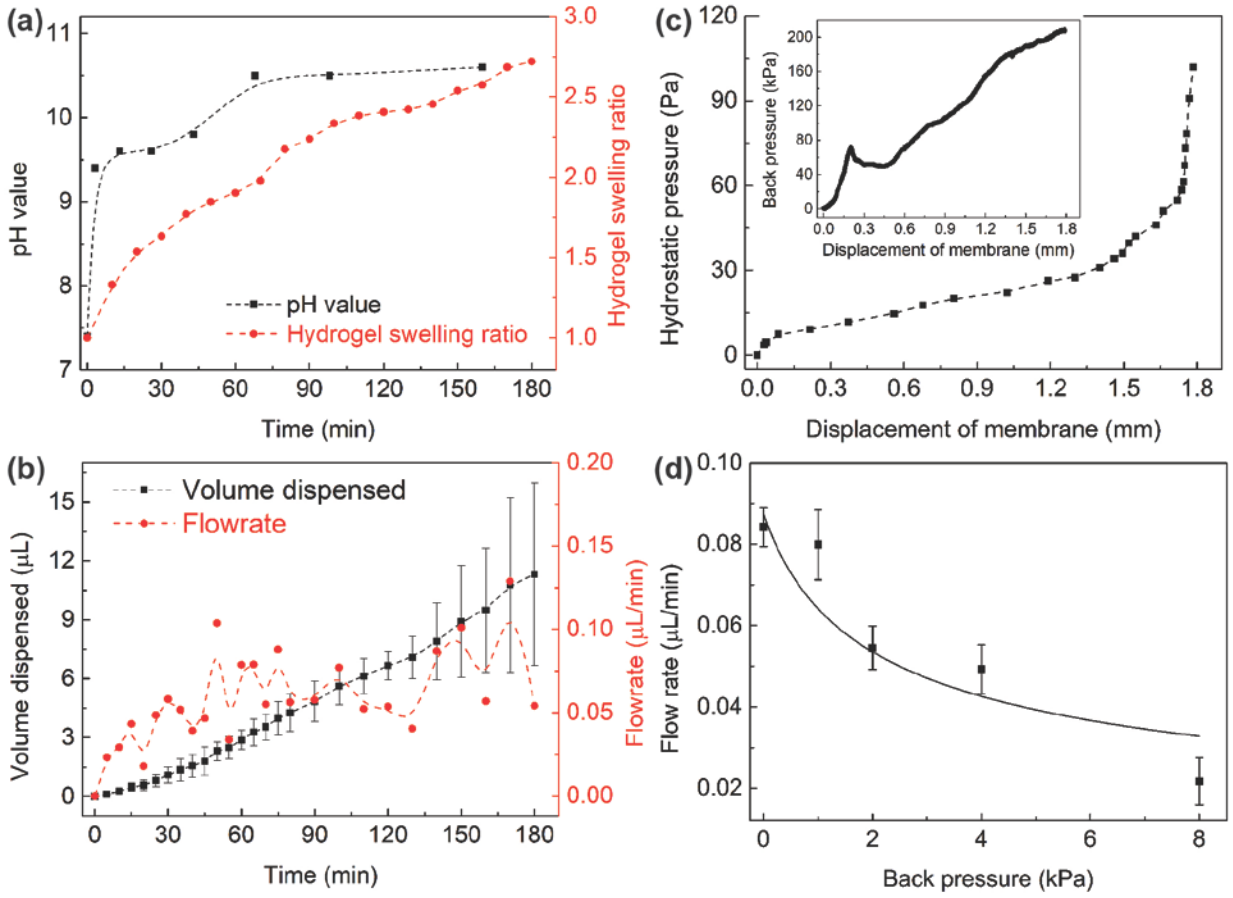


Figure 6.7 (a) pH within 0.5 mm of the cathode over time, and free swelling of pH-responsive hydrogel; (b) Volume dispensed by pH-regulated pump at minimal backpressure (< 100 Pa) shows a linear response over 180 minutes; (c) Backpressure (hydrostatic) as a function of membrane deflection. Inset: hydrogel pressure required for membrane deflection (206.8 kPa at maximum deflection); (d) Flow rate vs. backpressure.

Figure 6.8 shows the comparison of the drug delivery capacity between the 2 × 2 array and the single cell that up to 180 minutes, the single cell release a 11.31 μL while the array reaches almost 4 times larger volume of 49.89 μL. This experiment confirms the linearly relationship between the enhanced drug delivery capacity and the increased number of the single cell. Moreover, with the help of the laser micro-machining, the n × n array can be scaled into much smaller sizes to provide a higher resolution matching to the infected regions.

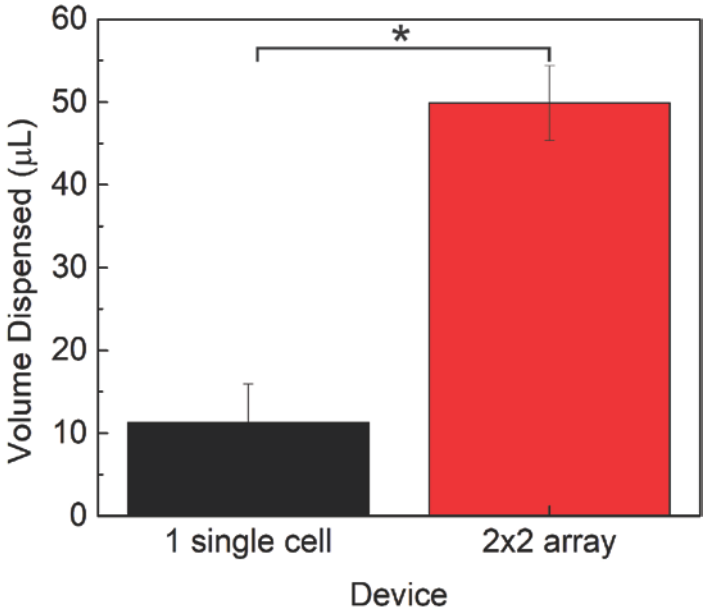


Figure 6.8 Expereimental comparison of the drug delivery capacity between the 2 × 2 array and the single cell for 180 minutes shows a 4 times increase of the released drug by using the array (49.89 μL) instead of the single cell (11.31 μL).

So far the fabricated wound dressing patch successfully demonstrates the pH-regulated autonomous drug delivery capabilities by using both a single cell and a 2 × 2 array, however, there exists a simplified version of this device by using another type of pH-sensitive hydrogel. This pH-sensitive hydrogel is the poly 2-hydroxyethyl methacrylate -co- N,N-dimethylaminoethyl methacrylate (HEMA-co-DMAEMA), a type of cationic pH hydrogel; its swelling kinetics is opposite to that of the poly (mAA-co-AAm) gel (mainly used in this work) as it will swell when the pH decreases and shrink when the pH increases [111], [112]. Therefore, at the region without infection (low pH level), this hydrogel can be designed to swell and cover the entire porous membrane, thus no drug (or a very limited amount) is released; and at the region with infection (high pH level), the gel will shrink and expose the drug to be released through the pores on the gel bond substrate, Figure 6.9 (a)-(b). By using this manner, the deflectable thin membrane is eliminated and the gel chamber and the drug reservoir are combined together, which thus facilitates a more rapid fabrication and reduces the cost. Note that as the gel is not hydrophobic, it is possible for the drug to diffuse through the gel to the outside, but this process assumes to be slow and volume-limited. Therefore, the balance between the wasted drug and the improved fabrication process is worth to be further fully investigated through more characterization (a future work).

Figure 6.9 (c) shows the swelling behavior of the poly (HEMA-co-DMAEMA) gel in different pH solution from 4 to 10 that the swelling ratio of the gel can reach 2.5 times the surface area within 1 hour of curing at pH 4 and deceases to 0.75 times at pH 10. According to this experimental result, the maximum window for the drug releasing is ~70% (calculated as 1-0.75/2.5 = 0.7) area of the porous membrane, which can be further tuned by setting the pH where the hydrogel is designed to fully cover the porous substrate from 4 to other values. For example, if the blocking pH value is set to 6, where the swelling ratio is ~2, then the maximum window to deliver the drug becomes to 1 – 0.75/2 = 62.5%. Therefore, using this pH sensitive hydrogel enables a simplification of the fabrication process and concomitant offers a more economical pH-dependent autonomous drug delivery protocol.

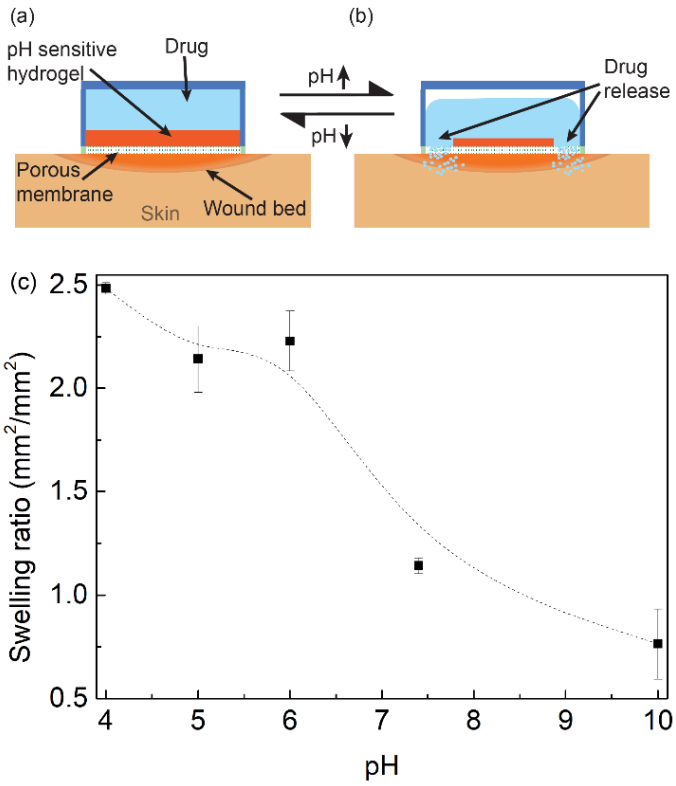


Figure 6.9 (a)-(b) The conceptial illustration of the pH-regulated drug delivery dressings using a different type of pH-sensitive hydrogel. When the pH level is low, the swollen gel covers the entire porous membrane, thus stopping the drug release; when the pH level is high, the shrinken gel exposes ~70% area of the porous membrane, thus delivering the drug. (c) The swelling behavior of the poly (HEMA-co-DMAEMA) gel in different pH buffer solutions shows that the gel swell/deswells as pH decrease/increases.

# 7. CONCLUSION

This described doctoral research aimed at utilizing the $CO_2$ laser to fabricate a rapid and scalable micromachining of pH-sensitive hydrogels for in vivo sensing and actuation bio-applications. When this hydrogel encounters a change in external chemical stimuli, pH in this work, it will swell or shrink; therefore this volumetric response can be used as a transducer for coupling the chemical stimuli concentration to a detectable electrical signal or as a chemo-mechanical engine to deflect a polymeric thin membrane to accomplish a mechanical work. In order to better fulfill a variable requirements, like sensing rate or actuation force which are based on the size-dependent swelling kinetics of the hydrogel, it is preferable to pattern/engineer the hydrogel into the designed patterns. Among the typical micro-machining techniques, like UV-lithography and micro-molding, $CO_2$ laser system has its unique advantages for its cost-effective and high-throughput, which is thus chose to micro-pattern the hydrogel for three different bio-applications. In this chapter, the conclusions including the summary and the prospective research direction of each scheme will be discussed.

In the chapter 2, the typical pH-sensitive hydrogels and their applications in drug delivery and wireless sensing are introduced that the hydrogel is usually used as the drug carriers to release the drug through their swelling/shrinking or degradation/decomposition induced by the external physical/chemical stimuli; while in the wireless sensing, the composite gel (mixing the micro/nano functional particles into the gel matrix) simplifies the conventional hydrogel volumetric regulated wireless sensing, like ferrogel or silicagel. Aiming to improve the efficiency of the above described drug delivery methods, this work promotes two pH-regulated autonomous drug delivery devices, whose detailed demonstration are in the chapter 5 and 6.

Chapter 3 discussed the mechanism and theory of the laser thermal ablation that the ablated pattern within a single laser beam scanning can be controlled by tuning the laser beam intensity and radius, and both of their increase are able to create a larger feature, and vice versa. On the other hand, the thermal and optical properties of the hydrogel will continuously change responsive to the hydrogel deformation, which also would affect the quality of the laser-machining. Latter, a series experiment and characterization identified an optimal timing for conducting the laser micro-machining on the hydrogel to create a combination of maximum features, including ablated width, sidewall quality and resolution; it is at 1~2 hours drying after the gelation where the

hydrogel loses 35%~65% weight, which can be applied to a wide range of different thick hydrogel from 0.5 to 2 mm. Finally, the proof of the concept is demonstrated that the laser micro-machining technique can be applied to the hydrogel to create a scalable pattern under a rapid and cost-effective fabrication manner.

Chapter 4 focuses on the characterization of the hydrogel swelling in pH solution. At first the principle of the pH-sensitive hydrogel swelling is discussed as the counterbalance between the elastic retractive force (inward) from the hydrogel chains and the ionic osmotic pressure (outward) in the gel. Then, the swelling kinetics of the laser micro-machined hydrogel is characterized. The experiment demonstrates both the size and pH regulated swelling pattern of the hydrogel that the smaller dimension, the faster swelling rate; the higher pH, the larger swelling ratio. Next, several other important parameters are also tested through the characterization of the composite gel swelling performance. The result shows that the temperature and ionization have a positive effect on the hydrogel swelling while the crosslink density has a negative effect, matching the theoretical analysis. Finally, the hydrogel swelling induced actuation capabilities are measured. Similar to the laser-machined hydrogel, the hydrogel integrated actuators also presents a size and pH dependent performance that the bigger size or higher pH, the larger deflection of a flexible PDMS membrane. Therefore, through the laser micro-machining process, different micro-gel patterns can be rapid fabricated to fulfill different mechanical works.

The chapter 5 presented an autonomous smart capsule (9 mm in diameter and 22 mm in length) that can release its payload in the GI-tract after a tunable time delay following its passage from intestine into the small intestine. This was accomplished by using a hydrogel-based pH-triggered switch to discharge a capacitor and melt a taut nylon fuse holding a release cap through a pre-stressed rubber band. The swelling kinetics of the hydrogel and mechanical design of the switch was used to adjust the delay-time from the initiation of the swelling (passing from an acidic milieu to an alkaline one) to the closure of the switch and discharge of the capacitor. The delay could be set to within ±5 min after one hour in the small intestine (start of the swelling) increasing to ±40 min after 4 hours.

The chapter 6 developed a low-cost flexible passive patch for slow drug delivery in wound healing applications by featuring a scalable layer-by-layer fabrication technique. The patch can achieve flow rates as small as < 0.1 µl/min over an extended period of time (3 hours) at backpressures of up to 8 kPa, thus making it suitable for incorporation into wound dressings

requiring slow drug release. Using the same fabrication procedure, this patch can be expanded to a 2 × 2 array, which can release 4 times volume of a single cell. Moreover, a simplified version of the autonomous drug delivery dressings can be achieved by using poly (HEMA-co-DMAEMA) gel, which swells/shrinks as the pH decrease/increases. The result shows that the drug delivery rate can be controlled by tuning the size of the hydrogel at its equilibrium swollen state. Therefore, this wound dressing patch is able to fulfill different drug delivery requirement by either creating an n × n array or a simplified design, defined by the swelling kinetics of the selected pH-sensitive hydrogels and both featuring a layer-by-layer rapid manufactory.

# 8. FUTURE WORK

The future work can be divided into two parts that one focuses on the expanded characterization of the laser micro-machining and the swelling kinetic behavior of the hydrogel; the other is concentrated at the complemental work of the two applications.

## 8.1 Laser micro-machining on the pH-sensitive hydrogel

In this work, the laser-machining on the hydrogel has been analyzed on a 5 mm length laser ablation under one single laser beam scan, and the future work can focus on quality characterization of laser micro-machining on hydrogels within longer laser beam scan, at least cm scale, in order to achieve large scale massive micro-gels films manufactory. That is because compared to laser-engineering a single line, any complicated pattern involves the combination of multiple single laser beam scanning, curved or straight lines; and then the laser induced thermal energy is easy to be accumulated at the line-line intersections, thus causing an over etching at those places and consequently affecting the morphology of fabricated patterns. Moreover, the degree of heat accumulation is strongly dependent on the sequence of the laser ablation, which can be understood by the physical overlap of the laser beam coverage. For example, a single hydrogel square can be laser-fabricated by ablating four intersected straight lines, two vertical and two horizontal, with the fabrication procedure set to different orders. One method is to laser ablate the horizontal lines and then the vertical lines, Figure 8.1 (a); and the other can follow a clockwise direction to accomplish the square, Figure 8.1 (b). It is reasonable to conclude that the former method is expected to create more sharp corners as the heat at the four corners of the square is allowed to have more time to be dissipated than that of the latter, which however has a compromised (reduced) heat dissipation window and consequently dumps more heat (thus more thermal damage) to the corners. In addition, it is evidence that it is also feasible to modify the integrity of the designed patterns by controlling the length of the lines, as the longer line, the longer window of heat dissipation, combined with the method in the Figure 8.1 (a).

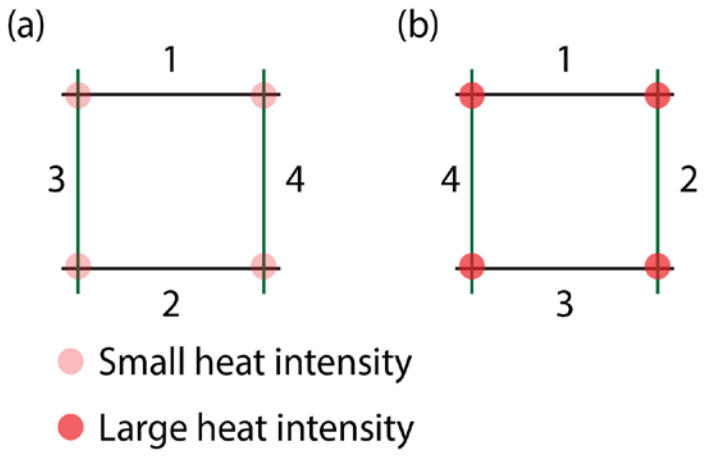


Figure 8.1 Conceptial illustion of laser-michaning a hydrogel square following the beam albation sequances of (a) horizontal-to-vertical direction; (b) clockwise direction of intercalation of one horizontol and one vertical.

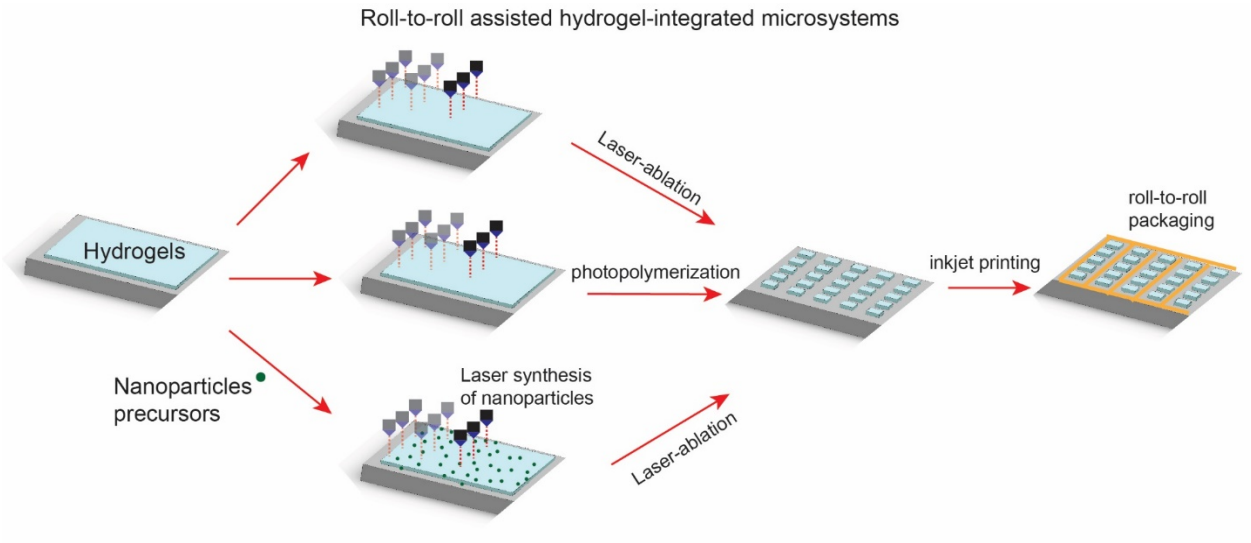


Figure 8.2 Conceptial illustion of laser-michaning and fabricate different hydrogels based micro-devices through a multifunictional roll-to-roll platform.

Actually, one major part of the future work can focus on the end-to-end micro-machining the hydrogels and fabricating the integrated system through a multiple function roll-to-roll platform, like Mirwec. As this platform can incorporate multiple rapid prototyping techniques, like laser system or inkjet printing, several different type of hydrogels are capable of being fabricated or micro-machined. Therefore, this manner offers a various methods to fabricate different types of environmental sensitive hydrogel integrated micro-systems. For example, the platform can directly

use the laser system to micro-machine the hydrogel or polymerize a photo-curable pregel solution into a crosslinked hydrogel or synthesize the embedded nanoparticles in the hydrogel network; then after laser micro-machining, the patterned micro-gels can be packaged using the inkjet printing to accomplish the final construction of the device, Figure 8.2.

## 8.2 Swelling kinetic research of the laser micro-machined hydrogel

The future work of hydrogel swelling kinetics can be divided into two parts that one is the continuous study of the swelling performance of the laser-machined hydrogels and the other is the extended experiment of the actuation capabilities of the hydrogel integrated pumping system. Regarding the swelling performance of the hydrogels, the pH range used in the current work is from 4 to 7, while a wider range can be extend to higher alkaline value as different pH ranges are required for certain distinct phases of wound healing, [113]–[115]. Up to a higher pH level, the poly (MAA-co-AAM) gel, which is the pH-sensitive hydrogel mainly used throughout the whole work, is expected to swell more or faster but within a limited degree as the largest volumetric transition of the poly (MAA-co-AAM) gel is between pH 5 to 6 [116], [117]. On the other hand, the detection limit or the sensitivity of the wireless sensing system integrating the hydrogel is one of the key value to assess a chemical sensor, whose experiment can be conducted by investigating the hydrogel deformation degree on a smaller pH step, like 0.2, instead of 1 (used in this work). By accomplishing these two set of characterization, a more comprehensive profile of the hydrogel swelling would be achieved.

Regarding the actuation performance of the hydrogel, the current experiments are concentrated at the fixed thickness of the thin PDMS membrane (0.12 mm) and the variant micro-gel patterns. Actually, different thick membranes would also affect the actuation capability of the hydrogel integrated pumping system. There are two steps that can quickly complete this extensive work. At first, a cantilever can be fixed on a universal test machine and slight put on top of a hydrogel. When the hydrogel is swelling by absorbing the water from the pH solution underneath through a porous substrate, the hydrogel would push the cantilever to deflect at the free end; therefore, by measuring the maximum deflection of the cantilever at the equilibrium swelling of the hydrogel from the following equation:

$$\delta_{max} = \frac{pl^3}{3EI} \qquad (8.1)$$

, where $\delta_{max}$ is the maximum cantilever deflection, $p$ is the load, $l$ is the cantilever length, E is the cantilever stiffness and I is the moment of inertia of the cantilever, the load also the force of the hydrogel exerting on the cantilever when it swelling can be calculated. At the same time, different patterns of the hydrogel are fabricated and their swelling deformation are monitored, thus the relationship of the mechanical force from the hydrogel swelling and the hydrogel patterns can be established, Figure 8.3 (a). The second step is to measure the maximum deflection of different thick PDMS membrane by using the universal test machine, thence the relationship between the PDMS membrane deflection and the required force is built, Figure 8.3 (b). Finally, by combining the two set of experiments, we are able to accomplish a quantitative temporal profile between the laser-machined hydrogel pattern and the deflection of flexbile PDMS membrane.

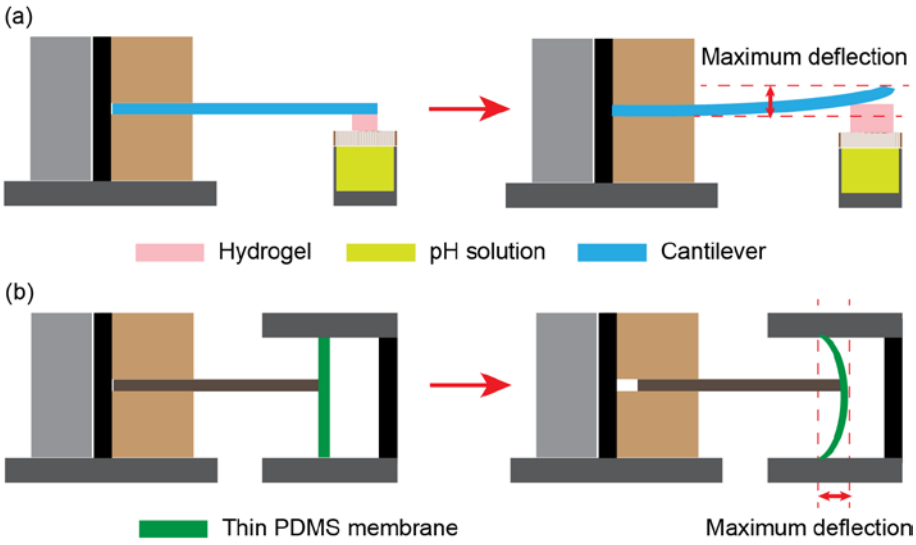


Figure 8.3 (a) Illustion of the hydrogel swelling outward force pushing the free end of a one-end fixed cantilever; (b) Demonstration of the measurement of the mechanical force used to deflect a thin PDMS membrane.

## 8.3 Biomedical applications of the laser-machined pH-sensitive hydrogel

From the chapter 5 to 6, two biomedical applications based on the hydrogel are introduced, including two autonomous drug delivery devices for chronic wound dressing and small intestine targeted drug release respectively. Except for the validation of their functionalities in large animal models, there are still some future work which can be rapidly finished after the complete of the extended characterization of both the hydrogel swelling and actuation performance as these two

features are the essential basis to accomplish all the three applications.

Regarding the smart capsule, one of its key feature is the tunability of the drug release, whose accuracy can reach ±5 min after one hour in the small intestine increasing to ±40 min after 4 hours; hence, the continuous work can focus on the improvement of the precision or higher resolution of the release time. Currently, the isolation gap to close the original opened electrical switch is set to the step of 0.2 mm, so the extended characterization can start by setting the gap down to 0.1 mm per step. Actually, as the time delay controllability is mainly dependent on the actuation capabilities of the hydrogel based pump; therefore, a preliminary conclusion of whether the improvement of the tunability can be achieve or not is able to be provided after finishing the future work of the actuation characterization. Moreover, since the deflection of flexbile PDMS membrane is linearly proportional to the load induced by the hydrogel swelling, the 0.1 mm per step or higher spatial resolution is achievable theoretically.

Regarding the pH-regulated chronic wound dressing, the future work would be concentrated at the robustness test at first. Currently, all the characterization of the drug delivery performance of this device is on a flat platform, and thus the further test can be set to put the device upon a curvature place. Under this situation, the device would be folded into a certain degree, which could against the drug out of the original opened outlets (the two hydrophobic microchannels). Therefore, the test protocol wound consist of selecting several typical curvature to represent the form of human arms or foot (the positions that the chronic would occurs frequently) at first and then measuring the drug volume from folding the device and the hydrogel swelling respectively. In addition, the current drug delivery capability is based on a 4 mm × 1 mm hydrogel film, and the pattern of the hydrogel can be further laser-machined to smaller size; therefore, the improvement of both the spatial resolution and coverage of the drug delivery can be achieved by increasing the 2 × 2 array to n × n (n > 2) at the same time.

## 8.4 Machining learning incorporated into the hydrogel micro-machining

Recently, machining learning become an advanced computational tool that is significantly incorporated and will continuously involve into all aspects of the health care or medical regions, like prediction, prevention or personalization, [118]–[121]. The same concept actually can be applied into the laser-machining of hydrogels that as different sensing or actuating biomedical applications have different requirement regarding to the hydrogel size-dependent swelling kinetics,

which are also regulated by the external environmental stimuli, all the measurement results from a variety of the combination of these factors can be collected as the input for the machine learning; therefore, a profile/pattern between the micro-machined hydrogel and the integrated system performance is expected to be achieve, whose establishment would in turn guide the initial design and processing of laser micro-fabrications, Figure 8.4.

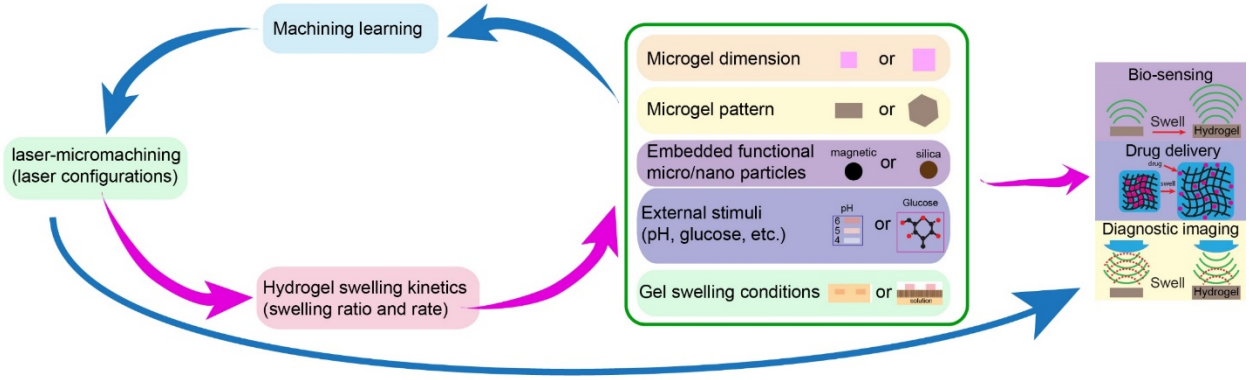


Figure 8.4 Illustion of the hydrogel swelling kinetics regulated and biomedical applications targeted expeiment results as the input for the machining learning, which can be used in turn to guide the laser micro-machining process.

## 8.5 Conclusion

The sections above outline various research directions to further develop this work with the ultimate goal being the development of the rapid and scalable laser micro-patterned pH-sensitive hydrogels, which can expand their applications into more micro biomedical systems requiring a high tempo-spatial resolution/controllability.

# REFERENCES


[1] R. A. Siegel, Y. Gu, M. Lei, A. Baldi, E. E. Nuxoll, and B. Ziaie, “Hard and soft micro- and nanofabrication: An integrated approach to hydrogel-based biosensing and drug delivery,” *J. Control. Release*, vol. 141, no. 3, pp. 303–313, 2010.

[2] P. Gupta, K. Vermani, and S. Garg, “Hydrogels: From controlled release to pH-responsive drug delivery,” *Drug Discov. Today*, vol. 7, no. 10, pp. 569–579, 2002.

[3] S. A.-A. and G. O. P. Syed K. H. Gulrez, “World ’s largest Science , Technology & Medicine Open Access book publisher Hydrogels : Methods of Preparation , Characterisation and Applications,” in *Progress in Molecular and Environmental Bioengineering - From Analysis and Modeling to Technology Applications*, 2011, p. 118.

[4] R. A. Siegel, “Stimuli sensitive polymers and self regulated drug delivery systems: A very partial review,” *J. Control. Release*, vol. 190, pp. 337–351, 2014.

[5] T. Garg, S. Singh, and A. Goyal, “Stimuli-sensitive hydrogels: an excellent carrier for drug and cell delivery,” *Crit. Revews Ther. Drug Carr. Syst.*, vol. 30, no. 5, pp. 369–409, 2013.

[6] R. Masteiková, Z. Chalupová, Z. Sklubalová, and C. Z. Masteikova R, “Stimuli-sensitive hydrogels in controlled and sustained drug delivery.,” *Medicina (Kaunas).*, vol. 39 Suppl 2, no. 2, pp. 19–24, 2003.

[7] X. Zhao, J. Kim, C. A. Cezar, N. Huebsch, K. Lee, K. Bouhadir, and D. J. Mooney, “Active scaffolds for on-demand drug and cell delivery,” *Proc. Natl. Acad. Sci. U. S. A.*, vol. 108, no. 1, pp. 67–72, 2011.

[8] R. Bashir, J. Z. Hilt, O. Elibol, A. Gupta, and N. A. Peppas, “Micromechanical cantilever as an ultrasensitive pH microsensor,” *Appl. Phys. Lett.*, vol. 81, no. 16, pp. 3091–3093, 2002.

[9] A. Baldi, Y. Gu, P. E. Loftness, R. A. Siegel, and B. Ziaie, “A hydrogel-actuated environmentally sensitive microvalve for active flow control,” *J. Microelectromechanical Syst.*, vol. 12, no. 5, pp. 613–621, 2003.

[10] J. H. Holtz and S. A. Asher, “Polymerized colloidal crystal hydrogel films as intelligent chemical sensing materials.,” *Nature*, vol. 389, pp. 829–832, 1997.

[11] M. Lei, A. Baldi, E. Nuxoll, R. A. Siegel, and B. Ziaie, “Hydrogel-based microsensors for wireless chemical monitoring,” *Biomed. Microdevices*, vol. 11, no. 3, pp. 529–538, 2009.

[12] A. Richter, G. Paschew, S. Klatt, J. Lienig, K.-F. Arndt, and H.-J. P. Adler, “Review on Hydrogel-based pH Sensors and Microsensors,” *Sensors*, vol. 8, no. 1, pp. 561–581, 2008.

[13] J. H. Park, A. Kim, H. Jiang, S. H. Song, J. Zhou, and B. Ziaie, “A Wireless Chemical Sensing Scheme using Ultrasonic Imaging of Silica-Particle-Embedded Hydrogels (Silicagel),” *Sensors Actuators B Chem.*, vol. 259, pp. 552–559, 2018.

[14] S. Singamaneni and V. V. Tsukruk, “Buckling instabilities in periodic composite polymeric materials,” *Soft Matter*, vol. 6, no. 22, p. 5681, 2010.

[15] Y. LiChunfang Li, Z. Hu, Y. Li, and C. Li, “Pattern formation of constrained acrylamide/sodium acrylate copolymer gels in acetone/water mixture,” *J. Chem. Phys.*, vol. 100, no. 4637, 1994.

[16] T. Tanaka, “KINETICS OF PHASE TRANSITION IN POLYMER GELS,” *Physica*, vol. 140A, pp. 261–268, 1986.

[17] M. D. Tang, A. P. Golden, and J. Tien, “Molding of Three-Dimensional Microstructures of Gels,” *J. Am. Chem. Soc.*, vol. 125, no. 43, pp. 12988–12989, 2003.

[18] B. Ziaie, A. Baldi, M. Lei, Y. Gu, and R. A. Siegel, “Hard and soft micromachining for BioMEMS: Review of techniques and examples of applications in microfluidics and drug delivery,” *Adv. Drug Deliv. Rev.*, vol. 56, no. 2, pp. 145–172, 2004.

[19] D. J. Beebe, J. S. Moore, J. M. Bauer, Q. Yu, R. H. Liu, C. Devadoss, and B.-H. Jo, “Functional hydrogel structures for autonomous flow control inside microfluidic channels : Abstract : Nature,” *Nature*, vol. 404, no. 6778, pp. 588–590, 2000.

[20] M. Lei, Y. D. Gu, A. Baldi, R. A. Siegel, and B. Ziaie, “Soft mold-dry etch: A novel hydrogel patterning technique for biomedical applications,” *Proc. 26th Annu. Int. Conf. Ieee Eng. Med. Biol. Soc. Vols 1-7*, vol. 26, p. 1983–1986 5459, 2004.

[21] Z. Ding, A. Salim, and B. Ziaie, “Squeeze-film hydrogel deposition and dry micropatterning.,” *Anal. Chem.*, vol. 82, no. 8, pp. 3377–82, 2010.

[22] A. R. Khare and N. a. Peppas, “Swelling/deswelling of anionic copolymer gels,” *Biomaterials*, vol. 16, no. 7, pp. 559–567, 1995.

[23] W. Oppermann, “Swelling Behavior and Elastic Properties of Ionic Hydrogels,” *Polyelectrolyte Gels - Prop. Prep. Appl.*, p. 159, 1992.

[24] D. Rees and T. H. Jenkins, “pH Profile of Gut as Measured by Radiotelemetry Capsule,” *Br. Med. J.*, vol. 2, no. April, pp. 104–106, 1972.

[25] D. F. Evans, G. Pye, R. Bramley, A. G. Clark, T. J. Dyson, and J. D. Hardcastle, “Measurement of Gastrointestinal Ph Profiles in Normal Ambulant Human-Subjects,” *Gut*, vol. 29, no. 8, pp. 1035–1041, 1988.

[26] A. A. Deshpande, C. T. Rhodes, and M. Danish, “**Intravaginal drug delivery**,” *Drug Dev. Ind. Pharm.*, vol. 18, no. 11–12, pp. 1225–1279, 1992.

[27] R. A. Siegel, M. Falamarzian, B. A. Firestone, and B. C. Moxley, “pH-Controlled release from hydrophobic/polyelectrolyte copolymer hydrogels,” *J. Control. Release*, vol. 8, no. 2, pp. 179–182, 1988.

[28] V. R. Patel and M. M. Amiji, “Preparation and characterization of freeze-dried chitosan-poly(ethylene oxide) hydrogels for site-specific antibiotic delivery in the stomach,” *Pharmaceutical Research*, vol. 13, no. 4. pp. 588–593, 1996.

[29] R. K. Mishra, K. Ramasamy, N. a. Ahmad, Z. Eshak, and a. B. a Majeed, “pH dependent poly[2-(methacryloyloxyethyl)trimetylammonium chloride-co-methacrylic acid]hydrogels for enhanced targeted delivery of 5-fluorouracil in colon cancer cells,” *J. Mater. Sci. Mater. Med.*, vol. 25, no. 4, pp. 999–1012, 2014.

[30] E. Ryjkina, H. Kuhn, H. Rehage, F. Müller, and J. Peggau, “pH-Responsive Polymer Microspheres: Rapid release of Encapsulated Material within the Range of Intracellular pH,” *Angew. Chem. Int. Ed. Engl.*, vol. 41, no. 6, pp. 983–6, 2002.

[31] K. E. Broaders, S. J. Pastine, S. Grandhe, and J. M. J. Frehet, “Acid-degradable solid-walled microcapsules for pH-responsive burst-release drug deliveryw,” *Chem. Commun*, vol. 47, pp. 665–667, 2011.

[32] N. Murthy, M. Xu, S. Schuck, J. Kunisawa, N. Shastri, and J. M. J. Frechet, “A macromolecular delivery vehicle for protein-based vaccines: Acid-degradable protein-loaded microgels,” *Proc. Natl. Acad. Sci.*, vol. 100, no. 9, pp. 4995–5000, 2003.

[33] C. Ramkissoon-Ganorkar, F. Liu, M. Baudys, and S. W. Kim, “Modulating insulin-release profile from pH / thermosensitive polymeric beads through polymer molecular weight,” *J. Control. Release*, vol. 59, no. 3, pp. 287–298, Jun. 1999.

[34] L. Wang, M. Liu, C. Gao, L. Ma, and D. Cui, “A pH-, thermo-, and glucose-, triple-responsive hydrogels: Synthesis and controlled drug delivery,” *React. Funct. Polym.*, vol. 70, pp. 159–167, 2009.

[35] C. M. Hassan, F. J. Doyle, and N. A. Peppas, “Dynamic Behavior of Glucose-Responsive Poly(methacrylic acid- g -ethylene glycol) Hydrogels,” *Macromolecules*, vol. 30, no. 20, pp. 6166–6173, 1997.

[36] G. Albin, T. A. Horbett, and B. D. Ratner, “Glucose sensitive membranes for controlled delivery of insulin: Insulin transport studies,” *J. Control. Release*, vol. 2, no. C, pp. 153–164, 1985.

[37] D. a LaVan, T. McGuire, and R. Langer, “Small-scale systems for in vivo drug delivery.,” *Nat. Biotechnol.*, vol. 21, no. 10, pp. 1184–1191, 2003.

[38] H. He, X. Cao, and L. J. Lee, “Design of a novel hydrogel-based intelligent system for controlled drug release,” *J. Control. Release*, vol. 95, no. 3, pp. 391–402, 2004.

[39] H. Li, G. Go, S. Y. Ko, J.-O. Park, and S. Park, “Magnetic actuated pH-responsive hydrogel-based soft micro-robot for targeted drug delivery,” *Smart Mater. Struct.*, vol. 25, no. 2, p. 027001, 2016.

[40] C. R. Gordijo, K. Koulajian, A. J. Shuhendler, L. D. Bonifacio, H. Y. Huang, S. Chiang, G. A. Ozin, A. Giacca, and X. Y. Wu, “Nanotechnology-enabled closed loop insulin delivery device: In vitro and in vivo evaluation of glucose-regulated insulin release for diabetes control,” *Adv. Funct. Mater.*, vol. 21, no. 1, pp. 73–82, 2011.

[41] R. Mackay and B. Jacobson, “Endoradiosonde,” *Nature*, vol. 179, pp. 1239–1240, 1957.

[42] V. Sridhar and K. Takahata, “A hydrogel-based passive wireless sensor using a flex-circuit inductive transducer,” *Sensors Actuators, A Phys.*, vol. 155, no. 1, pp. 58–65, 2009.

[43] M. P. Orthner, G. Lin, M. Avula, S. Buetefisch, J. Magda, L. W. Rieth, and F. Solzbacher, “Hydrogel based sensor arrays (2 x 2) with perforated piezoresistive diaphragms for metabolic monitoring (in vitro),” *Sensors Actuators, B Chem.*, vol. 145, no. 2, pp. 807–816, 2010.

[44] G. Gerlach, M. Guenther, J. Sorber, G. Suchaneck, K. F. Arndt, and A. Richter, “Chemical and pH sensors based on the swelling behavior of hydrogels,” *Sensors Actuators, B Chem.*, vol. 111–112, no. SUPPL., pp. 555–561, 2005.

[45] M. Guenther, G. Gerlach, and T. Wallmersperger, “Piezoresistive biochemical sensors based on hydrogels,” *Microsyst. Technol.*, vol. 16, no. 5, pp. 703–715, 2010.

[46] C. L. Chang, Z. Ding, V. N. L. R. Patchigolla, B. Ziaie, and C. A. Savran, “Reflective diffraction gratings from hydrogels as biochemical sensors,” *IEEE Sens. J.*, vol. 12, no. 7, pp. 2374–2379, 2012.

[47] M. Ochoa, H. Jiang, J. H. Park, A. Otte, R. Pinal, and B. Ziaie, “Nanoparticle-enabled wireless monitoring and characterization of physical degradation kinetics in pharmaceutical gelatin films,” *Sensors Actuators, A Phys.*, vol. 241, 2016.

[48] H. Jiang, M. Ochoa, J. H. Park, A. Otte, R. Pinal, and B. Ziaie, “Wireless screenning of degradation kinetics in pharmaceutical gelatin films,” in *2015 Transducers - 2015 18th International Conference on Solid-State Sensors, Actuators and Microsystems, TRANSDUCERS 2015*, 2015.

[49] M. Lei, A. Baldi, E. Nuxoll, R. A. Siegel, and B. Ziaie, “A hydrogel-based implantable micromachined transponder for wireless glucose measurement.,” *Diabetes Technol. Ther.*, vol. 8, no. 1, pp. 112–122, 2006.

[50] S. H. Song, J. H. Park, G. Chitnis, R. a. Siegel, and B. Ziaie, “A wireless chemical sensor featuring iron oxide nanoparticle-embedded hydrogels,” *Sensors Actuators, B Chem.*, vol. 193, pp. 925–930, 2014.

[51] J. Shin, P. V. Braun, and W. Lee, “Fast response photonic crystal pH sensor based on templated photo-polymerized hydrogel inverse opal,” *Sensors Actuators, B Chem.*, vol. 150, no. 1, pp. 183–190, 2010.

[52] S. A. Asher and J. H. Holtz, “Polymerized colloidal crystal hydrogel film as intelligent chemical sensing materials,” *Nature*, vol. 389, no. 6653, pp. 829–832, 1997.

[53] S. H. Song, J. H. Park, G. Chitnis, R. A. Siegel, and B. Ziaie, “A wireless chemical sensor featuring iron oxide nanoparticle-embedded hydrogels,” *Sensors Actuators B Chem.*, vol. 193, pp. 925–930, Mar. 2014.

[54] J.T. Verdeyen, *laser-electronics-prentice-hall-1995*. 1995.

[55] S. Mishra and V. Yadava, “Laser Beam MicroMachining (LBMM) - A review,” *Opt. Lasers Eng.*, vol. 73, pp. 89–122, 2015.

[56] A. S. Holmes, “Laser fabrication and assembly processes for MEMS,” *Proc. SPIE*, vol. 4274, pp. 297–306, 2001.

[57] C. A. Aguilar, Y. Lu, S. Mao, and S. Chen, “Direct micro-patterning of biodegradable polymers using ultraviolet and femtosecond lasers,” *Biomaterials*, vol. 26, no. 36, pp. 7642–7649, 2005.

[58] M. A. Roberts, J. S. Rossier, P. Bercier, and H. Girault, “UV laser machined polymer substrates for the development of microdiagnostic systems,” *Anal. Chem.*, vol. 69, no. 11, pp. 2035–2042, 1997.

[59] D. Knittel and E. Schollmeyer, “Surface structuring of synthetic polymers by UV-laser irradiation. Part IV. Applications of excimer laser induced surface modification of textile materials,” *Polym. Int.*, vol. 45, no. 1, pp. 110–117, 1998.

[60] V. V. Kancharla and S. Chen, “Fabrication of biodegradable polymeric micro-devices using laser micromachining,” *Biomed. Microdevices*, vol. 4, no. 2, pp. 105–109, 2002.

[61] C. G. K. Malek, “Laser processing for bio-microfluidics applications (part II),” *Anal Bioanal Chem*, vol. 385, pp. 1362–1369, 2006.

[62] H. Klank, J. P. Kutter, and O. Geschke, “CO2-laser micromachining and back-end processing for rapid production of PMMA-based microfluidic systems,” *Lab Chip*, vol. 2, no. 4, p. 242, 2002.

[63] D. Snakenborg, H. Klank, and J. P. Kutter, “Microstructure fabrication with a Co2 laser system,” *J. Micromechanics Microengineering*, vol. 14, no. 2, pp. 182–189, 2004.

[64] D. Yuan and S. Das, “Experimental and theoretical analysis of direct-write laser micromachining of polymethyl methacrylate by CO2 laser ablation,” *J. Appl. Phys.*, vol. 101, no. 2, p. 024901, 2007.

[65] S. Darvishi, T. Cubaud, and J. P. Longtin, “Ultrafast laser machining of tapered microchannels in glass and PDMS,” *Opt. Lasers Eng.*, vol. 50, pp. 210–214, 2011.

[66] A. L. Mckenzie, “How far does thermal damage extend beneath the surface of CO 2 laser incisions?,” *Phys. Med. Biol. Phys. Med. Biol*, vol. 28, no. 8, pp. 905–912, 1983.

[67] A. Issa, D. Brabazon, and M. S. J. Hashmi, “3D transient thermal modelling of laser microchannel fabrication in lime-soda glass,” *J. Mater. Process. Technol.*, vol. 207, no. 1–3, pp. 307–314, 2008.

[68] X. Xie, D. Li, T.-H. Tsai, J. Liu, P. V. Braun, and D. G. Cahill, “Thermal Conductivity, Heat Capacity, and Elastic Constants of Water-Soluble Polymers and Polymer Blends,” *Macromolecules*, vol. 49, no. 3, pp. 972–978, 2016.

[69] J. a Viator, B. Choi, G. M. Peavy, S. Kimel, and J. S. Nelson, “Spectra from 2.5-15 microm of tissue phantom materials, optical clearing agents and ex vivo human skin: implications for depth profiling of human skin.,” *Phys. Med. Biol.*, vol. 48, no. 2, pp. N15-24, 2003.

[70] J. Rička and T. Tanaka, “Swelling of Ionic Gels: Quantitative Performance of the Donnan Theory,” *Macromolecules*, vol. 17, no. 12, pp. 2916–2921, 1984.

[71] L. Brannon-Peppas and N. A. Peppas, “Equilibrium swelling behavior of pH-sensitive hydrogels,” *Chem. Eng. Sci.*, vol. 46, no. 3, pp. 715–722, 1991.

[72] K. S. De, N. R. Aluru, B. Johnson, W. C. Crone, D. J. Beebe, and J. Moore, “Equilibrium swelling and kinetics of pH-responsive hydrogels: Models, experiments, and simulations,” *J. Microelectromechanical Syst.*, vol. 11, no. 5, pp. 544–555, 2002.

[73] K. Gawel, D. Barriet, M. Sletmoen, and B. T. Stokke, “Responsive Hydrogels for Label-Free signal transduction within biosensors,” *Sensors*, vol. 10, no. 5, pp. 4381–4409, 2010.

[74] J. P. Baker, H. W. Blanch, and J. M. Prausnitzt, “Swelling properties of acrylamide-based ampholytic hydrogels: comparison of experiment with theory,” *Polymer (Guildf).*, vol. 36, no. 5, pp. 1061–1069, 1995.

[75] F. Ganji, S. Vasheghani-Farahani, and E. Vasheghani-Farahani, “Theoretical Description of Hydrogel Swelling: A Review,” *Iran. Polym. J.*, vol. 19, no. 5, pp. 375–398, 2010.

[76] R. Huggins, “Statistical Mechanics of Cross-Linked Polymer Networks,” *J. Adhes.*, vol. 11, no. 11, pp. 521–526, 1943.

[77] M. E. Weber, D. G. Cooper, J. H. Vera, and E. V. Farahani, “Swelling of Ionic Gels in Electrolyte Solutions,” *Ind. Eng. Chem. Res.*, vol. 29, no. 4, pp. 554–560, 1990.

[78] Y. Li and T. Tanaka, “Kinetics of swelling and shrinking of gels,” *J. Chem. Phys.*, vol. 92, no. 2, pp. 1365–1371, 1990.

[79] H. Jiang, W. Yu, J. Zhou, and B. Ziaie, “A pH-SENSITIVE HYDROGEL-BASED SMART SWITCH FOR GI-TRACT PAYLOAD RELEASE,” *Proc. IEEE Int. Conf. Micro Electro Mech. Syst.*, pp. 510–513, 2017.

[80] H. Jiang, W. Yu, M. Oscai, and B. Ziaie, “A Smart Capsule with a Hydrogel-Based pH-Triggered Release Switch for GI-Tract Site-Specific Drug Delivery,” *IEEE Trans. Biomed. Eng.*, "DOI: 10.1109/TBME.2018.2818463", 2018.

[81] R. Liu, S. Liang, X.-Z. Tang, D. Yan, X. Li, and Z.-Z. Yu, “Tough and highly stretchable graphene oxide/polyacrylamide nanocomposite hydrogels,” *J. Mater. Chem.*, vol. 22, p. 14160, 2012.

[82] K. Van Durme, B. Van Mele, W. Loos, and F. E. Du Prez, “Introduction of silica into thermo-responsive poly(N-isopropyl acrylamide) hydrogels: A novel approach to improve response rates,” *Polymer (Guildf).*, vol. 46, pp. 9851–9862, 2005.

[83] S. G. Starodoubtsev, N. A. Churochkina, and A. R. Khokhlov, “Hydrogel Composites of Neutral and Slightly Charged Poly(acrylamide) Gels with Incorporated Bentonite. Interaction with Salt and Ionic Surfactants,” *Langmuir*, vol. 16, pp. 1529–1534, 2000.

[84] S. H. Behrens and D. G. Grier, “The charge of glass and silica surfaces,” *J. Chem. Phys.*, vol. 115, no. 14, pp. 6716–6721, 2001.

[85] I. R. Wilding, “Site-specific drug delivery in the gastrointestinal tract.” Critical Reviews™ in Therapeutic Drug Carrier Systems 17, no. 6 (2000).

[86] N. A. Liechty, W. B., Kryscio, D.R., Slaughter, B. V. and Peppas, “Polymers for drug delivery systems,” *Annu. Rev. Chem. Biomol. Eng.*, vol. 1, pp. 149–173, 2010.

[87] K. Sato, K. Yoshida, S. Takahashi, and J. I. Anzai, “PH- and sugar-sensitive layer-by-layer films and microcapsules for drug delivery,” *Adv. Drug Deliv. Rev.*, vol. 63, no. 9, pp. 809–821, 2011.

[88] A. Göpferich, “Bioerodible implants with programmable drug release,” *J. Control. Release*, vol. 44, no. 2–3, pp. 271–281, 1997.

[89] I. Wilding, P. Hirst, and a Connor, “Development of a new engineering-based capsule for human drug absorption studies.,” *Pharm. Sci. Technolo. Today*, vol. 3, no. 11, pp. 385–392, 2000.

[90] I. R. Wilding and D. V Prior, “Remote controlled capsules in human drug absorption (HDA) studies.,” *Crit. Rev. Ther. Drug Carrier Syst.*, vol. 20, no. 6, pp. 405–431, 2003.

[91] M. E. A. McGirr, S. M. McAllister, E. E. Peters, A. W. Vickers, A. F. Parr, and A. W. Basit, “The use of the InteliSite?? Companion device to deliver mucoadhesive polymers to the dog colon,” *Eur. J. Pharm. Sci.*, vol. 36, no. 4–5, pp. 386–391, 2009.

[92] W. Yu, R. Rahimi, M. Ochoa, R. Pinal, and B. Ziaie, “A smart capsule with GI-tract-location-specific payload release,” *IEEE Trans. Biomed. Eng.*, vol. 62, no. 9, pp. 2289–2295, 2015.

[93] P. J. Van Der Schaar, J. F. Dijksman, H. Broekhuizen-De Gast, J. Shimizu, N. Van Lelyveld, H. Zou, V. Iordanov, C. Wanke, and P. D. Siersema, “A novel ingestible electronic drug delivery and monitoring device,” *Gastrointest. Endosc.*, vol. 78, no. 3, pp. 520–528, 2013.

[94] Y. Qiu and K. Park, “Environment-sensitive hydrogels for drug delivery,” *Adv. Drug Deliv. Rev.*, vol. 64, no. SUPPL., pp. 49–60, 2012.

[95] D. N. Bateman and T. a Whittingham, “Measurement of gastric emptying by real-time ultrasound.,” *Gut*, vol. 23, no. 6, pp. 524–527, 1982.

[96] D. Cassilly, S. Kantor, L. C. Knight, a. H. Maurer, R. S. Fisher, J. Semler, and H. P. Parkman, “Gastric emptying of a non-digestible solid: Assessment with simultaneous SmartPill pH and pressure capsule, antroduodenal manometry, gastric emptying scintigraphy,” *Neurogastroenterol. Motil.*, vol. 20, no. 4, pp. 311–319, 2008.

[97] L. Marciani, P. A. Gowland, A. Fillery-travis, P. Manoj, J. Wright, A. Smith, P. Young, R. Moore, R. C. Spiller, L. Marciani, P. A. Gowland, A. Fillery-travis, P. Manoj, J. Wright, A. Smith, P. Young, R. Moore, R. C. Spiller, P. A. Gowland, A. Fillery-, P. Manoj, J. Wright, A. Smith, P. Young, R. Moore, and R. C. S. As-, “Assessment of antral grinding of a model solid meal with echo-planar imaging,” *Am. J. Physiol. Gastrointesti liver phsiol*, vol. 280, pp. 844–849, 2001.

[98] F. Kong and R. P. Singh, “Disintegration of solid foods in human stomach,” *J. Food Sci.*, vol. 73, no. 5, pp. 67–80, 2008.

[99] A. Tharakan, I. T. Norton, P. J. Fryer, and S. Bakalis, “Mass transfer and nutrient absorption in a simulated model of small intestine,” *J. Food Sci.*, vol. 75, no. 6, 2010.

[100] A. Stojadinovic, J. W. Carlson, G. S. Schultz, T. A. Davis, and E. A. Elster, “Topical advances in wound care,” *Gynecol. Oncol.*, vol. 111, pp. S70–S80, 2008.

[101] L. K. Branski, G. G. Gauglitz, D. N. Herndon, and M. G. Jeschke, “A review of gene and stem cell therapy in cutaneous wound healing,” *burns*, vol. 35, pp. 171–180, 2009.

[102] M. Ochoa, R. Rahimi, and B. Ziaie, “Flexible sensors for chronic wound management,” *IEEE Rev. Biomed. Eng.*, vol. 7, pp. 73–86, 2014.

[103] J. S. Boateng, K. H. Matthews, H. N. E. Stevens, and G. M. Eccleston, “Wound healing dressings and drug delivery systems: A review,” *J. Pharm. Sci.*, vol. 97, no. 8, pp. 2892–2923, 2008.

[104] T. R. Dargaville, B. L. Farrugia, J. A. Broadbent, S. Pace, Z. Upton, and N. H. Voelcker, “Sensors and imaging for wound healing: A review,” *Biosens. Bioelectron.*, vol. 41, no. 1, pp. 30–42, 2013.

[105] T. Thimma Reddy and A. Takahara, “Simultaneous and sequential micro-porous semi-interpenetrating polymer network hydrogel films for drug delivery and wound dressing applications,” *Polymer (Guildf).*, vol. 50, no. 15, pp. 3537–3546, 2009.

[106] V. Ntziachristos, a G. Yodh, M. Schnall, and B. Chance, “Concurrent MRI and diffuse optical tomography of breast after indocyanine green enhancement.,” *Proc. Natl. Acad. Sci. U. S. A.*, vol. 97, no. 6, pp. 2767–2772, 2000.

[107] R. A. Shimkunas, E. Robinson, R. Lam, S. Lu, X. Xu, X. Q. Zhang, H. Huang, E. Osawa, and D. Ho, “Nanodiamond-insulin complexes as pH-dependent protein delivery vehicles,” *Biomaterials*, vol. 30, no. 29, pp. 5720–5728, 2009.

[108] S. Schreml, R. J. Meier, O. S. Wolfbeis, M. Landthaler, R.-M. Szeimies, and P. Babilas, “2D luminescence imaging of pH in vivo.,” *Proc. Natl. Acad. Sci. U. S. A.*, vol. 108, pp. 2432–2437, 2011.

[109] H. Wells, J. Youmans, and D. M. Jr, “Tissue pressure (intracutaneous, subcutaneous, and intramuscular) as related to venous pressure, capillary filtration, and other factors,” *J. Clin. …*, pp. 489–499, 1938.

[110] M. Ochoa, C. Mousoulis, and B. Ziaie, “Polymeric microdevices for transdermal and subcutaneous drug delivery,” *Adv. Drug Deliv. Rev.*, vol. 64, no. 14, pp. 1603–1616, 2012.

[111] C. S. Satish and H. G. Shivakumar, “Formulation and evaluation of self-regulated insulin delivery system based on poly (HEMA-co-DMAEMA) hydrogels,” *J. Macromol. Sci.*, vol. 44, no. January, pp. 379–387, 2007.

[112] T. Traitel, Y. Cohen, and J. Kost, “Characterization of glucose-sensitive insulin release systems in simulated in vivo conditions,” *Biomaterials*, vol. 21, no. 16, pp. 1679–1687, 2000.

[113] D. A. Jankowska, M. B. Bannwarth, C. Schulenburg, G. Faccio, K. Maniura-Weber, R. M. Rossi, L. Scherer, M. Richter, and L. F. Boesel, “Simultaneous detection of pH value and glucose concentrations for wound monitoring applications,” *Biosens. Bioelectron.*, vol. 87, pp. 312–319, 2017.

[114] L. A. Schneider, A. Korber, S. Grabbe, and J. Dissemond, “Influence of pH on wound-healing: A new perspective for wound-therapy?,” *Arch. Dermatol. Res.*, vol. 298, no. 9, pp. 413–420, 2007.

[115] M. A. Khan, U. Ansari, and M. N. Ali, “Real-time wound management through integrated pH sensors: a review,” *Sens. Rev.*, vol. 35, no. 2, pp. 183–189, 2015.

[116] S. Matsumura, A. R. Hlil, C. Lepiller, J. Gaudet, D. Guay, Z. Shi, S. Holdcroft, and A. S. Hay, “Introduction of pH-Sensitivity into Mechanically Strong Nanoclay Composite Hydrogels Based on N-isopropylacrylamide,” *Am. Chem. Soc. Polym. Prepr. Div. Polym. Chem.*, vol. 49, no. 1, pp. 511–512, 2008.

[117] H. Ni, H. Kawaguchi, and T. Endo, “Preparation of pH-sensitive hydrogel microspheres of poly(acrylamide-co-methacrylic acid) with sharp pH–volume transition,” *Colloid Polym. Sci.*, vol. 285, no. 7, pp. 819–826, 2007.

[118] J. Larry Jameson and D. L. Longo, “Precision Medicine—Personalized, Problematic, and Promising,” *Obstet. Gynecol. Surv.*, vol. 70, no. 10, pp. 612–614, 2015.

[119] C. Wang, P. Xu, L. Zhang, J. Huang, K. Zhu, and C. Luo, “Current Strategies and Applications for Precision Drug Design,” *Front. Pharmacol.*, vol. 9, no. July, pp. 1–19, 2018.

[120] N. E. W. Engla, N. D. Journal, and J. D. Cherry, “A New Initiative on Precision Medicine,” *N. Engl. J. Med.*, pp. 1–4, 2012.

[121] M. Puri, A. Solanki, T. Padawer, S. M. Tipparaju, W. A. Moreno, and Y. Pathak, *Introduction to Artificial Neural Network (ANN) as a Predictive Tool for Drug Design, Discovery, Delivery, and Disposition: Basic Concepts and Modeling. Basic Concepts and Modeling*. Elsevier Inc., 2015.

# VITA

Hongjie Jiang received the M.S. degree in electrical engineering from the Beijing Institute of Technology, Beijing, China in 2005. He is currently pursuing a Ph.D. degree in electrical and computer engineering at Purdue University. Since 2013 he has been a research assistant with the Ziaie Biomedical Microdevices Laboratory at Purdue. His research focuses on the development of rapid and scalable micro-machined hydrogels integrated platforms for biomedical applications, including the pH-regulated drug delivery for chronic dermal wound (wound dressing) and GI tract (smart capsule).

# PUBLICATIONS

## JOURNAL PUBLICATIONS (7)

**H. Jiang**, W. Yu, M. Oscai, and B. Ziaie, "A Smart Capsule with a Hydrogel-Based pH-Triggered Release Switch for GI-Tract Site-Specific Drug Delivery," *IEEE Transactions on Biomedical Engineering*, vol. PP, 2018.

M. Ochoa, **H. Jiang**, J. H. Park, A. Otte, R. Pinal, and B. Ziaie, "Nanoparticle-enabled wireless monitoring and characterization of physical degradation kinetics in pharmaceutical gelatin films," *Sens. Actuators A: Phys.*, vol. 241, 2016, pp. 238–244.

J.H. Park, A. Kim, **H. Jiang**, S.H.Song, J. Zhou and B. Ziaie, "A wireless chemical sensing scheme using ultrasonic imaging of silica-particle-embedded hydrogels (silicagel),"*Sensors and Actuators B, 259 (2018),* 552–559.

**H. Jiang**, M. Ochoa, V. Jain, and B. Ziaie, "A laser-customizable insole for selective topical oxygen delivery to diabetic foot ulcers", *MRS communication*, 1-7, 2018.

**H. Jiang**, M. Ochoa, and B. Ziaie, "Laser-treated glass platform for rapid wicking-driven transport and particle separation in bio-microfluidics," *ACS Applied Materials & Interfaces*, 2018 (under review).

**H. Jiang**, J. H. Park, and B. Ziaie, "Susceptibility of Stimuli-Responsive Hydrogels with Embedded Magnetic Microparticles," *Applied Physical Letters*, 2018 (under review).

Zhou. J, Samaddar. S, Ochoa. M, Rahimi. **R, Jiang H**, Thompson. D.H, and Ziaie. B. "A Rapid 3D-Print-Assisted Fabrication for Biodegradable Microneedles Loaded with DNA Complex." *J Controlled Release,* 2018 (under review).

**CONFERENCES PUBLICATIONS (11)**

**H. Jiang**, W. Yu, J. Zhou, and B. Ziaie, "A pH-sensitive hydrogel-based smart switch for GI-tract payload release", *MEMS 2017, Las Vegas, USA, 2017*, pp. 510513.

**H. Jiang**, R. Rahimi, M. Ochoa, T. Parupudi, and B. Ziaie, "A pH-regulated drug delivery device for targeting infected regions in chronic dermal wounds", *MicroTAS 2016, Dublin, Ireland*.
W. Yu, J. Zhou, R. Rahimi, **H. Jiang**, M. Ochoa, and B. Ziaie, "Modular customizable 3d-printed batteries for wearable applications", *MicroTAS 2016, Dublin, Ireland*.

J. Zhou, A. Kim, M. Ochoa, **H. Jiang**, and B. Ziaie, "An ultrasonically powered micropump for on-demand in-situ drug delivery", *MEMS 2016, Shanghai, China, 2016*, pp. 349352.

**H. Jiang**, M. Ochoa, J.H. Park, A. Otte, R. Pinal, and B. Ziaie, "Wireless screening of degradation kinetics in pharmaceutical gelatin films", *Transducers 2015, Anchorage, AK, 2015*.

M. Ochoa, **H. Jiang**, R. Rahimi, and B. Ziaie, "Laser treated glass platform with rapid wicking-driven transport and particle separation capabilities", *MEMS 2015, Estoril, Portugal, 2015*.

M. Ochoa, R. Rahimi, **H. Jiang**, and B. Ziaie, "Laser surface-treated glass with wicking capability for microfluidics", *MicroTAS 2015, San Antonio, TX, 2015*.

**H. Jiang**, V. Jain, M. Ochoa, and B. Ziaie, "A low-cost insole using selective laser-engineered PDMS to provide topical oxygen therapy for diabetic foot ulcers", *2018 MRS spring meeting & exhibit*.

**H. Jiang**, Y. Wuyang, R. Rahimi, and B. Ziaie, "A biodegradable sensor housed in 3d printed porous tube for in-situ soil nitrate detection", *Hilton Head Workshop 2018: A Solid-State Sensors, Actuators and Microsystems Workshop*.

R. Rahimi, M. Ochoa, **H. Jiang,** and B. Ziaie, “facile fabrication of low-cost passive wireless humidity sensor for smart packaging via all-laser processing of metalized paper”, *Hilton Head Workshop 2018: A Solid-State Sensors, Actuators and Microsystems Workshop*.

M. Ochoa, R. Rahimi, J. Zhou, **H. Jiang**, etc., “A manufacturable smart dressing with oxygen delivery and sensing capability for chronic wound management”, *Micro and Nanotechnology Sensors, Systems, and Applications X, Orlando, FL, 2018*.